Generalisation of Theory and Algorithms for the Configurational Temperature Nosè-Hoover Thermostat

by

Derrick Beckedahl

Submitted in fulfilment of the academic requirements for the degree of Master of Science in Physics in the School of Chemistry and Physics, University of kwaZulu-Natal Durban/Pietermaritzburg.

December 2015

Supervisor: Prof. Alessandro Sergi
Co-supervisors: Prof. Francesco Petruccione and Dr. Daniel Uken

Name: ALESSANDRO SERGI Date: 25/01/2016 Signature: Alessandro Sergi
Name: Francesco Petruccione Date: 25/01/2016 Signature: Petruccione
Name: ..... Date: ..... Signature: .....

Abstract

In this dissertation we reformulate the configurational temperature Nosè-Hoover thermostat proposed by Braga and Travis (C. Braga and K.P. Travis, 2005), using the antisymmetric matrix formalism found in (A. Sergi, 2003). By exploiting the properties of this formalism, and utilising the concept behind the Nosè-Hoover chain thermostat, we extend our reformulated thermostat to obtain a hybrid configurational-kinetic chain thermostat. This is done with a view to achieving an ergodic sampling of phase space. We derive an integration algorithm, based upon the symmetric Trotter factorisation of the Liouville operator, as well as symplectic position and velocity Verlet integrations schemes, for purposes of comparison. In the case of systems possessing non-harmonic and non-linear interaction potentials, a position-dependent harmonic approximation scheme is presented. The thermostats and integration schemes were tested on one-dimensional harmonic and quartic oscillators, where it was found that the hybrid configurational-kinetic temperature Nosè-Hoover chain thermostat overcame the ergodicity problem, and the integration scheme based on the Trotter factorisation was the best performing.

Declaration

I, Derrick Beckedahl, declare that

(i) The research reported in this thesis, except where otherwise indicated, is my original research.

(ii) This thesis has not been submitted for any degree or examination at any other university.

(iii) This thesis does not contain other persons' data, pictures, graphs or other information, unless specifically acknowledged as being sourced from other persons.

(iv) This thesis does not contain any other persons' writing, unless specifically acknowledged as being sourced from other researchers. Where other written sources have been quoted, then:

  (a) their words have been rewritten but the general information attributed to them has been referenced;

  (b) where their exact words have been used, their writing has been placed inside quotation marks, and referenced.

(v) Where I have reproduced a publication of which I am author, co-author or editor, I have indicated in detail which part of the publication was actually written by myself alone and have fully referenced such publications.

(vi) This thesis does not contain text, graphics or tables copied and pasted from the Internet, unless specifically acknowledged, and the source being detailed in the thesis and in the References sections.

Signed .....

Preface

Conferences

During the course of this research, the following conferences were attended:

1. "Quantum Information Processing, Communication and Control 2014", Alpine Heath, Drakensberg, KZN, 3 - 7 November 2014.
2. "Quantum Simulation and Quantum Walks 2014", Pumula Beach Hotel, South Coast, KZN, 24 - 28 November 2014.
3. "Mini-workshop on Quantum Dynamics and Non-Hermitian Hamiltonians", UKZN - Pietermaritzburg, 3 - 8 December 2014.
4. "Non-equilibrium physics of driven-dissipative many-body systems", Palm Dune Beach Lodge, North Coast, KZN, 21 - 25 September 2015.

Publications

The research presented in this thesis is based on the following publication:

1. "On the Configurational Temperature Nosè-Hoover Thermostat"; D. Beckedahl, E. Obaga, D. Uken, A. Sergi and M. Ferrario. Submitted to *Computer Physics Communications*, November 2015.

This publication is reproduced in Appendix E.

Acknowledgements

I would like to thank my supervisor, Prof. Alessandro Sergi, for his constant motivation and support, as well as my co-supervisors, Prof. Francesco Petruccione and Dr. Daniel Uken, for their assistance and feedback during this work. Thank you to my parents for their support, encouragement and understanding and for providing me with the tools I needed to get to this point in my life. Further, I wish to express my gratitude to my fellow research group members for all their assistance and the good times. I would also like to thank my friends who have been so understanding during the writing process; I will not name you, but you know who you are. Finally I would like to acknowledge the financial support from the National Institute for Theoretical Physics (NITheP) which afforded me the privilege of participating in various conferences during this work, as well as the University of kwaZulu-Natal and the National Research Foundation (NRF) for funding this research.

Contents

List of Figures

Chapter 1

Introduction

Theoretical physics uses mathematical models to describe, and predict, natural phenomena, whilst experimental physics uses tools to investigate these natural phenomena. Computational physics provides a means of comparing, through computer simulation, theoretical models and experimental results [1, 2], particularly in cases where the models have no analytical solution. The accuracy of a particular model can be investigated through its numerical solution. If the model is found to be a valid one, comparisons can then be drawn between experimental results and results from the computer simulation of the model. If predictions made using the model are found to agree, to within acceptable numerical error, with results of experiments, then one can use the results from a computer simulation of the model to gain new insights into the physical systems [1, 2]. In addition to this, computer simulation has an advantage over physical experiments in that experimental conditions which lead to a physical experiment being extremely difficult or impossible (for example very high temperature and pressure), can still be used in a computer simulation [1].

The field of computer simulation uses two main techniques, namely Monte Carlo (MC) and molecular dynamics (MD). The Monte Carlo technique makes use of randomly generated numbers, whilst MD is used to obtain dynamical information about systems, by solving the classical equations of motion [1]. This dissertation will focus on a method used in MD simulations known as extended systems dynamics, which was first introduced by Andersen in 1980 [3], specifically thermostats.

Extended systems are a non-Hamiltonian theory, most often used to replicate thermodynamical baths (which physically require a very large number of degrees of freedom) within computer simulations [4]. Thermostats are a form of extended system

used to simulate thermodynamic heat baths, or thermal reservoirs. Some commonly used thermostats include the Gaussian [5], the Langevin [6, 7] and the Nosè-Hoover (NH) [8, 9] and Nosè-Hoover chain (NHC) thermostats [10], all of which control the kinetic temperature of the system to which they are attached.

Recently a new type of thermostat, referred to as a configurational thermostat as it controls the configurational temperature of a system [11, 12], has been derived. The configurational temperature was first used as a means of checking the codes used in MC simulations [13], and has been shown to be equivalent to the kinetic temperature at equilibrium in the microcanonical ensemble [14]. This new configurational thermostat has advantages over the more traditional kinetic schemes, in non-equilibrium simulations [15]. One such an advantage arises from the need, when using a kinetic thermostat scheme, to know the form of the local streaming velocity. The local streaming velocity is necessary in order to calculate the correct thermal contribution. This form however, is not known in general, leading to the onset of fictitious string phases [16–18]. The generation of non-zero off-diagonal stresses has also been observed [19], when using kinetic thermostat schemes. A configurational thermostat scheme is not subject to these difficulties, and thus is more appealing than kinetic schemes.

In the work presented in this dissertation, we reformulate the configurational temperature Nosè-Hoover (CTNH) thermostat of Braga and Travis [20] into a phase space description, following the antisymmetric matrix formalism of [21]. We then proceed to extend this reformulated thermostat, utilising the same concept behind the NHC thermostat. This is done in order to overcome the issue of the CTNH thermostat not achieving an ergodic sampling of phase space, particularly in the case of stiff systems. We refer to this extended thermostat as a hybrid configurational-kinetic temperature Nosè-Hoover (CKTNH) chain thermostat. Three integration algorithms are developed for each of the two thermostats (both the CTNH and hybrid CKTNH chain thermostats), where a position-dependent, harmonic approximation (PDHA) is presented for systems with non-harmonic and non-linear interaction potentials. The thermostats, along with the integration schemes, are tested by simulating a one dimensional harmonic oscillator (single well potential) system as well as a one dimensional quartic oscillator (double well potential) system.

The work presented in this dissertation, together with an extension provided by Mr. E. Obaga, whereby the CTNH thermostat was applied to a three-dimensional

variation of the Lennard-Jones potential (referred to as a Weeks-Chandler-Andersen (WCA) fluid), has been submitted to the journal Computer Physics Communications, and is currently in the review process.

In Chap. 2 we introduce and discuss the thermodynamic temperature and its relevance within the field of Thermostatistics. Chapter 3 compares Hamiltonian and non-Hamiltonian theories. The underlying algebraic bracket of each of these theories is also discussed, along with constant temperature dynamics. The NH and NHC thermostats are further discussed within this chapter. In Chap. 4 configurational thermostats are discussed, and our work is introduced. The integration algorithms for our proposed thermostats are provided in Chap. 5, with the models used and simulation results being presented in Chap. 6. Finally, conclusions and future research are given in Chap. 7.

Chapter 2

Temperature in Thermostatistics

Thermodynamics is the theory which links the motion of particles on the microscopic scale to the measurement of observable quantities on the macroscopic scale [22, 23]. It is well known that a variety of different microscopic states, or microstates, lead to the same value for a measured macroscopic observable. Hence it is reasonable to assume that the fluctuations on the microscopic scale average out over the duration of the measurement of the macroscopic observable [22, 23]. This averaging is accounted for through use of the so called *ensemble concept*. An ensemble consists of all possible, unique microstates which correspond to a common set of macroscopic observables [22]. Each system within the ensemble evolves under the same microscopic laws of motion, but starts from a different set of initial conditions. Therefore at any instant in time, each member of the ensemble will be a unique microstate, distinguishable from all other members [22].

In order to obtain the value for a particular macroscopic observable, one needs to take an average over the ensemble [22, 23]. For a given macroscopic observable, A, the relation to its corresponding microscopic function, $a = a(\mathbf{X})$, which is itself a function of the phase space vector $\mathbf{X}$, is given by [22]

$$A = \langle a\left(\mathbf{X}\right)\rangle = \int \mathrm{d}\mathbf{X}\, f\left(\mathbf{X}, t\right) a\left(\mathbf{X}\right) \ , \tag{2.1}$$

where $f\left(\mathbf{X}, t\right)$ is referred to as the *phase space distribution function*, or the *phase space probability density*. The phase space distribution function is defined such that the quantity $f\left(\mathbf{X}, t\right) \mathrm{d}\mathbf{X}$ is equal to the fraction of ensemble members which occupy the volume element of phase space $\mathrm{d}\mathbf{X}$, at time t [22]. The phase space probability density

therefore has the properties

$$f(\mathbf{X}, t) \geq 0$$
$$\int \mathrm{d}\mathbf{X} f(\mathbf{X}, t) = 1 \, .$$

Different ensembles are defined for different sets of macroscopic properties, and are equivalent within the thermodynamic limit [22]. The thermodynamic limit is defined as the limit in which $N \to \infty$ and $V \to \infty$ in such a way that $N/V =$ constant [22, 24]. In practice, measurements are only performed on a single system, as opposed to over an ensemble of systems. The value obtained, however, is still an average, but it is an average in time as opposed to an average over an ensemble. This leads to the conclusion that ensemble averages are equivalent to time averages [3, 22]. This equivalence of ensemble and time averages is known as the *ergodic hypothesis* [22], and can be mathematically expressed [22] as

$$A = \langle a \rangle = \lim_{t \to \infty} \frac{1}{t} \int_0^t \mathrm{d}t' a\left(\mathbf{X}\left(t'\right)\right) \, . \tag{2.2}$$

A system is said to be ergodic if, given an infinite amount of time, all possible system configurations, which correspond to the constant energy hypersurface in phase space, are realised [22]. Physically, this implies that the dynamics of the system sample all possible phase space points.

We consider a general system consisting of N particles in three dimensions, which we describe in phase space using the $6N$-dimensional vector $\mathbf{X} = (q, p)$, where q and p represent the particles' positions and momenta respectively, and a multi-dimensional notation has been used. The Hamiltonian of the system is given by

$$\mathcal{H}(\mathbf{X}) = \mathcal{K}(p) + \mathcal{U}(q) \, , \tag{2.3}$$

where $\mathcal{K}(p)$ and $\mathcal{U}(q)$ represent the kinetic and potential energy of the system, respectively. From the theory of thermodynamics, we know that the temperature of the system is given by the following relation [22, 24]:

$$\frac{1}{T} = \left(\frac{\partial S}{\partial E}\right)_{V,N} \, , \tag{2.4}$$

where T is the temperature, S the entropy, V the volume, N the number of particles in the system and E is the total energy of the system. Recently, a microcanonical definition of the temperature of a system has been derived, by Rugh [11, 25], and is

given by

$$\frac{1}{k_{\mathrm{B}}T} = \left\langle \nabla_{\mathbf{X}} \cdot \frac{\nabla_{\mathbf{X}}\mathcal{H}}{|\nabla_{\mathbf{X}}\mathcal{H}|^2} \right\rangle + \mathcal{O}\left(\frac{1}{N}\right) , \tag{2.5}$$

where k_{B} is the Boltzmann constant, $\mathcal{H}$ the Hamiltonian of the system and $\nabla_{\mathbf{X}}$ is the gradient operator in phase space. This expression, given by Eq. (2.5), has since been generalised, by Jepps *et al.* [12], to

$$k_{\mathrm{B}}T \approx \frac{\langle \nabla_{\mathbf{X}}\mathcal{H} \cdot \Omega(\mathbf{X}) \rangle}{\langle \nabla_{\mathbf{X}} \cdot \Omega(\mathbf{X}) \rangle} , \tag{2.6}$$

where $\Omega(\mathbf{X})$ is an arbitrary vector field which satisfies the following two relations:

$$0 < \langle |\nabla_{\mathbf{X}}\mathcal{H} \cdot \Omega(\mathbf{X})| \rangle < \infty ,$$
$$0 < \langle |\nabla_{\mathbf{X}} \cdot \Omega(\mathbf{X})| \rangle < \infty .$$

From Eq. (2.6) one is able to obtain two useful expressions for the system temperature, by choosing $\Omega(\mathbf{X}) = \boldsymbol{\chi}\,(\nabla_{\mathbf{X}}\mathcal{H})$, where $\boldsymbol{\chi}$ is a matrix such that $(\nabla_{\mathbf{X}}\mathcal{H})\boldsymbol{\chi}(\nabla_{\mathbf{X}}\mathcal{H}) \neq 0$. The first expression is acquired by choosing the matrix elements, χ_{ij}, as δ_{ij} (the Krönecker delta) if i and j correspond to momentum variables and zero otherwise. With this choice for the matrix $\boldsymbol{\chi}$, Eq. (2.6) becomes

$$k_{\mathrm{B}}T_{\mathrm{kin}} = \frac{\left\langle |\nabla_{\mathbf{p}}\mathcal{K}(p)|^2 \right\rangle}{\left\langle |\nabla^2_{\mathbf{p}}\mathcal{K}(p)| \right\rangle} = \frac{\langle p^2/m^2 \rangle}{\langle D \sum_i (1/m_i) \rangle} , \tag{2.7}$$

where it is assumed that the kinetic energy of the system, $\mathcal{K}(p)$, can be expressed in the form $\mathcal{K}(p) = \frac{1}{2}\sum_i \left(p_i^2/m_i\right)$. In Eq. (2.7), D denotes the dimensionality of the system, and $\nabla_{\mathbf{p}}$ represents the momentum gradient. The index i, which runs over all degrees of freedom, has been introduced to indicate, without ambiguity, a summation operation. The expression in Eq. (2.7) provides a means of determining the so called kinetic temperature, T_{kin}, and in the case where the particles in the system have identical mass values, Eq. (2.7) reduces to the equipartition theorem: $DNk_{\mathrm{B}}T_{\mathrm{kin}} = \langle p^2/m \rangle$.

The second expression is obtained by choosing the elements of $\boldsymbol{\chi}$ as δ_{ij} if i and j correspond to coordinate variables and zero otherwise. With this choice, a configurational expression for the temperature is obtained, from Eq. (2.6), as

$$k_{\mathrm{B}}T_{\mathrm{conf}} = \frac{\left\langle |\nabla_q \mathcal{U}(q)|^2 \right\rangle}{\left\langle \sum_i \nabla^2_{q_i}\mathcal{U}(q) \right\rangle} , \tag{2.8}$$

where ∇_q denotes the phase space position gradient. Eq. (2.8) differs from the expression introduced by Rugh in Ref. [11]. The temperature, T_{conf}, defined in Eq. (2.8), was used by Braga and Travis to introduce a configurational temperature Nosè-Hoover (CTNH) thermostat [20]. This is discussed further in Chap. 4.

Chapter 3

Non-Hamiltonian Dynamics

3.1 Hamiltonian Theory

The algebra which underpins Hamiltonian theory belongs to a class of algebra known as a Lie algebra. In order to define what it means for an algebra to be considered a Lie algebra, we consider a set of mathematical objects, (a, b, c), belonging to a mathematical space. We define a generic bracket, denoted by $\{\cdots, \cdots\}$, with the following properties

$$\{a, b\} = -\{b, a\} \,, \tag{3.1a}$$

$$\{a + b, c\} = \{a, c\} + \{b, c\} \,, \tag{3.1b}$$

$$\{ga, b\} = g\{a, b\} \,, \tag{3.1c}$$

where g is a complex number. Equation (3.1a) states the antisymmetry of the bracket while Eqs. (3.1b) and (3.1c) state the bracket's linearity, both with respect to constants and to members of the mathematical space. For the algebra to be considered a Lie algebra, the bracket must also satisfy the so called Jacobi relation [26], given by

$$\mathcal{J} = \{a, \{b, c\}\} + \{b, \{c, a\}\} + \{c, \{a, b\}\} = 0 \,, \tag{3.2}$$

which shows that the bracket algebra is not associative [26]. Any algebra which satisfies the properties given by Eqs. (3.1) and Eq. (3.2) is said to be a Lie algebra. For the Hamiltonian description in the classical case, this bracket algebra is given by the Poisson bracket, defined as

$$\{a, b\} = \frac{\partial a}{\partial q_i}\frac{\partial b}{\partial p_i} - \frac{\partial a}{\partial p_i}\frac{\partial b}{\partial q_i} \,, \tag{3.3}$$

where the Einstein summation convention has been used and q_i and p_i denote the generalised coordinate and momentum, respectively, of the ith particle. The requirement

for a bracket algebra to be considered as Hamiltonian is that it be a Lie algebra [26, 27], in other words that it satisfies the properties given by Eqs. (3.1) and (3.2).

One can see that if elements of this mathematical space are time independent (they denote conserved quantities), then a bracket of said elements will also be conserved (time independent). The total time derivative of an element of the mathematical space, say a, can be expressed in terms of the Poisson bracket [26, 27] as follows

$$\frac{\mathrm{d}a}{\mathrm{d}t} = \{a, H\} + \frac{\partial a}{\partial t} \,, \tag{3.4}$$

where $a = a(q, p, t)$ is a function of phase space and H is the Hamiltonian of the system. From Eq. (3.4) one can see that if the quantity a is time independent the corresponding equation of motion will be given by

$$\frac{\mathrm{d}a}{\mathrm{d}t} = \{a, H\} \,. \tag{3.5}$$

If a quantity's total time derivative is equal to zero, then that quantity is said to be a constant of motion. From Eq. (3.5), and the antisymmetry property of the Poisson bracket, one can see that if the Hamiltonian is not explicitly time dependent, it is a constant of motion [26, 27]. Similarly if two quantities, say a and b, obey a Hamiltonian bracket algebra and are constants of motion, then a bracket of these two quantities will also be a constant of motion [26]

$$\{\{a, b\}, H\} = 0 \,, \tag{3.6}$$

which shows that the algebra underlying Hamiltonian theory is left invariant under time translations.

3.2 Non-Hamiltonian Theory

Non-Hamiltonian systems are characterised by equations of motion which cannot be obtained from Lagrangian or Hamiltonian functions [22]. Such systems can be particularly useful within molecular dynamics (MD) simulations. One can see this by considering a system in contact with a constant temperature thermal bath. If one were to simulate such a system using Hamiltonian dynamics, one would need to consider not only the degrees of freedom of the system, but also the degrees of freedom of the bath to which the system is coupled. This is not a feasible task as, by definition, a thermodynamic reservoir has a large number of degrees of freedom; too many for the

memory constraints of modern computers [4, 22]. A technique within MD, which was first introduced by Andersen in 1980 [3], and is frequently used, is known as *extended systems* [1, 21]. This technique involves the coupling of *ad hoc* dynamical variables to the system under study. The desired ensemble is chosen through the way in which the *ad hoc* variables are coupled to the system, as this affects the way in which the MD simulation samples the phase space trajectory [21, 28].

We define an antisymmetric matrix $\mathcal{B}_{ij} = -\mathcal{B}_{ji}$, with elements which are general functions of the phase space point $\mathbf{x} = (\mathbf{q}, \mathbf{p})$, where, following convention, the generalised coordinates come first [29]. With this, one can introduce the non-Hamiltonian bracket operation [29], $\{\cdots, \cdots\}$, defined by

$$\{a, b\} = \sum_{i,j=1}^{2N} \frac{\partial a}{\partial x_i} \mathcal{B}_{ij} \frac{\partial b}{\partial x_j} \,, \tag{3.7}$$

where the dimension of phase space is equal to $2N$. We postulate that the equations of motion can be expressed in the form

$$\dot{x}_i = \{x_i, \mathcal{H}\} = \sum_{j=1}^{2N} \mathcal{B}_{ij} \frac{\partial \mathcal{H}}{\partial x_j} \,, \qquad i = 1, \ldots, 2N \,, \tag{3.8}$$

where $\mathcal{H}$ is a given Hamiltonian [21, 29]. In the case where the Hamiltonian is time independent one can see that it will be a constant of motion, assuming that the algebra defining the phase space flow is given by the bracket operation [29] in Eq. (3.7)

$$\frac{\mathrm{d}\mathcal{H}}{\mathrm{d}t} = \{\mathcal{H}, \mathcal{H}\} = \sum_{i,j=1}^{2N} \frac{\partial \mathcal{H}}{\partial x_i} \mathcal{B}_{ij} \frac{\partial \mathcal{H}}{\partial x_j} = 0 \,. \tag{3.9}$$

With the exception of the requirement of $\mathcal{B}$ being antisymmetric, the property stated by Eq. (3.9) is very general [21, 29].

One can easily verify that the Jacobi relation, stated in Eq. (3.2), is not satisfied by the bracket algebra of Eq. (3.7)

$$\mathcal{J} \neq 0 \,. \tag{3.10}$$

To evaluate the time translation variance of the non-Hamiltonian bracket, we consider the Jacobi relation between the Hamiltonian, $\mathcal{H}$, and two arbitrary variables of phase space, a and b

$$\{a, \{b, \mathcal{H}\}\} + \{b, \{\mathcal{H}, a\}\} + \{\mathcal{H}, \{a, b\}\} = \mathcal{R} \,. \tag{3.11}$$

Using the definition of the bracket operation given by Eq. (3.7), one finds [29]

$$\mathcal{R} = \sum_{i,j,k,n}^{2N} \frac{\partial a}{\partial x_i}\frac{\partial b}{\partial x_k}\frac{\partial \mathcal{H}}{\partial x_n}\left(\mathcal{B}_{ij}\frac{\partial \mathcal{B}_{kn}}{\partial x_j} + \mathcal{B}_{nj}\frac{\partial \mathcal{B}_{ik}}{\partial x_j} + \mathcal{B}_{kj}\frac{\partial \mathcal{B}_{ni}}{\partial x_j}\right) . \tag{3.12}$$

Equation (3.12) can be rearranged [29] to obtain

$$\{\{a,b\},\mathcal{H}\} = \{\dot{a},b\} + \{a,\dot{b}\} + \mathcal{R} , \tag{3.13}$$

$$\Rightarrow \frac{\mathrm{d}}{\mathrm{d}t}\{a,b\} = \{\dot{a},b\} + \{a,\dot{b}\} + \mathcal{R} , \tag{3.14}$$

where in the last step the postulate of Eq. (3.8) was used. One can see, from Eq. (3.14), that the bracket algebra defined by Eq. (3.7) is not time translation invariant [29]. From this one can infer that, unlike in the case of the Hamiltonian bracket algebra, the non-Hamiltonian bracket of two constants of motion is not itself a constant of motion.

The phase space compressibility, κ, is defined as

$$\kappa = \sum_{i,j=1}^{2N} \frac{\partial \mathcal{B}_{ij}}{\partial x_i}\frac{\partial \mathcal{H}}{\partial x_j} . \tag{3.15}$$

In the Hamiltonian case the phase space compressibility is zero, however, in general this is not so for non-Hamiltonian phase space flows [21, 29], defined by the bracket of Eq. (3.7). It has been shown [21, 22, 29–31] that the compressibility is used to describe the statistical mechanical properties of non-Hamiltonian systems, as well as the ensemble distribution. Thus for a given conserved quantity of an extended system, one is able to select a desired ensemble by using the definition in Eq. (3.15) and exploiting the generality of the antisymmetric matrix $\mathcal{B}$.

3.3 Constant Temperature Dynamics

In reality most experiments are conducted under conditions of constant temperature [22]. Thus in order for MD simulations to be compared with experimental results, for checking the accuracy of the numerical approximations or the model used, the simulations need to be performed within a corresponding ensemble. Such an ensemble is known as the canonical ensemble and is characterised by the number of particles (N), the volume of the system (V) and the system temperature (T), each being kept constant. This constant temperature is achieved by placing the system in contact with a thermal reservoir, or heat bath. By definition a thermal reservoir is a system which is large

enough such that any finite change in the energy of the system will not affect the overall temperature of said system [22, 23]. As has been previously mentioned (section 3.2), of the multiple ways in which to replicate the effects of a heat bath, a common choice for MD simulations is that of extended systems. The concept behind extended systems dynamics is to introduce one or more degrees of freedom into the system, which are representative of the thermal reservoir. The resulting extended system is then simulated [1]. Two of the most commonly used kinetic schemes, namely the Nosè-Hoover and the Nosè-Hoover Chain thermostats, are introduced in the following sections. A configurational scheme is introduced and discussed in Ch. 4.

3.3.1 Nosè-Hoover Thermostat

The Nosè-Hoover thermostat, which was first introduced in Ref. [8], has an extended system Hamiltonian given by

$$\mathcal{H}^{\mathrm{NH}} = \sum_{i=1}^{N} \frac{p_i^2}{2m_i} + \phi\left(q\right) + \frac{p_s^2}{2M_s} + g k_{\mathrm{B}} T s \;, \tag{3.16}$$

where p_i and m_i are the generalised momentum and mass of the ith particle respectively, $\phi\left(q\right)$ is the potential energy function of the system using a multidimensional notation for the generalised coordinates. The last two terms in Eq. (3.16) can be thought of as the kinetic and potential energies of the reservoir respectively, where p_s is the conjugate momentum of the fictitious thermostat variable s, M_s is a parameter which acts as a mass for the motion of s, k_{B} is Boltzmann's constant, g is a constant equal to the number of degrees of freedom of the system and T is the temperature of the heat bath. Following the postulate of Eq. (3.8), we can express this extended system's equations of motion as

$$\dot{\mathbf{x}} = \{\mathbf{x}, \mathcal{H}^{\mathrm{NH}}\} = \sum_{j,k} \frac{\partial \mathbf{x}}{\partial x_j} \mathcal{B}^{\mathrm{NH}}_{jk} \frac{\partial \mathcal{H}^{\mathrm{NH}}}{\partial x_k} \;, \tag{3.17}$$

where the phase space point is given by $\mathbf{x} = (q, s, p, p_s)$. By choosing the antisymmetric matrix, $\mathcal{B}^{\mathrm{NH}}$, as

$$\mathcal{B}^{\mathrm{NH}} = \begin{bmatrix} 0 & 0 & 1 & 0 \\ 0 & 0 & 0 & 1 \\ -1 & 0 & 0 & -p \\ 0 & -1 & p & 0 \end{bmatrix} \;, \tag{3.18}$$

the equations of motion for the Nosè-Hoover thermostat can be expressed explicitly as

$$\dot{q} = \frac{p}{m} \,, \tag{3.19a}$$

$$\dot{s} = \frac{p_s}{M_s} \,, \tag{3.19b}$$

$$\dot{p} = -\frac{\partial \phi\left(q\right)}{\partial q} - p\frac{p_s}{M_s} \,, \tag{3.19c}$$

$$\dot{p}_s = \frac{p^2}{m} - g k_{\mathrm{B}} T \,. \tag{3.19d}$$

The second term in Eq. (3.19c) can be thought of as a feedback term, allowing for energy transfer between the reservoir and the physical system. From Eq. (3.15) we see that the phase space compressibility for this extended system is given by

$$\kappa^{\mathrm{NH}} = \sum_{j,k} \frac{\partial \mathcal{B}_{jk}^{\mathrm{NH}}}{\partial x_j} \frac{\partial \mathcal{H}^{\mathrm{NH}}}{\partial x_k} = -\frac{p_s}{M_s} = -\dot{s} \,. \tag{3.20}$$

3.3.2 Nosè-Hoover Chain Thermostat

The Nosè-Hoover thermostat has limitations, namely that for small or stiff systems the dynamics achieved are not ergodic [10]. A solution to this, proposed by Martyna *et al* [10], is the so called Nosè-Hoover Chain (NHC) thermostat. The concept of the NHC thermostat is to attach an additional thermostat to the one which is attached to the physical system, forming a chain of thermostats. This is so as to increase the fluctuations in the thermostat variables and, if necessary, the thermostat chain can be extended [10]. In this section we will only consider the case of a chain of length two, where thermostat 1 is attached to the physical system and thermostat 2 is attached to thermostat 1. In this case the phase space point is given by $\mathbf{x} = (q, s_1, s_2, p, p_{s_1}, p_{s_2})$ and the extended Hamiltonian is

$$\mathcal{H}^{\mathrm{NHC}} = \sum_{i=1}^{N} \frac{p_i^2}{2m_i} + \phi\left(q\right) + \frac{p_{s_1}^2}{2M_{s_1}} + \frac{p_{s_2}^2}{2M_{s_2}} + g k_{\mathrm{B}} T \left(s_1 + s_2\right) \,, \tag{3.21}$$

where the notation used is the same as that for the Nosè-Hoover thermostat and the subscripts correspond to the thermostat number. Again using the postulate of Eq. (3.8), the equations of motion are given by

$$\dot{\mathbf{x}} = \{\mathbf{x}, \mathcal{H}^{\mathrm{NHC}}\} = \sum_{j,k} \frac{\partial \mathbf{x}}{\partial x_j} \mathcal{B}_{jk}^{\mathrm{NHC}} \frac{\partial \mathcal{H}^{\mathrm{NHC}}}{\partial x_k} \,, \tag{3.22}$$

with the antisymmetric matrix being given by

$$\mathcal{B}^{\mathrm{NHC}} = \begin{bmatrix} 0 & 0 & 0 & 1 & 0 & 0 \\ 0 & 0 & 0 & 0 & 1 & 0 \\ 0 & 0 & 0 & 0 & 0 & 1 \\ -1 & 0 & 0 & 0 & -p & 0 \\ 0 & -1 & 0 & p & 0 & -p_{s_1} \\ 0 & 0 & -1 & 0 & p_{s_1} & 0 \end{bmatrix} . \tag{3.23}$$

Expressed explicitly, the equations of motion for the NHC thermostat are as follows

$$\dot{q} = \frac{p}{m} , \tag{3.24a}$$

$$\dot{s}_1 = \frac{p_{s_1}}{M_{s_1}} , \tag{3.24b}$$

$$\dot{s}_2 = \frac{p_{s_2}}{M_{s_2}} , \tag{3.24c}$$

$$\dot{p} = -\frac{\partial \phi(q)}{\partial q} - p\frac{p_{s_1}}{M_{s_1}} , \tag{3.24d}$$

$$\dot{p}_{s_1} = \frac{p^2}{m} - gk_{\mathrm{B}}T - p_{s_1}\frac{p_{s_2}}{M_{s_2}} , \tag{3.24e}$$

$$\dot{p}_{s_2} = \frac{p_{s_1}^2}{M_{s_1}} - gk_{\mathrm{B}}T . \tag{3.24f}$$

Using Eq. (3.15), the phase space compressibility for this extended system is given by

$$\kappa^{\mathrm{NHC}} = \sum_{j,k} \frac{\partial \mathcal{B}_{jk}^{\mathrm{NHC}}}{\partial x_j} \frac{\partial \mathcal{H}^{\mathrm{NHC}}}{\partial x_k} = -\frac{p_{s_1}}{M_{s_1}} - \frac{p_{s_2}}{M_{s_2}} = -\left(\dot{s}_1 + \dot{s}_2\right) . \tag{3.25}$$

Chapter 4

Configurational Thermostats

A configurational expression for the temperature was first used by Butler *et al* [13] as a means of verifying Monte Carlo simulations. A thermostatting scheme based on the configurational expression for the temperature was first introduced by Delhommelle and Evans [32], and was applied to liquid chlorine being subjected to shear flow. The expression for the temperature used in formulating this thermostat [32, 33] was the same as that derived by Rugh [11, 25], and is given in Eq. (2.5). The temperature expression is quoted below for the reader's convenience

$$\frac{1}{k_{\mathrm{B}}T} = \left\langle \nabla_{\mathbf{X}} \cdot \frac{\nabla_{\mathbf{X}}\mathcal{H}}{|\nabla_{\mathbf{X}}\mathcal{H}|^2} \right\rangle + \mathcal{O}\left(\frac{1}{N}\right) \ .$$

The concept of a configurational temperature thermostat was later explored by Braga and Travis [20] and a new thermostat, which was derived in the same spirit as the well known Nosè-Hoover (NH) thermostat, was developed. This Braga and Travis thermostat is further discussed in the following section (Sec. 4.1), and will henceforth be referred to as the BT thermostat.

4.1 Braga and Travis Formulation

The approach followed by Braga and Travis was similar to that used by Hoover when formulating the kinetic temperature NH thermostat, namely equations of motion were proposed with consideration of the Langevin equation [20]. An expression for the rate of change of a friction coefficient, appearing in the equations of motion, was derived such that the canonical ensemble distribution was obtained [20]. Assuming that the

Hamiltonian of the physical system can be expressed in the form

$$\mathcal{H}(q,p) = \frac{p^2}{2m} + U(q) \ , \tag{4.1}$$

where a multidimensional notation has been used and $U(q)$ denotes the potential function, one can propose the following equations of motion for the BT thermostat [20]

$$\dot{q} = \frac{p}{m} - \eta \frac{\partial U(q)}{\partial q} \ , \tag{4.2a}$$

$$\dot{p} = -\frac{\partial U(q)}{\partial q} \ , \tag{4.2b}$$

$$\dot{\eta} = ? \ , \tag{4.2c}$$

where η is the thermostat variable and the second term on the right hand side of Eq. (4.2a) is the feedback term between the reservoir and the system. The right hand side of Eq. (4.2c) is to be determined.

We can express the phase space probability density of the extended system, $\rho(q,\eta,p)$, as a product of the canonical distribution, $\rho_{\mathrm{NVT}}(q,p)$, and a density function of the thermostat variable η, $g(\eta)$

$$\rho(q,\eta,p) = \rho_{\mathrm{NVT}}(q,p)\, g(\eta) \ , \tag{4.3}$$

$$\text{where} \qquad \rho_{\mathrm{NVT}}(q,p) \propto \mathrm{e}^{-\beta \mathcal{H}(q,p)} \ . \tag{4.4}$$

This is possible due to q, p and η being independent variables [20]. For such an extended system, one can express the steady-state Liouville equation as

$$\dot{q}\frac{\partial \rho}{\partial q} + \dot{p}\frac{\partial \rho}{\partial p} + \dot{\eta}\frac{\partial \rho}{\partial \eta} + \rho\left(\frac{\partial \dot{q}}{\partial q} + \frac{\partial \dot{p}}{\partial p} + \frac{\partial \dot{\eta}}{\partial \eta}\right) = 0 \ . \tag{4.5}$$

Under the assumption that the right hand side of Eq. (4.2c) is a function solely of variables of the physical system, $\dot{\eta} = \dot{\eta}(q,p)$, the term $\partial\dot{\eta}/\partial\eta$ becomes zero. Calculating the nonzero terms in Eq. (4.5) one obtains

$$\frac{\partial \rho}{\partial q} = -\beta\rho \frac{\partial U(q)}{\partial q} \ , \tag{4.6a}$$

$$\frac{\partial \rho}{\partial p} = -\beta\rho \frac{p}{m} \ , \tag{4.6b}$$

$$\frac{\partial \rho}{\partial \eta} = \rho \frac{\partial \ln(g)}{\partial \eta} \ , \tag{4.6c}$$

$$\frac{\partial \dot{q}}{\partial q} = -\eta \frac{\partial^2 U(q)}{\partial^2 q} \ . \tag{4.6d}$$

By substituting Eqs. (4.6) and the equations of motion Eqs. (4.2a) and (4.2b) into Eq. (4.5), we obtain

$$\dot{\eta}\rho\frac{\partial \ln g}{\partial \eta} - \eta\rho\frac{\partial^2 U(q)}{\partial q^2} + \eta\rho\beta\left(\frac{\partial U(q)}{\partial q}\right)^2 = 0 \,, \tag{4.7}$$

which leads to the equation for $\dot{\eta}$

$$\dot{\eta} = \frac{-\beta\eta}{\left(\frac{\partial \ln(g)}{\partial \eta}\right)}\left[\left(\frac{\partial U(q)}{\partial q}\right)^2 - k_{\mathrm{B}}T\frac{\partial^2 U(q)}{\partial q^2}\right] \,. \tag{4.8}$$

Owing to the earlier assumption that $\dot{\eta}$ is independent of η, the ratio

$$\frac{\left(\frac{\partial \ln(g)}{\partial \eta}\right)}{-\beta\eta} = M_\eta \,, \tag{4.9}$$

must be constant, where the quantity M_η can be viewed as the thermostat mass [20]. Thus the equations of motion for the BT thermostat are

$$\dot{q} = \frac{p}{m} - \eta\frac{\partial U(q)}{\partial q} \,, \tag{4.10a}$$

$$\dot{p} = -\frac{\partial U(q)}{\partial q} \,, \tag{4.10b}$$

$$\dot{\eta} = \frac{1}{M_\eta}\left[\left(\frac{\partial U(q)}{\partial q}\right)^2 - k_{\mathrm{B}}T\frac{\partial^2 U(q)}{\partial q^2}\right] \,. \tag{4.10c}$$

These equations of motion have the following conserved quantity

$$\mathcal{H}_\eta = \frac{p^2}{2m} + U(q) + M_\eta\frac{\eta^2}{2} + k_{\mathrm{B}}T\int_0^t\left[\eta\left(t'\right)\left(\frac{\partial^2 U(q)}{\partial q^2}\right)\right]\mathrm{d}t' \,. \tag{4.11}$$

4.2 Phase-Space Formulation of the Configurational Temperature Nosè-Hoover Thermostat

By definition phase space is even-dimensional [26, 27]. Thus the BT thermostat is not in a phase space description, which would be useful for further generalisations. In order to cast this thermostat in a phase space description, we introduce the fictitious variable ζ with associated conjugate momentum $p_\zeta = \eta M_\zeta$. By defining $M_\zeta = M_\eta$ one can introduce the conserved quantity

$$\mathcal{H}^\zeta = \frac{p^2}{2m} + U(q) + \frac{p_\zeta^2}{2M_\zeta} + k_{\mathrm{B}}T\zeta \,, \tag{4.12}$$

with phase space equations of motion

$$\dot{q} = \frac{p}{m} - \frac{p_\zeta}{M_\zeta}\frac{\partial U\left(q\right)}{\partial q} \,, \tag{4.13a}$$

$$\dot{\zeta} = G\left(q\right)\frac{p_\zeta}{M_\zeta} \,, \tag{4.13b}$$

$$\dot{p} = -\frac{\partial U\left(q\right)}{\partial q} \,, \tag{4.13c}$$

$$\dot{p}_\zeta = F_\zeta\left(q\right) \,, \tag{4.13d}$$

where

$$G\left(q\right) = \frac{\partial^2 U\left(q\right)}{\partial q^2} \,, \tag{4.14a}$$

$$F_\zeta\left(q\right) = \left(\frac{\partial U\left(q\right)}{\partial q}\right)^2 - k_{\mathrm{B}}T\left(\frac{\partial^2 U\left(q\right)}{\partial q^2}\right) \,. \tag{4.14b}$$

The equations of motion Eqs. (4.13) can be expressed using the antisymmetric matrix notation discussed in Chap. 3 by defining the extended phase space point as $\mathbf{x} = (q, \zeta, p, p_\zeta)$. Thus the equations of motion, in matrix form, are given as

$$\dot{x}_i = \sum_{j=1}^{6N+2} \mathcal{B}_{ij}^{\mathrm{CTNH}} \frac{\partial \mathcal{H}^\zeta}{\partial x_j} \,, \qquad (i = 1, \ldots, 6N+2) \,, \tag{4.15}$$

where the antisymmetric matrix, $\mathcal{B}^{\mathrm{CTNH}}$, is given by

$$\mathcal{B}^{\mathrm{CTNH}} = \begin{bmatrix} 0 & 0 & 1 & -\left(\frac{\partial U(q)}{\partial q}\right) \\ 0 & 0 & 0 & G\left(q\right) \\ -1 & 0 & 0 & 0 \\ \left(\frac{\partial U(q)}{\partial q}\right)^T & -G\left(q\right) & 0 & 0 \end{bmatrix} . \tag{4.16}$$

A compact notation has been used in Eq. (4.16) to represent the column vector $(\partial U/\partial q)$ and its transpose $(\partial U/\partial q)^T$, as well as for the $3N \times 3N$ block diagonal matrices.

Under the assumption of ergodicity, the thermostat described by Eqs. (4.12) and (4.13) causes the dynamics of the system to canonically sample phase space. Using the definition, Eq. (3.15), provided in Chap. 3, we find that the phase space compressibility for this extended system is given by

$$\kappa^{\mathrm{CTNH}} = \sum_{j,k=1}^{6N+2} \frac{\partial \mathcal{B}_{jk}^{\mathrm{CTNH}}}{\partial x_j}\frac{\partial \mathcal{H}^\zeta}{\partial x_k} = -G\left(q\right)\frac{p_\zeta}{M_\zeta} = -\dot{\zeta} \,. \tag{4.17}$$

This ergodicity assumption however is not valid when concerning stiff systems. A solution to this problem is provided, and discussed, in the following section, Sec. 4.3.

4.3 Hybrid Thermostat (Ergodic Phase-Space Sampling)

A solution to the problem of ergodicity when dealing with stiff systems was achieved by utilising the same concept of the Nosè-Hoover chain (NHC) thermostat, discussed in Sec. 3.3.2, namely creating a chain of thermostats. We consider a hybrid thermostat chain which consists of a configurational temperature thermostat attached to the physical system, which is itself thermostatted by a kinetic temperature standard Nosè-Hoover thermostat. Such a thermostat will henceforth be referred to as a hybrid Configurational-Kinetic Temperature Nosè-Hoover (CKTNH) chain thermostat.

To introduce the hybrid CKTNH chain thermostat, we define the following conserved quantity

$$\mathcal{H}^{\zeta s} = \frac{p^2}{2m} + U\left(q\right) + \frac{p_\zeta^2}{2M_\zeta} + \frac{p_s^2}{2M_s} + k_{\mathrm{B}}T\left(\zeta + s\right) \ , \tag{4.18}$$

where ζ is the configurational thermostat variable, with associated mass M_ζ and momentum p_ζ, and s is the kinetic thermostat variable, with associated mass M_s and momentum p_s. The equations of motion are

$$\dot{q} = \frac{p}{m} - \frac{p_\zeta}{M_\zeta}\frac{\partial U\left(q\right)}{\partial q} \ , \tag{4.19a}$$

$$\dot{\zeta} = G\left(q\right)\frac{p_\zeta}{M_\zeta} \ , \tag{4.19b}$$

$$\dot{s} = \frac{p_s}{M_s} \ , \tag{4.19c}$$

$$\dot{p} = -\frac{\partial U\left(q\right)}{\partial q} \ , \tag{4.19d}$$

$$\dot{p}_\zeta = F_\zeta\left(q\right) - p_\zeta\frac{p_s}{M_s} \ , \tag{4.19e}$$

$$\dot{p}_s = \frac{p_\zeta^2}{M_\zeta} - k_{\mathrm{B}}T \ , \tag{4.19f}$$

where the functions $G\left(q\right)$ and $F_\zeta\left(q\right)$ are defined as in Eqs. (4.14)

$$G\left(q\right) = \frac{\partial^2 U\left(q\right)}{\partial q^2} \ , \tag{4.20a}$$

$$F_\zeta\left(q\right) = \left(\frac{\partial U\left(q\right)}{\partial q}\right)^2 - k_{\mathrm{B}}T\left(\frac{\partial^2 U\left(q\right)}{\partial q^2}\right) \ . \tag{4.20b}$$

Defining the extended phase space point as $\tilde{\mathbf{x}} = (q, \zeta, s, p, p_\zeta, p_s)$, the equations of motion are expressed in matrix form as

$$\dot{\tilde{x}}_i = \sum_j \mathcal{B}_{ij}^{\mathrm{CKTNH}}\frac{\partial \mathcal{H}^{\zeta s}}{\partial \tilde{x}_j} \ , \tag{4.21}$$

where the antisymmetric matrix $\mathcal{B}^{CKTNH}$ is given by

$$\mathcal{B}^{\mathrm{CKTNH}} = \begin{bmatrix} 0 & 0 & 0 & 1 & -\left(\frac{\partial U(q)}{\partial q}\right) & 0 \\ 0 & 0 & 0 & 0 & G\left(q\right) & 0 \\ 0 & 0 & 0 & 0 & 0 & 1 \\ -1 & 0 & 0 & 0 & 0 & 0 \\ \left(\frac{\partial U(q)}{\partial q}\right)^{T} & -G\left(q\right) & 0 & 0 & 0 & -p_{\zeta} \\ 0 & 0 & -1 & 0 & p_{\zeta} & 0 \end{bmatrix} . \tag{4.22}$$

Under the assumption of ergodicity the hybrid CKTNH chain thermostat, described by Eqs. (4.18) and (4.19), causes the dynamics of the physical system to canonically sample phase space, even in the case of stiff systems. Using the definition, Eq. (3.15), provided in Chap. 3, we find that the phase space compressibility for this extended system is given by

$$\kappa^{\mathrm{CKTNH}} = \sum_{j,k} \frac{\partial \mathcal{B}_{jk}^{\mathrm{CTNH}}}{\partial \tilde{x}_j} \frac{\partial \mathcal{H}^{\zeta s}}{\partial \tilde{x}_k} = -G\left(q\right) \frac{p_{\zeta}}{M_{\zeta}} - \frac{p_s}{M_s} = -\left(\dot{\zeta} + \dot{s}\right) . \tag{4.23}$$

Integration schemes for both the CTNH thermostat and the hybrid CKTNH chain thermostat are discussed in Chap. 5.

Chapter 5

Algorithms of Integration

The phase space equations of motion of the two thermostats were integrated using symplectic position and velocity Verlet algorithms. For comparison purposes, we also present a time-reversible integration scheme, based on the symmetric Trotter expansion of the Liouville propagator.

The symplectic integrators preserve the volume of the phase space of the system being investigated. Symplectic integrators are therefore more stable than the proposed reversible integrator, as more constraints are imposed upon the system by the symplectic integrators than by the reversible integrator.

Although the symplectic integrators are the more stable option, they have with them their own drawbacks (as will be shown in Sec. 5.1), namely that integrating some of the associated equations of motion requires iteration. It is for these drawbacks that we propose the integration scheme based upon the symmetric Trotter decomposition of the Liouville propagator. The reversible integration scheme also has its drawbacks (shown in Sec. 5.2) which are overcome through the use of a position-dependent, harmonic approximation (PDHA) scheme. This PDHA scheme is outlined in Sec 5.2.1.

5.1 Symplectic

If one considers the equations of motion in the following form

$$\dot{q} = H_p(q,p) \ , \tag{5.1a}$$

$$\dot{p} = -H_q(q,p) \ , \tag{5.1b}$$

where $H_p = \partial H/\partial p, H_q = \partial H/\partial q$, whilst H denotes the Hamiltonian of the system of interest, and (q, p) can be interpreted as multidimensional coordinates. The symplectic formulation of the velocity Verlet algorithm is given by

$$p\big(t+\tau/2\big) = p(t) - \frac{\tau}{2} H_q\big(q(t), p(t+\tau/2)\big) \ , \tag{5.2a}$$

$$q\big(t+\tau\big) = q(t) + \frac{\tau}{2}\Big[H_p\big(q(t), p(t+\tau/2)\big) + H_p\big(q(t+\tau), p(t+\tau/2)\big)\Big] \ , \tag{5.2b}$$

$$p\big(t+\tau\big) = p(t+\tau/2) - \frac{\tau}{2} H_q\big(q(t+\tau), p(t+\tau/2)\big) \ , \tag{5.2c}$$

while the symplectic formulation of the position Verlet algorithm is given by

$$q\big(t+\tau/2\big) = q(t) + \frac{\tau}{2} H_p\big(q(t+\tau/2), p(t)\big) \ , \tag{5.3a}$$

$$p\big(t+\tau\big) = p(t) - \frac{\tau}{2}\Big[H_q\big(q(t+\tau/2), p(t)\big) + H_q\big(q(t+\tau/2), p(t+\tau)\big)\Big] \ , \tag{5.3b}$$

$$q\big(t+\tau\big) = q(t+\tau/2) + \frac{\tau}{2} H_p\big(q(t+\tau/2), p(t+\tau)\big) \ . \tag{5.3c}$$

From equations (5.2a) and (5.2b) one can see that for the symplectic velocity Verlet algorithm, the momentum at time $t + \tau/2$ and the position at time $t + \tau$ are both dependent upon themselves. The same occurs in the symplectic position Verlet algorithm regarding the position and momentum respectively (refer to equations (5.3a) and (5.3b)).

This problem of self-dependence was overcome by making two assumptions. The first assumption which we made was that for a given coordinate, or momentum, value at a given time t, the next value (at time $t + \tau$ or at time $t + \tau/2$) would be within the region of the given value (at time t). The motivation behind this assumption was that a small time-step was used for the integration and hence the propagation of the dynamics would not contain large fluctuations between consecutive points. The second assumption made was that over several iterations, the variables in equations (5.2a), (5.2b), (5.3a) and (5.3b) will tend to their true values. The motivation behind this assumption is that it is reasonable to assume that the value of the variable at the next time step will be close to its value at the current time. Therefore by using an iterative procedure the value at the next time step changes on each iteration, whilst the value at the current time remains the same across all iterations.

This solution was coded such that both an iteration limit and a tolerance limit were accepted as input into the program. When calculating values that are self-dependent, the first iteration uses the value at time t in place of the self-dependent quantity to

estimate the value at the next time step. Each consecutive iteration uses the estimated value from the previous iteration in place of the self-dependent quantity, in order to calculate an improved, estimated value. This iteration process is repeated until either the number of iterations reaches the iteration limit, or the difference between consecutive iteration values is less than or equal to the tolerance. Once either condition is reached, the last value calculated for the variable at the next time step is taken to be the numerically correct one.

5.1.1 Symplectic Integrator for the CTNH Thermostat

For the configurational temperature Nosè-Hoover (CTNH) thermostat, in a phase space description, the equations of motion are as follows

$$\dot{q} = \frac{p}{m} + \frac{p_\zeta}{M_\zeta} F(q) \,, \tag{5.4a}$$

$$\dot{\zeta} = \frac{p_\zeta}{M_\zeta} \frac{\partial^2 \mathcal{U}(q)}{\partial q^2} \,, \tag{5.4b}$$

$$\dot{p} = -\frac{\partial \mathcal{U}\,(q)}{\partial q} = F(q) \,, \tag{5.4c}$$

$$\dot{p}_\zeta = \left(\frac{\partial \mathcal{U}(q)}{\partial q} \right)^2 - k_B T \frac{\partial^2 \mathcal{U}(q)}{\partial q^2} \,. \tag{5.4d}$$

Hence, the symplectic velocity Verlet algorithm, for the phase space CTNH thermostat, is as follows

$$p(t + \tau/2) = p(t) + \frac{\tau}{2} F\big(q(t)\big) \,, \tag{5.5a}$$

$$p_\zeta(t + \tau/2) = p_\zeta(t) + \frac{\tau}{2} F_\zeta\big(q(t)\big) \,, \tag{5.5b}$$

$$q(t + \tau) = q(t) + \tau \frac{p(t + \tau/2)}{m} + \frac{\tau}{2} \frac{p_\zeta(t + \tau/2)}{M_\zeta} \Big[F\big(q(t)\big) + F\big(q(t + \tau)\big) \Big] \,, \tag{5.5c}$$

$$\zeta(t + \tau) = \zeta(t) + \frac{\tau}{2} \frac{p_\zeta(t + \tau/2)}{M_\zeta} \Big[G\big(q(t)\big) + G\big(q(t + \tau)\big) \Big] \,, \tag{5.5d}$$

$$p(t + \tau) = p(t + \tau/2) + \frac{\tau}{2} F\big(q(t + \tau)\big) \,, \tag{5.5e}$$

$$p_\zeta(t + \tau) = p_\zeta(t + \tau/2) + \frac{\tau}{2} F_\zeta\big(q(t + \tau)\big) \,, \tag{5.5f}$$

and the symplectic position Verlet algorithm reads

$$q(t+\tau/2) = q(t) + \frac{\tau}{2}\frac{p(t)}{m} + \frac{\tau}{2}\frac{p_\zeta(t)}{M_\zeta}F\big(q(t+\tau/2)\big) \,, \tag{5.6a}$$

$$\zeta(t+\tau/2) = \zeta(t) + \frac{\tau}{2}\frac{p_\zeta(t)}{M_\zeta}G\big(q(t+\tau/2)\big) \,, \tag{5.6b}$$

$$p(t+\tau) = p(t) + \tau F\big(q(t+\tau/2)\big) \,, \tag{5.6c}$$

$$p_\zeta(t+\tau) = p_\zeta(t) + \tau F_\zeta\big(q(t+\tau/2)\big) \,, \tag{5.6d}$$

$$q(t+\tau) = q(t+\tau/2) + \frac{\tau}{2}\frac{p(t+\tau)}{m} + \frac{\tau}{2}\frac{p_\zeta(t+\tau)}{M_\zeta}F\big(q(t+\tau/2)\big) \,, \tag{5.6e}$$

$$\zeta(t+\tau) = \zeta(t+\tau/2) + \frac{\tau}{2}\frac{p_\zeta(t+\tau)}{M_\zeta}G\big(q(t+\tau/2)\big) \,, \tag{5.6f}$$

where Eqs. (5.5c) and (5.6a) need to be iterated.

5.1.2 Symplectic Integrator for the CKTNH Hybrid Thermostat

Following the same reasoning as for the CTNH thermostat, one obtains for the hybrid configurational-kinetic temperature Nosè-Hoover (CKTNH) thermostat

$$p(t+\tau/2) = p(t) + \frac{\tau}{2}F(q(t)) \,, \tag{5.7a}$$

$$p_\zeta(t+\tau/2) = p_\zeta(t) - \frac{\tau}{2}\frac{p_s(t+\tau/2)}{M_s}p_\zeta(t+\tau/2) + \frac{\tau}{2}F_\zeta(q(t)) \,, \tag{5.7b}$$

$$p_s(t+\tau/2) = p_s(t) + \frac{\tau}{2}\frac{p_\zeta^2(t+\tau/2)}{M_\zeta} - \frac{\tau}{2}k_\mathrm{B}T \,, \tag{5.7c}$$

$$q(t+\tau) = q(t) + \tau\frac{p(t+\tau/2)}{m} + \frac{\tau}{2}\frac{p_\zeta(t+\tau/2)}{M_\zeta}\left[F(q(t)) + F(q(t+\tau))\right] \,, \tag{5.7d}$$

$$\zeta(t+\tau) = \zeta(t) + \frac{\tau}{2}\frac{p_\zeta(t+\tau/2)}{M_\zeta}\left[G(q(t)) + G(q(t+\tau))\right] \,, \tag{5.7e}$$

$$s(t+\tau) = s(t) + \tau\frac{p_s(t+\tau/2)}{M_s} \,, \tag{5.7f}$$

$$p(t+\tau) = p(t+\tau/2) + \frac{\tau}{2}F(q(t+\tau)) \,, \tag{5.7g}$$

$$p_\zeta(t+\tau) = p_\zeta(t+\tau/2) - \frac{\tau}{2}\frac{p_s(t+\tau/2)}{M_s}p_\zeta(t+\tau/2) + \frac{\tau}{2}F_\zeta(q(t+\tau)) \,, \tag{5.7h}$$

$$p_s(t+\tau) = p_s(t+\tau/2) + \frac{\tau}{2}\frac{p_\zeta^2(t+\tau/2)}{M_\zeta} - \frac{\tau}{2}k_\mathrm{B}T \,, \tag{5.7i}$$

where Eqs. (5.7b)-(5.7d) must be iterated.

The symplectic position Verlet algorithm for the hybrid CKTNH chain thermostat

reads

$$q(t+\tau/2) = q(t) + \frac{\tau}{2}\frac{p(t)}{m} + \frac{\tau}{2}\frac{p_\zeta(t)}{M_\zeta}F(q(t+\tau/2)) \,, \tag{5.8a}$$

$$\zeta(t+\tau/2) = \zeta(t) + \frac{\tau}{2}\frac{p_\zeta(t)}{M_\zeta}G(q(t+\tau/2)) \,, \tag{5.8b}$$

$$s(t+\tau/2) = s(t) + \frac{\tau}{2}\frac{p_s(t)}{M_s} \,, \tag{5.8c}$$

$$p(t+\tau) = p(t) + \tau F(q(t+\tau/2)) \,, \tag{5.8d}$$

$$p_\zeta(t+\tau) = p_\zeta(t) + \tau F_\zeta(q(t+\tau/2)) - \frac{\tau}{2M_s}\left[p_s(t)p_\zeta(t) + p_s(t+\tau)p_\zeta(t+\tau)\right] \,, \tag{5.8e}$$

$$p_s(t+\tau) = p_s(t) + \frac{\tau}{2M_\zeta}\left[p_\zeta^2(t) + p_\zeta^2(t+\tau)\right] - \tau k_\mathrm{B}T \,, \tag{5.8f}$$

$$q(t+\tau) = q(t+\tau/2) + \frac{\tau}{2}\frac{p(t+\tau)}{m} + \frac{\tau}{2}\frac{p_\zeta(t+\tau)}{M_\zeta}F(q(t+\tau/2)) \,, \tag{5.8g}$$

$$\zeta(t+\tau) = \zeta(t+\tau/2) + \frac{\tau}{2}\frac{p_\zeta(t+\tau)}{M_\zeta}G(q(t+\tau/2)) \,, \tag{5.8h}$$

$$s(t+\tau) = s(t+\tau/2) + \frac{\tau}{2}\frac{p_s(t+\tau)}{M_s} \,, \tag{5.8i}$$

where Eq. (5.8a) and Eqs. (5.8e)-(5.8f) must be iterated.

5.2 Time-Reversible

The time reversible integration scheme was obtained by following the methodology in [34]. Consider the equations of motion for the CTNH thermostat

$$\dot{q} = \frac{p}{m} + F(q)\frac{p_\zeta}{M_\zeta} \,, \tag{5.9a}$$

$$\dot{\zeta} = G(q)\frac{p_\zeta}{M_\zeta} \,, \tag{5.9b}$$

$$\dot{p} = -\frac{\partial U}{\partial q} \,, \tag{5.9c}$$

$$\dot{p}_\zeta = F_\zeta(q) \,, \tag{5.9d}$$

where $F(q)$ is the force acting on the system coordinates q and

$$G(q) = \frac{\partial^2 \mathcal{U}}{\partial q^2} \,, \tag{5.10a}$$

$$F_\zeta(q) = \left(\frac{\partial \mathcal{U}}{\partial q}\right)^2 - k_\mathrm{B}T\frac{\partial^2 \mathcal{U}}{\partial q^2} \,. \tag{5.10b}$$

One can define the following Liouville operators

$$L_1^{\mathrm{CTNH}} = \left(\frac{p}{m} + F(q)\frac{p_\zeta}{M_\zeta}\right)\frac{\partial}{\partial q}\,, \tag{5.11a}$$

$$L_2^{\mathrm{CTNH}} = F(q)\frac{\partial}{\partial p}\,, \tag{5.11b}$$

$$L_3^{\mathrm{CTNH}} = G(q)\frac{p_\zeta}{M_\zeta}\frac{\partial}{\partial \zeta}\,, \tag{5.11c}$$

$$L_4^{\mathrm{CTNH}} = F_\zeta(q)\frac{\partial}{\partial p_\zeta}\,. \tag{5.11d}$$

The total Liouville operator is therefore given by $L^{\mathrm{CTNH}} = \sum_{i=1}^{4} L_i^{\mathrm{CTNH}}$. We introduce the propagators associated to each of the Liouville operators in Eqs. (5.11)

$$U_\alpha^{\mathrm{CTNH}}(\tau) = \exp\left(\tau L_\alpha^{\mathrm{CTNH}}\right)\,, \qquad \alpha = 1,\ldots,4\,, \tag{5.12}$$

where τ denotes the time step. The total propagator for the system is therefore given by

$$\begin{aligned}
U^{\mathrm{CTNH}}(\tau) &= \exp\left(\tau\left[L_1^{\mathrm{CTNH}} + L_2^{\mathrm{CTNH}} + L_3^{\mathrm{CTNH}} + L_4^{\mathrm{CTNH}}\right]\right) \\
&\simeq \exp\left(\frac{\tau}{4}L_4^{\mathrm{CTNH}}\right)\exp\left(\frac{\tau}{2}L_3^{\mathrm{CTNH}}\right)\exp\left(\frac{\tau}{4}L_4^{\mathrm{CTNH}}\right) \\
&\quad\times \exp\left(\frac{\tau}{2}L_2^{\mathrm{CTNH}}\right)\exp\left(\tau L_1^{\mathrm{CTNH}}\right)\exp\left(\frac{\tau}{2}L_2^{\mathrm{CTNH}}\right) \\
&\quad\times \exp\left(\frac{\tau}{4}L_4^{\mathrm{CTNH}}\right)\exp\left(\frac{\tau}{2}L_3^{\mathrm{CTNH}}\right)\exp\left(\frac{\tau}{4}L_4^{\mathrm{CTNH}}\right) \\
&= U_4^{\mathrm{CTNH}}\left(\frac{\tau}{4}\right)U_3^{\mathrm{CTNH}}\left(\frac{\tau}{2}\right)U_4^{\mathrm{CTNH}}\left(\frac{\tau}{4}\right)U_2^{\mathrm{CTNH}}\left(\frac{\tau}{2}\right)U_1^{\mathrm{CTNH}}(\tau) \\
&\quad\times U_2^{\mathrm{CTNH}}\left(\frac{\tau}{2}\right)U_4^{\mathrm{CTNH}}\left(\frac{\tau}{4}\right)U_3^{\mathrm{CTNH}}\left(\frac{\tau}{2}\right)U_4^{\mathrm{CTNH}}\left(\frac{\tau}{4}\right)\,,
\end{aligned} \tag{5.13}$$

where a symmetric Trotter factorisation has been used twice, successively. One can calculate the action of the propagators U_α^{CTNH} for $\alpha = 2,3,4$ by considering the identity $\exp\left(c\frac{\partial}{\partial x}\right)f(x) \equiv f(x+c)$ where c is an arbitrary constant and $f(x)$ an arbitrary function. Thus the action of the propagators is

$$p \to p + \tau F(q)\Big\} : U_2^{\mathrm{CTNH}}(\tau)\,, \tag{5.14a}$$

$$\zeta \to \zeta + \tau G(q)\frac{p_\zeta}{M_\zeta}\Bigg\} : U_3^{\mathrm{CTNH}}(\tau)\,, \tag{5.14b}$$

$$p_\zeta \to p_\zeta + \tau F_\zeta(q)\Big\} : U_4^{\mathrm{CTNH}}(\tau)\,. \tag{5.14c}$$

However, one cannot determine the action of the propagator $U_1^{\mathrm{CTNH}}(\tau)$ for a general potential $U(q)$.

For the case of quadratic potentials $\mathcal{U}(q) = (1/2)kq^2$ (i.e.: the force $F(q)$ is linear in q), one can substitute the Liouville operator L_1^{CTNH} with another operator $L_{1,h}^{\mathrm{CTNH}}$, given by

$$L_{1,h}^{\mathrm{CTNH}} = \left(\frac{p}{m} - kq\frac{p_\zeta}{M_\zeta}\right)\frac{\partial}{\partial q} \,. \tag{5.15}$$

The action of the associated propagator, $U_{1,h}^{\mathrm{CTNH}}(\tau)$, can be analytically determined by solving the differential equation $\dot{q} = L_{1,h}^{\mathrm{CTNH}} q$. This is demonstrated in App. A, with the result found to be

$$q \to q\exp\left(-\tau k\frac{p_\zeta}{M_\zeta}\right) + \tau\frac{p}{m}\exp\left(-\tau\frac{k}{2}\frac{p_\zeta}{M_\zeta}\right)\left[\frac{\sinh\left(\tau\frac{k}{2}\frac{p_\zeta}{M_\zeta}\right)}{\tau\frac{k}{2}\frac{p_\zeta}{M_\zeta}}\right] \Bigg\} : U_{1,\mathrm{h}}^{\mathrm{CTNH}}(\tau) \,. \tag{5.16}$$

It is difficult to use the propagator U^{CTNH} as defined in Eq. (5.13) as one does not generally know the action of the propagator U_1^{CTNH}. However, assuming a continuous and sufficiently smooth potential, it is possible for one to use a linear approximation in place of the force. Such an approximation is discussed in Sec. 5.2.1.

For the case of the hybrid CKTNH chain thermostat, the equations of motion are given by Eqs. 4.19

$$\dot{q} = \frac{p}{m} - \frac{p_\zeta}{M_\zeta}\frac{\partial U(q)}{\partial q} \,, \tag{5.17a}$$

$$\dot{\zeta} = G(q)\frac{p_\zeta}{M_\zeta} \,, \tag{5.17b}$$

$$\dot{s} = \frac{p_s}{M_s} \,, \tag{5.17c}$$

$$\dot{p} = -\frac{\partial U(q)}{\partial q} \,, \tag{5.17d}$$

$$\dot{p}_\zeta = F_\zeta(q) - p_\zeta\frac{p_s}{M_s} \,, \tag{5.17e}$$

$$\dot{p}_s = \frac{p_\zeta^2}{M_\zeta} - k_{\mathrm{B}}T \,. \tag{5.17f}$$

Following the same procedure as for the CTNH thermostat, we define the following

Liouville operators

$$L_1^{\mathrm{CKTNH}} = \left(\frac{p}{m} + F(q)\frac{p_\zeta}{M_\zeta}\right)\frac{\partial}{\partial q} = L_1^{\mathrm{CTNH}}\,, \tag{5.18a}$$

$$L_2^{\mathrm{CKTNH}} = F(q)\frac{\partial}{\partial p} = L_2^{\mathrm{CTNH}}\,, \tag{5.18b}$$

$$L_3^{\mathrm{CKTNH}} = G(q)\frac{p_\zeta}{M_\zeta}\frac{\partial}{\partial \zeta} = L_3^{\mathrm{CTNH}}\,, \tag{5.18c}$$

$$L_4^{\mathrm{CKTNH}} = \frac{p_s}{M_s}\frac{\partial}{\partial s}\,, \tag{5.18d}$$

$$L_5^{\mathrm{CKTNH}} = F_\zeta(q)\frac{\partial}{\partial p_\zeta} = L_4^{\mathrm{CTNH}}\,, \tag{5.18e}$$

$$L_6^{\mathrm{CKTNH}} = -p_\zeta\frac{p_s}{M_s}\frac{\partial}{\partial p_\zeta}\,, \tag{5.18f}$$

$$L_7^{\mathrm{CKTNH}} = \left(\frac{p_\zeta^2}{M_\zeta} - k_{\mathrm{B}}T\right)\frac{\partial}{\partial p_s}\,, \tag{5.18g}$$

with the total Liouville operator being given by $L^{\mathrm{CKTNH}} = \sum_{i=1}^{7} L_i^{\mathrm{CKTNH}}$. Utilising the same methodology as before, we find that the associated propagators are given by

$$\begin{aligned} U_1^{\mathrm{CKTNH}}(\tau) &= \exp\left[\tau\left(\frac{p}{m} + F(q)\frac{p_\zeta}{M_\zeta}\right)\frac{\partial}{\partial q}\right] \\ &= U_1^{\mathrm{CTNH}}(\tau)\,, \end{aligned} \tag{5.19a}$$

$$\begin{aligned} U_2^{\mathrm{CKTNH}}(\tau) &= \exp\left[\tau F(q)\frac{\partial}{\partial p}\right] \\ &= U_2^{\mathrm{CTNH}}(\tau)\,, \end{aligned} \tag{5.19b}$$

$$U_3^{\mathrm{CKTNH}}(\tau) = \exp\left[\tau\left(G(q)\frac{p_\zeta}{M_\zeta}\frac{\partial}{\partial \zeta} + \frac{p_s}{M_s}\frac{\partial}{\partial s}\right)\right]\,, \tag{5.19c}$$

$$\begin{aligned} U_4^{\mathrm{CKTNH}}(\tau) &= \exp\left[\tau F_\zeta(q)\frac{\partial}{\partial p_\zeta}\right] \\ &= U_4^{\mathrm{CTNH}}(\tau)\,, \end{aligned} \tag{5.19d}$$

$$U_5^{\mathrm{CKTNH}}(\tau) = \exp\left[-\tau p_\zeta\frac{p_s}{M_s}\frac{\partial}{\partial p_\zeta}\right]\,, \tag{5.19e}$$

$$U_6^{\mathrm{CKTNH}}(\tau) = \exp\left[\tau\left(\frac{p_\zeta^2}{M_\zeta} - k_{\mathrm{B}}T\right)\frac{\partial}{\partial p_s}\right]\,. \tag{5.19f}$$

Hence the total propagator can be approximated as

$$\begin{aligned} U^{\mathrm{CKTNH}}(\tau) = &\left[\prod_{\alpha=1}^{3} U_{7-\alpha}^{\mathrm{CKTNH}}\left(\frac{\tau}{4}\right)\right] U_3^{\mathrm{CKTNH}}\left(\frac{\tau}{2}\right)\left[\prod_{\alpha=1}^{3} U_{7-\alpha}^{\mathrm{CKTNH}}\left(\frac{\tau}{4}\right)\right] \\ &\times U_2^{\mathrm{CKTNH}}\left(\frac{\tau}{2}\right) U_1^{\mathrm{CKTNH}}(\tau)\, U_2^{\mathrm{CKTNH}}\left(\frac{\tau}{2}\right) \\ &\times \left[\prod_{\alpha=1}^{3} U_{7-\alpha}^{\mathrm{CKTNH}}\left(\frac{\tau}{4}\right)\right] U_3^{\mathrm{CKTNH}}\left(\frac{\tau}{2}\right)\left[\prod_{\alpha=1}^{3} U_{7-\alpha}^{\mathrm{CKTNH}}\left(\frac{\tau}{4}\right)\right]\,, \end{aligned} \tag{5.20}$$

where a symmetric Trotter factorisation has been used as before.

5.2.1 Position-Dependent Harmonically Approximated

In order to obtain a time-reversible integration algorithm for systems where the force is non-linear in q, one can use a Taylor series expansion, arrested to second order, of the potential. The Taylor series expansion is taken about the coordinate q at time t and an approximate expression for the force is calculated. This expression is substituted in place of the true force in Eq. (5.9a) and a new propagator is obtained, the action of which is determined in the same manner as before. The result is

$$q \to q\exp\left(-\tau B\right) + \tau A \exp\left(-\frac{\tau B}{2}\right)\left[\frac{\sinh\left(\frac{\tau B}{2}\right)}{\frac{\tau B}{2}}\right]\Bigg\} : \tilde{U}_{1,\mathrm{h}}^{\mathrm{CTNH}}(\tau)\ , \tag{5.21}$$

where

$$\begin{aligned} A &= \frac{p}{m} + \frac{p_\zeta}{M_\zeta}\left[F\left(q_t\right) + q_t G\left(q_t\right)\right]\ , \\ B &= \frac{p_\zeta}{M_\zeta} G\left(q_t\right)\ , \end{aligned}$$

and q_t is the coordinate q, at time t, about which the Taylor series expansion was taken. A detailed derivation of Eq. (5.21) is provided in App. B.

At each time step the value which was used for q_t was the coordinate value at that time. This is equivalent to expanding about a different point at each time step, and has the effect of locally approximating the potential function to an harmonic potential. The motivation behind this choice is to minimise the error incurred from using an approximated potential function, as opposed to the true potential function.

5.2.2 Higher Order Integrators

In order to improve the numerical accuracy of the integration algorithms proposed in Secs. 5.2 and 5.2.1, one can introduce additional schemes to be used in conjunction with the proposed algorithm. Two such techniques are the Yoshida higher order integration scheme [35, 36] and a multiple time step procedure [34, 37]. With the implementation of these two schemes, the propagator for the CTNH thermostat extended system can

be expressed as

$$U^{\mathrm{CTNH}}(\tau) = \left[\prod_{n=1}^{n_{\mathrm{yosh}}}\prod_{m=1}^{m_{\mathrm{step}}}\left(U_4^{\mathrm{CTNH}}\left(\frac{w_n}{m_{\mathrm{step}}}\frac{\tau}{4}\right)U_3^{\mathrm{CTNH}}\left(\frac{w_n}{m_{\mathrm{step}}}\frac{\tau}{2}\right)U_4^{\mathrm{CTNH}}\left(\frac{w_n}{m_{\mathrm{step}}}\frac{\tau}{4}\right)\right)\right] \times U_2^{\mathrm{CTNH}}\left(\frac{\tau}{2}\right)U_1^{\mathrm{CTNH}}(\tau)\,U_2^{\mathrm{CTNH}}\left(\frac{\tau}{2}\right) \times \left[\prod_{n=1}^{n_{\mathrm{yosh}}}\prod_{m=1}^{m_{\mathrm{step}}}\left(U_4^{\mathrm{CTNH}}\left(\frac{w_n}{m_{\mathrm{step}}}\frac{\tau}{4}\right)U_3^{\mathrm{CTNH}}\left(\frac{w_n}{m_{\mathrm{step}}}\frac{\tau}{2}\right)U_4^{\mathrm{CTNH}}\left(\frac{w_n}{m_{\mathrm{step}}}\frac{\tau}{4}\right)\right)\right], \tag{5.22}$$

where n_{yosh} is the number of Yoshida integration steps and m_{step} is the number of iterations in the multiple time step procedure. The Yoshida weights, w_n, are defined [35, 36] as

$$\left.\begin{aligned} w_1 = w_3 &= \tfrac{1}{\left(2-2^{1/3}\right)} \\ w_2 &= 1-2w_1 \end{aligned}\right\} : n_{\mathrm{yosh}} = 3\,, \tag{5.23a}$$

$$\left.\begin{aligned} w_1 = w_2 = w_4 = w_5 &= \tfrac{1}{\left(4-4^{1/3}\right)} \\ w_3 &= 1-4w_1 \end{aligned}\right\} : n_{\mathrm{yosh}} = 5\,. \tag{5.23b}$$

Using the same notation as before, the system propagator for the hybrid CKTNH thermostat can be expressed as

$$U^{\mathrm{CKTNH}}(\tau) = \left[\prod_{n=1}^{n_{\mathrm{yosh}}}\prod_{m=1}^{m_{\mathrm{step}}}\left(\prod_{\alpha=1}^{3}U_{7-\alpha}^{\mathrm{CKTNH}}\left(\frac{w_n}{m_{\mathrm{step}}}\frac{\tau}{4}\right)\right) \times U_3^{\mathrm{CKTNH}}\left(\frac{w_n}{m_{\mathrm{step}}}\frac{\tau}{2}\right)\left(\prod_{\alpha=1}^{3}U_{3+\alpha}^{\mathrm{CKTNH}}\left(\frac{w_n}{m_{\mathrm{step}}}\frac{\tau}{4}\right)\right)\right] \times U_2^{\mathrm{CKTNH}}\left(\frac{\tau}{2}\right)U_1^{\mathrm{CKTNH}}(\tau)\,U_2^{\mathrm{CKTNH}}\left(\frac{\tau}{2}\right) \times \left[\prod_{n=1}^{n_{\mathrm{yosh}}}\prod_{m=1}^{m_{\mathrm{step}}}\left(\prod_{\alpha=1}^{3}U_{7-\alpha}^{\mathrm{CKTNH}}\left(\frac{w_n}{m_{\mathrm{step}}}\frac{\tau}{4}\right)\right) \times U_3^{\mathrm{CKTNH}}\left(\frac{w_n}{m_{\mathrm{step}}}\frac{\tau}{2}\right)\left(\prod_{\alpha=1}^{3}U_{3+\alpha}^{\mathrm{CKTNH}}\left(\frac{w_n}{m_{\mathrm{step}}}\frac{\tau}{4}\right)\right)\right]. \tag{5.24}$$

For both the CTNH thermostat and the hybrid CKTNH chain thermostat, the techniques implemented above, for the purpose of improving numerical accuracy, are applied only to the propagators which act on the thermostat variables, not those which act on the physical system.

Chapter 6

Models and Results

The configurational temperature Nosè-Hoover (CTNH) and the hybrid configurational-kinetic temperature Nosè-Hoover (CKTNH) chain thermostats were tested on both the harmonic oscillator (single well potential) and the quartic oscillator (double well potential) systems. For each system, a single particle, in one dimension, was simulated. For each extended system that was considered, three runs were performed, each one implementing a different one of the integration algorithms (symplectic position Verlet (SPV), symplectic velocity Verlet (SVV) and symmetric Trotter propagator (STP)) discussed in Chap. 5. For convenience, the particle mass, m, and heat bath temperature, T, were set to unit values for all simulations. In other words

$$m = 1 \,, \tag{6.1a}$$

$$k_{\mathrm{B}} T = 1 \,. \tag{6.1b}$$

For a single, one-dimensional, harmonic oscillator, the potential energy function is given by

$$\mathcal{U}^{\mathrm{HO}}(q) = \frac{1}{2} k q^2 \,, \tag{6.2}$$

where q is the generalised particle coordinate and k is the spring constant. In the case of a single quartic oscillator, in one dimension, the potential energy function is given by

$$\mathcal{U}^{\mathrm{DW}}(q) = \frac{a}{4} q^4 + \frac{b}{2} q^2 \,, \tag{6.3}$$

where q is the generalised particle coordinate and the parameters a and b determine the width and depth, respectively, of the potential wells. The results presented in this

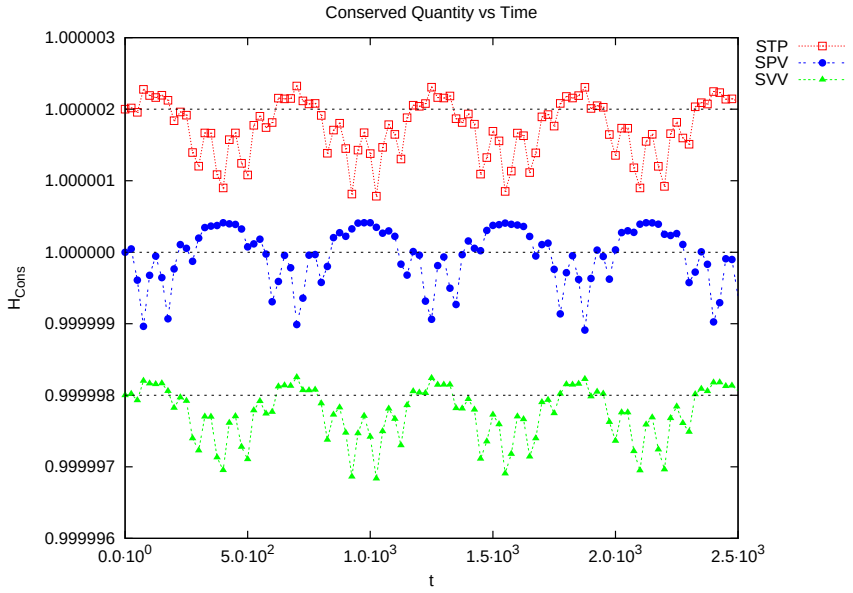

Figure 6.1a: Conserved quantity, $\mathcal{H}^{\zeta}$, versus time for an harmonic oscillator attached to a configurational temperature Nosè-Hoover (CTNH) thermostat, for each of the integration schemes discussed previously (symplectic position Verlet (SPV), symplectic velocity Verlet (SVV) and the symmetric Trotter propagator (STP) scheme). The results shown are each normalised to an initial value of one, with those for the STP algorithm being incremented by a constant factor of $2 \cdot 10^{-6}$, and those for the SVV algorithm being decremented by the same amount. The figure shows the numerical conservation of $\mathcal{H}^{\zeta}$, for each of the integration schemes implemented. The simulation results were obtained using a thermostat mass of $M_{\zeta} = 10$ and a time step of $\tau = 2.5 \cdot 10^{-3}$.

chapter were obtained using a spring constant value of $k = 1.0$, for the case of the quadratic potential, and parameter values of $a = 1.0$ and $b = -1.0$, for the quartic potential function. A table of the relevant parameter values used for each simulation is provided in App. C.

Figure 6.1a shows the numerical conservation of the conserved quantity, $\mathcal{H}^{\zeta}$, for an harmonic oscillator attached to a CTNH thermostat, for each of the integration algorithms discussed in Chap. 5. One can see that $\mathcal{H}^{\zeta}$ is conserved for each of the integration schemes implemented, as the fluctuations are of the order of 10^{-6}, which lies within acceptable numerical error. By using the intrinsic `stats` function of `gnuplot`, it was determined the average value of the extended Hamiltonian, using the symplectic

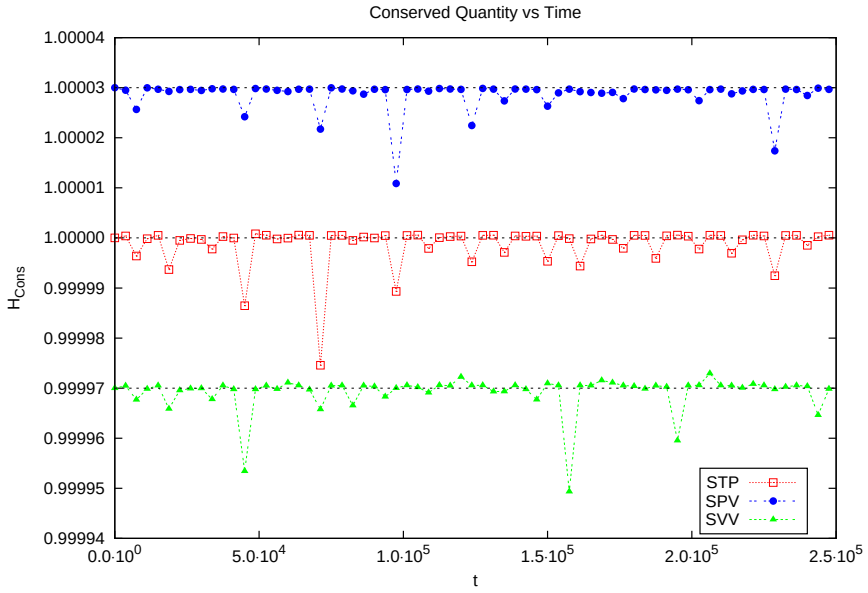

Figure 6.1b: Conserved quantity, $\mathcal{H}^{\zeta}$, versus time for a double well system attached to a configurational (CTNH) thermostat, showing numerical conservation of $\mathcal{H}^{\zeta}$ when using the symplectic position (SPV) and velocity (SVV) Verlet integration algorithms as well as for the symmetric Trotter propagator (STP) integration scheme. The results obtained using the symplectic integrators have been shifted by a constant factor of $3 \cdot 10^{-5}$. The simulations were conducted using a thermostat mass of $M_{\zeta} = 9.6 \cdot 10^{5}$ and a time step of $\tau = 2.5 \cdot 10^{-3}$ for each of the integration schemes.

integrators (SPV and SVV) was $0.9999999 \pm 3.8 \cdot 10^{-7}$ and $0.9999997 \pm 3.7 \cdot 10^{-7}$ respectively, where the error was taken to be the standard deviation. When implementing the STP integration scheme, the average value for the conserved quantity was found to be $0.9999997 \pm 3.9 \cdot 10^{-7}$, where again the error was taken to be the standard deviation. These values are as expected, owing to the conserved quantity being normalised to an initial value of 1. From these results, together with the semi-periodic nature of the fluctuations in $\mathcal{H}^{\zeta}$, we can conclude that the extended Hamiltonian is conserved to within the limits of numerical precision, by all three proposed integration algorithms. Shown in Fig. 6.1b is the numerical conservation of $\mathcal{H}^{\zeta}$ for the case of a quartic oscillator system attached to a CTNH thermostat. The results for each of the three integration algorithms (SPV, SVV, and STP) previously discussed are reflected in the figure. The average value of $\mathcal{H}^{\zeta}$, for this extended system, was found to be $0.999998 \pm 5.0 \cdot 10^{-6}$ using the STP integration scheme and $0.999999 \pm 3.3 \cdot 10^{-6}$ $0.999999 \pm 3.1 \cdot 10^{-6}$ when

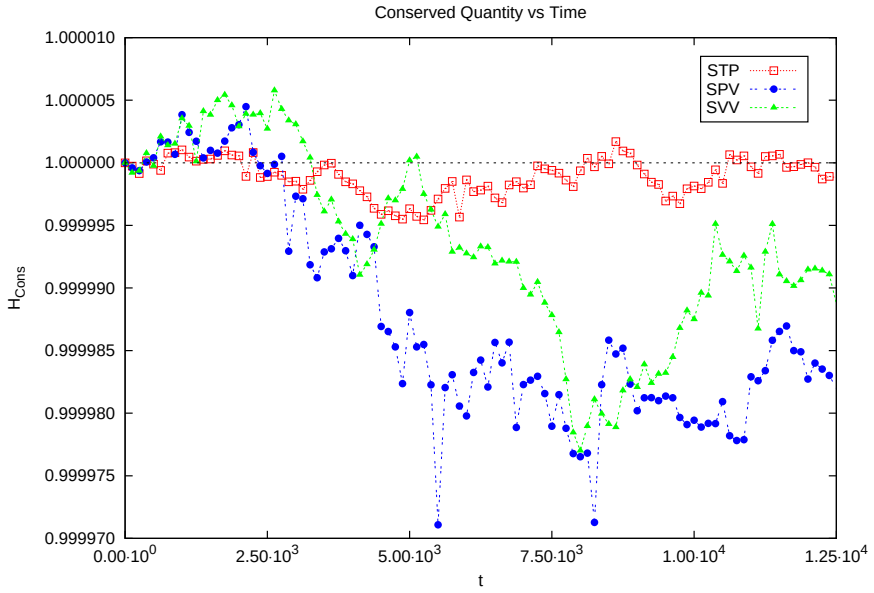

Figure 6.2a: Conserved quantity, $\mathcal{H}^{\zeta s}$, versus time for an harmonic oscillator attached to a hybrid configurational-kinetic temperature Nosè-Hoover (CKTNH) chain thermostat, showing the numerical conservation of the extended Hamiltonian ($\mathcal{H}^{\zeta s}$). The results were obtained using thermostat masses of $M_\zeta = 10$ and $M_s = 1$ and a time step of $\tau = 2.5 \cdot 10^{-3}$. Simulations were conducted using the symplectic position (SPV) and velocity (SVV) Verlet and the symmetric Trotter propagator (STP) integrators. The values shown in the figure have each been normalised to an initial value of one.

implementing the symplectic position and velocity Verlet integration algorithms respectively. These values were obtained by employing the `stats` function of `gnuplot`, where the standard deviations were taken to be the errors. With the exception of the occasional larger fluctuation, we can see that the fluctuations in the extended Hamiltonian are generally very small, for all the integration algorithms implemented. The lack of any overall drift in the values shows that, for this set of input parameters (as earlier mentioned, these are provided in App. C), the integration algorithms used are stable. This, together with the averages reported, lead one to conclude that the extended Hamiltonian, $\mathcal{H}^{\zeta}$, is conserved, to within the limits imposed by numerical precision, for each of the three integration schemes.

The numerical conservation of the extended Hamiltonian, $\mathcal{H}^{\zeta s}$, is shown in Figs. 6.2 for each of the three integration schemes (SPV, SVV and STP) and each of the systems used to investigate the hybrid CKTNH chain thermostat. As is shown in Fig. 6.2a, for

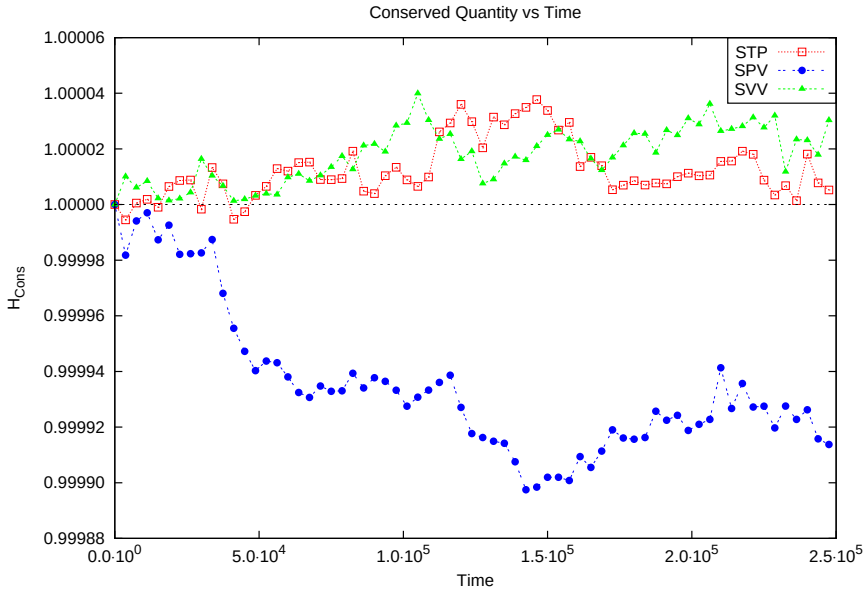

Figure 6.2b: Conserved quantity, $\mathcal{H}^{\zeta s}$, versus time for a quartic oscillator system attached to a hybrid configurational-kinetic temperature Nosè-Hoover (CKTNH) chain thermostat. The figure shows numerical conservation of $\mathcal{H}^{\zeta s}$ for each of the three integration schemes implemented (symplectic position Verlet (SPV), symplectic velocity Verlet (SVV) and symmetric Trotter propagator (STP)). Thermostat masses of $M_\zeta = 10^3$ and $M_s = 1$, and a time step of $\tau = 2.5 \cdot 10^{-3}$ were used.

the case of an harmonic oscillator attached to a hybrid CKTNH chain thermostat, the symplectic integrators quickly become unstable. This can be seen around the time $t = 2.50 \cdot 10^3$, where the values of the conserved quantity begin, on average, to drift toward zero, for both symplectic integrators (SPV and SVV). This reflects the occurrence of an instability in the integrator. The STP integration scheme on the other hand displays no such drift, and instead fluctuates around the initial value. These fluctuations are of the order of 10^{-6}, whilst the variations for the symplectic integrators are of the order of 10^{-5}. Through the use of `gnuplot`, it was determined that the average values of the extended Hamiltonian, for each of the integrators used, were found to be $0.999999 \pm 1.5 \cdot 10^{-6}$ for the STP scheme and $0.999988 \pm 8.6 \cdot 10^{-6}$ and $0.999993 \pm 7.3 \cdot 10^{-6}$ for the SPV and SVV schemes respectively. The errors were taken to be equivalent to the standard deviations. From these values we can conclude that the quantity $\mathcal{H}^{\zeta s}$ is numerically conserved by the integrators. However, the instability in the symplectic integrators, which is apparent from the figure, means that one must question

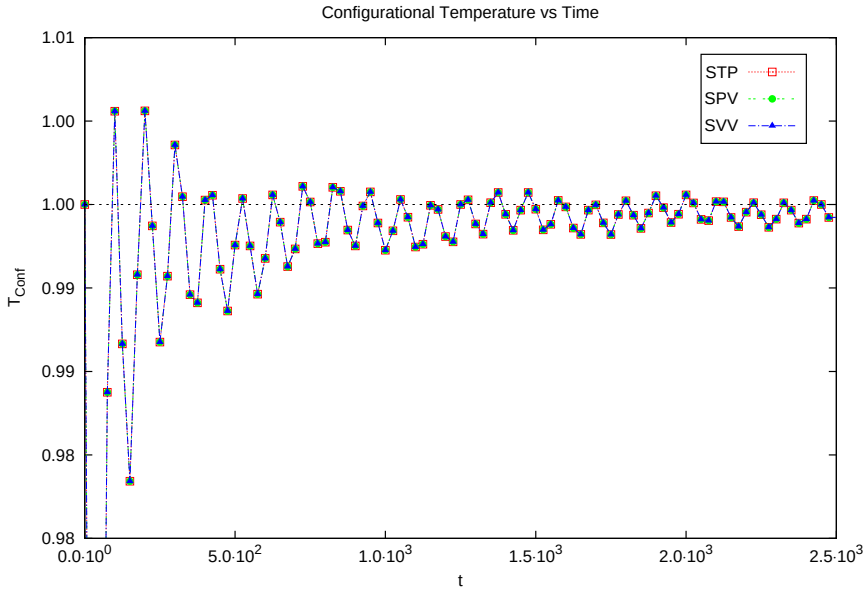

Figure 6.3a: Configurational temperature versus time for an harmonic oscillator attached to a configurational (CTNH) thermostat for the symplectic position (SPV) and velocity (SVV) Verlet algorithms as well as the symmetric Trotter propagator (STP) algorithm. The figure shows the convergence of the system configurational temperature to the input value, where the dashed line denotes the thermostat (input) temperature. The results were obtained using a thermostat mass of $M_\zeta = 10$ and a time step of $\tau = 2.5 \cdot 10^{-3}$, for each of the three integration schemes.

the reliability of the results obtained at long time scales when utilising said schemes. From Fig. 6.2b one can see a similar trend exists for the case of a quartic oscillator being thermostatted by a hybrid CKTNH chain thermostat. The symplectic position Verlet integration algorithm destabilizes around time $t = 2.5 \cdot 10^4$, as is evident by the overall drift towards zero. The conserved quantity for the SVV algorithm exhibits a drift toward two, which begins around the same time as for the SPV algorithm, however, the drift occurs more gradually than for the case of the harmonic oscillator. The STP integration scheme results in no discernible drift of the extended Hamiltonian. Both the STP and SVV schemes have fluctuations of the order of 10^{-5}, whilst the SPV schemes exhibits fluctuations of the order of 10^{-4}. Through use of the `stats` function found in `gnuplot`, it was determined that the average values for the extended Hamiltonian were $1.00001 \pm 1.1 \cdot 10^{-5}$ for the STP integrator, $0.99993 \pm 2.6 \cdot 10^{-5}$ for the SPV scheme and $1.000018 \pm 9.5 \cdot 10^{-6}$ for the SVV scheme, where the errors were taken

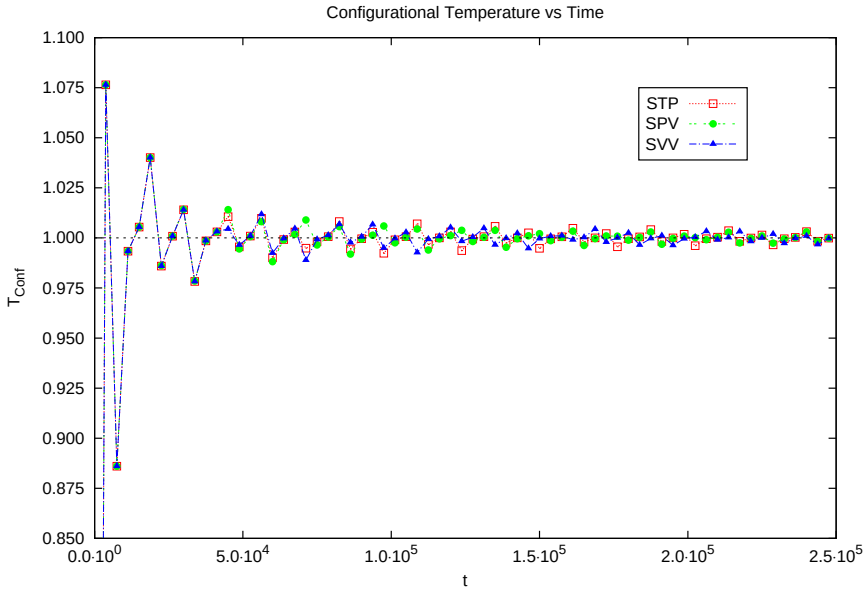

Figure 6.3b: Configurational temperature versus time for a quartic oscillator attached to a configurational temperature Nosè-Hoover (CTNH) thermostat, showing the convergence of the system configurational temperature to the input thermostat temperature. The dashed line denotes the temperature of the heat bath. Three separate simulations were performed, using the symplectic position (SPV) and velocity (SVV) Verlet integrators, as well as the symmetric Trotter propagator (STP) integration scheme. The results shown were obtained using a thermostat mass of $M_\zeta = 9.6 \cdot 10^5$ and a time step of $\tau = 2.5 \cdot 10^{-3}$.

to be the standard deviations. From these values we can conclude that the extended Hamiltonian was conserved, to within the limits imposed by numerical precision. From Figs. 6.1 one can see that, for the case of the CTNH thermostat, the three integration algorithms discussed in Chap. 5 numerically conserve the extended Hamiltonian, whilst being numerically stable. However, in the case of the hybrid CKTNH chain thermostat, the symplectic integrators become numerically unstable, as is shown in Figs. 6.2. The STP algorithm remains stable for both thermostats and leads to numerical conservation of the extended Hamiltonian, as is shown in Figs. 6.1 and 6.2.

When implementing a CTNH thermostatting scheme, the configurational temperature of the physical system, as defined by Eq. (2.8), quickly converges to the value of the thermostat temperature, as is shown in Figs. 6.3, and subsequently fluctuates around this value. In Fig. 6.3a, one can see that there exists a minimal difference

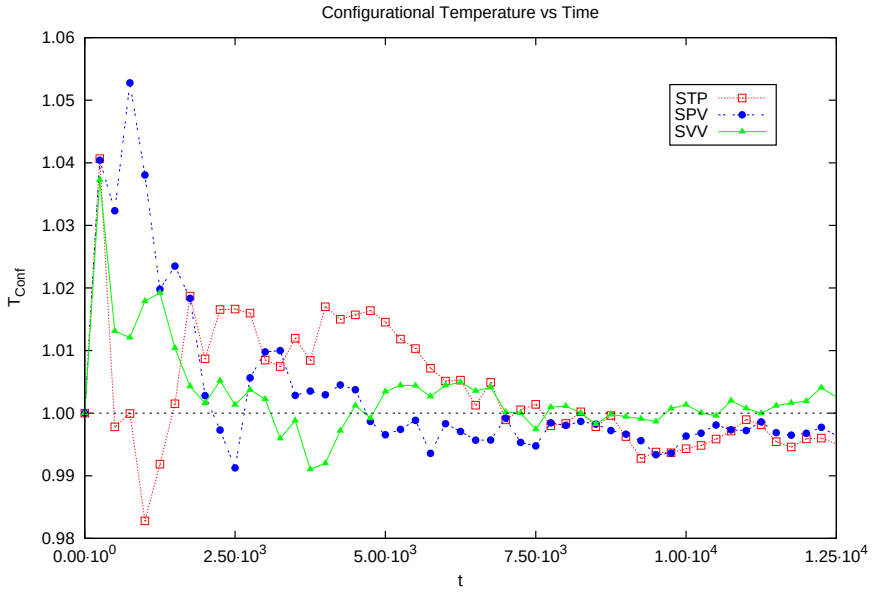

Figure 6.4a: Configurational temperature versus time for an harmonic oscillator system, simulated using a hybrid configurational-kinetic temperature Nosè-Hoover (CKTNH) chain thermostat, where the dashed line represents the temperature of the heat bath. The figure shows the configurational temperature of the physical system converging to the input temperature value. Thermostat masses of $M_\zeta = 10$ and $M_s = 1$ and a time step of $\tau = 2.5 \cdot 10^{-3}$ were used for each simulation conducted, where a different integration algorithm (symplectic position Verlet (SPV), symplectic velocity Verlet (SVV) or symmetric Trotter propagator (STP)) was used for each simulation.

between the results obtained for each of the three integration techniques used in the case of the harmonic oscillator, thermostatted by a CTNH thermostat. It was found, through use of the `stats` function of `gnuplot`, that the average value for the configurational temperature of the physical system was $0.9993 \pm 9.4 \cdot 10^{-4}$, where the error was taken to be the standard deviations, for each of the integration schemes used. The average was calculated after time $t = 7.5 \cdot 10^2$. This was done in an attempt to allow the system to reach thermal equilibrium with the heat bath. For the quartic oscillator, attached to a CTNH thermostat, there is an evident difference across the integration schemes (see Fig. 6.3b), however, this difference is small. Under the assumption that the physical system had reached thermal equilibrium by time $t = 7.5 \cdot 10^4$, the average value for the configurational temperature was determined to be $1.000 \pm 3.0 \cdot 10^{-3}$ for each of the integrators implemented. For both oscillators tested in the case of the

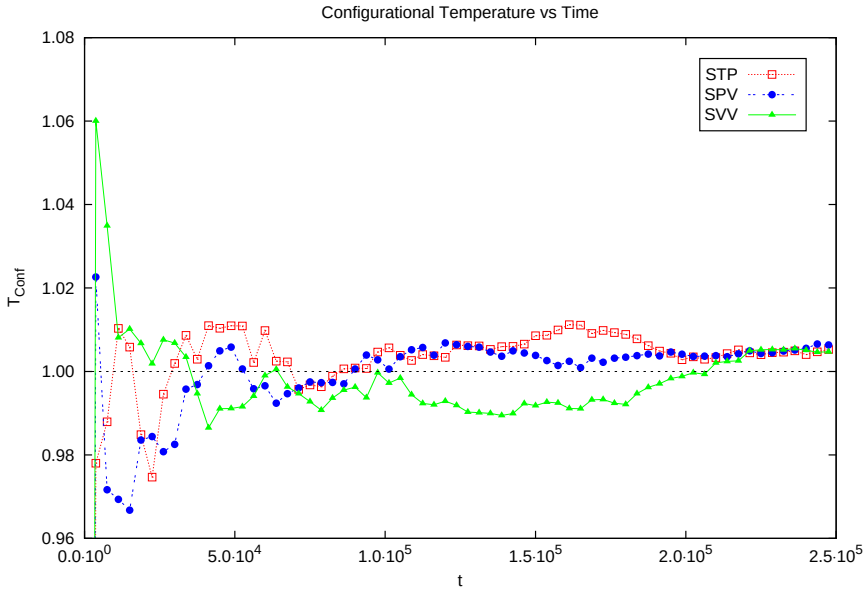

Figure 6.4b: Configurational temperature versus time for double well system attached to a hybrid configurational-kinetic temperature Nosè-Hoover (CKTNH) chain thermostat, showing the convergence of the physical system's configurational temperature to the input thermostat temperature. The temperature of the thermostat chain is denoted by the dashed line. A time step of $\tau = 2.5 \cdot 10^{-3}$, together with thermostat masses of $M_\zeta = 10^3$ and $M_s = 1$, were used to obtain the results for each integration scheme used (symplectic position Verlet (SPV), symplectic velocity Verlet (SVV) or symmetric Trotter propagator (STP)).

CTNH thermostat, the fluctuations around the input temperature value are small, as is shown by Figs. 6.3, and the configurational temperature of the physical system is well regulated by the CTNH thermostat, for the set of simulation input parameter values (as mentioned previously, these are provided in App. C). The configurational temperature of the systems thermostatted by a hybrid CKTNH chain thermostat has larger fluctuations around the thermostat temperature than for a CTNH thermostat, but still maintains the short convergence time. This can be seen in Figs. 6.4, where Fig. 6.4a shows the configurational temperature as a function of time for the case of an harmonic oscillator attached to a hybrid CKTNH chain thermostat, for each of the integration algorithms discussed, and Fig. 6.4b reflects the same information for the case of a quartic oscillator attached to a hybrid CKTNH chain thermostat. Using the same method as for the CTNH thermostat, it was found that, for the harmonic oscillator case, the

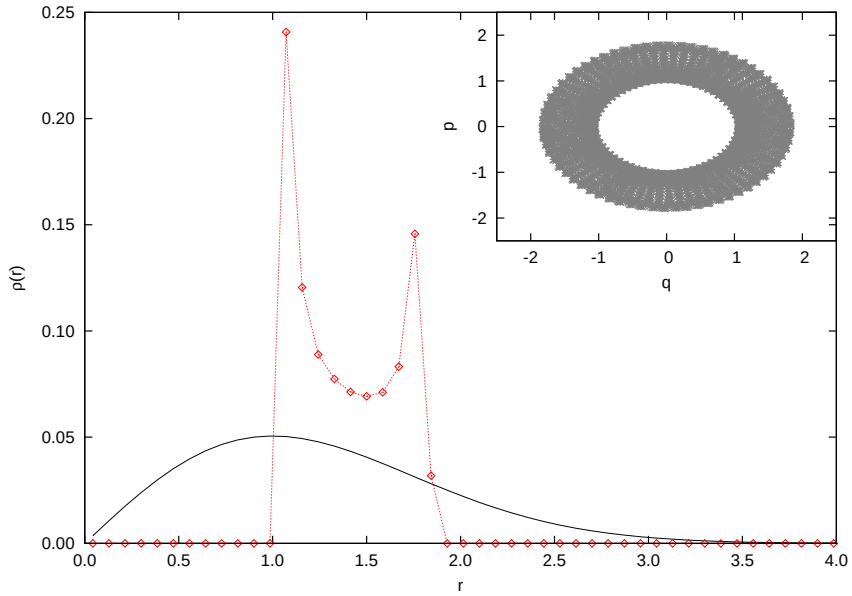

Figure 6.5a: Radial distribution in phase space (main figure) and occupied phase space (inset figure) for an harmonic oscillator attached to a configurational (CTNH) thermostat. Shown in the figure is the lack of ergodicity inherent in the CTNH thermostat, when simulating stiff systems. The equations of motion were integrated using the symplectic position Verlet (SPV) algorithm. The results were obtained using a thermostat mass of $M_\zeta = 10$ and a time step of $\tau = 2.5 \cdot 10^{-3}$.

average configurational temperatures were $1.003 \pm 7.9 \cdot 10^{-3}$ for the STP integration scheme and $0.998 \pm 4.2 \cdot 10^{-3}$ and $1.001 \pm 3.1 \cdot 10^{-3}$ for the SPV and SVV integration algorithms respectively. It was assumed that thermal equilibrium had been reached by the system after time $t = 2.0 \cdot 10^3$. For the quartic oscillator case, under the assumption that thermal equilibrium had been reached by time $t = 5.0 \cdot 10^4$, the configurational temperatures were determined to be $1.003 \pm 3.3 \cdot 10^{-3}$ and $0.996 \pm 5.0 \cdot 10^{-3}$ for the symplectic position and velocity Verlet integrators respectively, and $1.005 \pm 3.4 \cdot 10^{-3}$ for the STP integration scheme. For both thermostats the errors reported were taken to be equivalent to the standard deviations. One possible explanation for the larger fluctuations in the temperature when using a hybrid chain thermostat, is the difference in the temperatures being controlled (kinetic or configurational) by the respective thermostat, because thermostats allow for fluctuations in the temperature which is being regulated. Hence, the fluctuations from the kinetic temperature thermostat may be affecting the calculation of the physical system's configurational temperature. This has

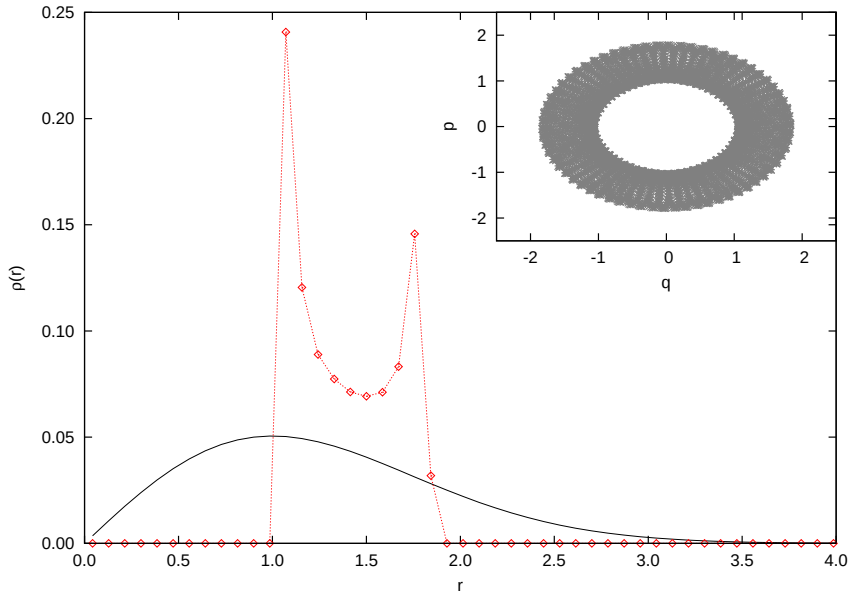

Figure 6.5b: Phase space radial distribution (main figure) for an harmonic oscillator attached to a configurational temperature Nosè-Hoover (CTNH) thermostat, with the occupied phase space shown in the inset figure, showing the non-ergodic property of the CTNH thermostat. The results shown were obtained using the symplectic velocity Verlet (SVV) integration scheme with a thermostat mass of $M_\zeta = 10$ and a time step of $\tau = 2.5 \cdot 10^{-3}$.

not been investigated in the current work, and is a topic for future investigation.

Figures 6.5 show the radial distribution in phase space for an harmonic oscillator system attached to a CTNH thermostat, with the inset figures reflecting the occupied phase spaces for the simulation run. Enlarged versions of the inset figures are provided in App. D, Figs. D.1 for the reader's convenience. Figures 6.5a and 6.5b were obtained using the symplectic position and velocity Verlet integrators respectively, whilst the STP integration scheme was used for Fig. 6.5c. One can clearly see from Figs. 6.5 that the radial distribution of phase space for the duration of the simulation differs significantly from the analytical distribution for the canonical ensemble, in the case of an harmonic oscillator thermostatted using a CTNH thermostat. By comparing the radial distributions presented in Figs. 6.5 one finds that each of the three integration schemes implemented result in the same distribution of phase space, different from that of the canonical ensemble. For each of the Figs. 6.5, the initial zero value for the radial distribution (for the range $0 < r < 1$) corresponds to the distinct void in the occupied

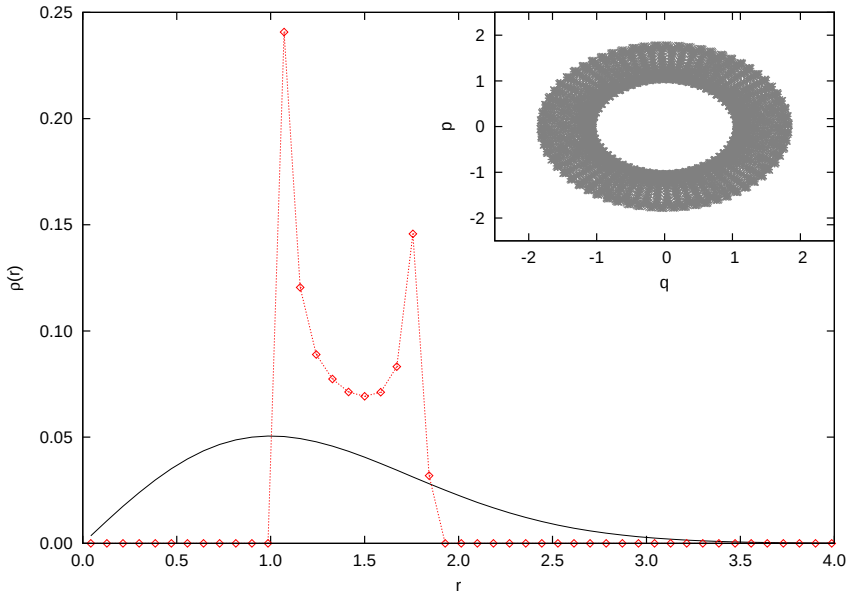

Figure 6.5c: Radial distribution of phase space (main figure) with the phase space occupied for the simulation (inset figure) for an harmonic oscillator attached to a configurational (CTNH) thermostat. The figure shows the loss of ergodicity, which arises when implementing the CTNH thermostat. The results were obtained using the symmetric Trotter propagator (STP) integration scheme and a thermostat mass of $M_\zeta = 10$. The time step used for the simulation was $\tau = 2.5 \cdot 10^{-3}$.

phase space. Figures 6.6 show the occupied phase spaces for a quartic oscillator attached to a CTNH thermostat, using each of the three integration algorithms discussed. Figures 6.6 (a) and (b) were obtained using the symplectic position and velocity Verlet integration algorithms respectively, whilst the STP integration scheme was used for Fig. 6.6 (c). For the reader's convenience, enlarged versions of Figs. 6.6 are provided in App. D, Figs. D.2. For each of the Figs. 6.6 one can see a distinct void in the occupied phase space for a quartic oscillator attached to a CTNH thermostat. Hence, by considering that the radial distribution of phase space differing from the analytical result is independent of the integrator used (see Figs. 6.5), and that a distinct void exists in the occupied phase spaces for both the harmonic and quartic oscillators (see inset Figs. 6.5 and Figs. 6.6), which is again independent of the integration scheme, one can deduce that the dynamics achieved when implementing a CTNH thermostat, on stiff systems, do not ergodically sample the phase space.

The radial distribution in phase space for an harmonic oscillator attached to a

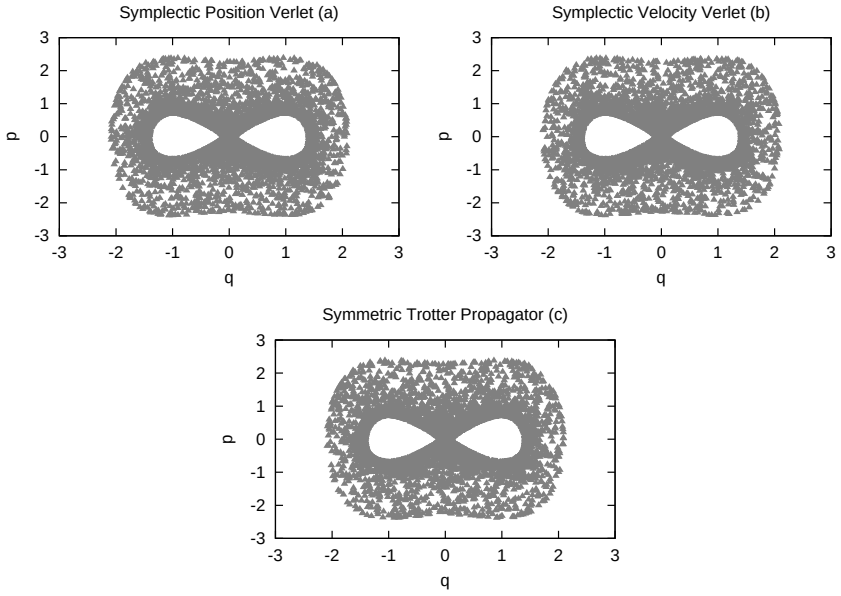

Figure 6.6: Occupied phase space for a quartic oscillator system attached to a configurational (CTNH) thermostat. The top left and right figures were obtained using the symplectic position (SPV) and velocity (SVV) Verlet algorithms, respectively, whilst the symmetric Trotter propagator (STP) integration scheme was used for the bottom figure. The figure shows the lack of ergodicity, arising from use of the CTNH thermostat. All three simulations were performed using a time step of $\tau = 2.5 \cdot 10^{-3}$ and a thermostat mass given by $M_\zeta = 9.6 \cdot 10^5$.

hybrid CKTNH chain thermostat is shown in Figs. 6.7, where Figs. 6.7a and 6.7b were obtained using the symplectic position and velocity Verlet integration algorithms respectively. Figure 6.7c was obtained using the STP integration scheme. Figures 6.7a and 6.7b show that small deviations from the analytical distribution are present when the symplectic integrators are used (around $r = 1$ for Fig. 6.7a and around $r = 0.75$ and $r = 1.5$ for Fig. 6.7b), however, these differences are within acceptable limits. Figure 6.7c shows that, when the STP integration scheme is implemented, the phase space distribution very closely resembles that of an harmonic oscillator in the canonical ensemble. Comparing the inset Figs. 6.7 with those of Figs. 6.5, we can see that by utilising a hybrid CKTNH chain thermostat, the occupied phase space no longer contains a void. For the reader's convenience, enlarged versions of the inset Figs. 6.7 are provided in App. D, Figs. D.3. Figures 6.8 show that the absence of voids in the occupied phase spaces also occurs for the case of a quartic oscillator attached to a

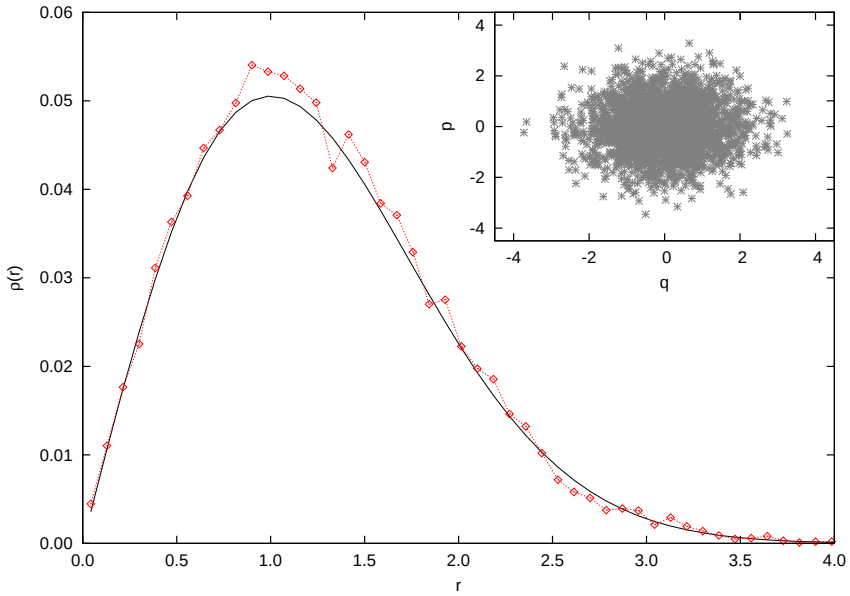

Figure 6.7a: Radial distribution of phase space (main figure) and occupied phase space (inset figure) for an harmonic oscillator attached to a hybrid configurational-kinetic temperature Nosè-Hoover (CKTNH) chain thermostat, where the solid line denotes the analytical distribution, showing that an ergodic sampling of phase space was achieved during the simulation. The results shown were obtained using the symplectic position Verlet (SPV) integration scheme, with thermostat masses of $M_\zeta = 10$ and $M_s = 1$ and a time step of $\tau = 2.5 \cdot 10^{-3}$.

hybrid CKTNH chain thermostat. Enlarged plots of the occupied phase space for each of the integration algorithms implemented are provided, for the reader's convenience, in App. D, Figs. D.4. The symplectic position and velocity Verlet integration algorithms were used to obtain Figs. 6.8 (a) and (b), respectively, whilst Fig. 6.8 (c) was obtained using the STP integration scheme. From the close resemblance between the phase space distribution, for an harmonic oscillator, obtained through simulation and that predicted by theory (see Figs. 6.7), together with the absence of any voids within the occupied phase spaces (see inset Figs. 6.7 and Figs. 6.8), we can conclude that the problem of ergodicity, which arises when using the CTNH thermostat, is rectified through the use of the hybrid CKTNH chain thermostat.

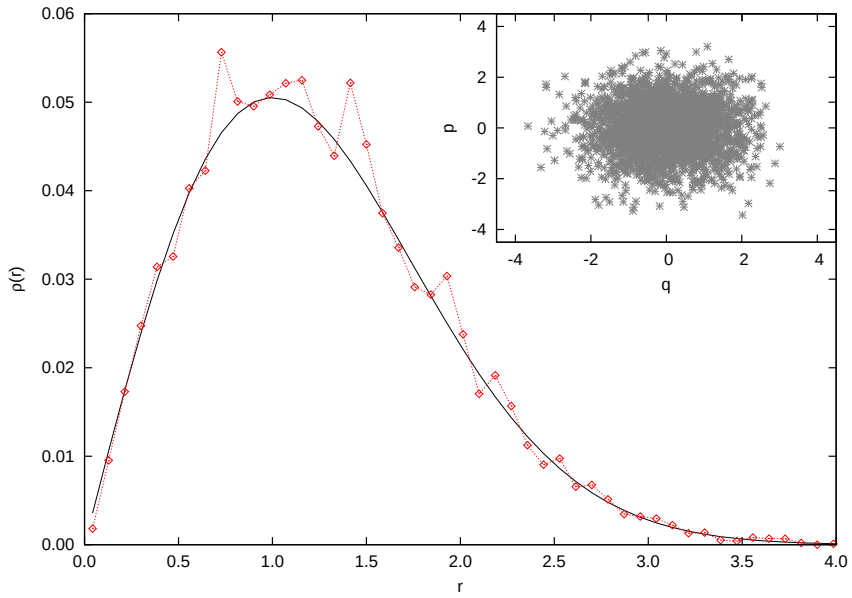

Figure 6.7b: Phase space radial distribution (main figure), where the solid line denotes the analytical distribution, for an harmonic oscillator attached to a hybrid configurational-kinetic temperature Nosè-Hoover (CKTNH) chain thermostat. The inset figure shows the phase space occupied for the simulation. The figure shows that the hybrid CKTNH chain thermostat leads the dynamics of the physical system to ergodically sample phase space. The symplectic velocity Verlet (SVV) algorithm, together with thermostat masses of $M_\zeta = 10$ and $M_s = 1$ and a time step of $\tau = 2.5 \cdot 10^{-3}$, were used to obtain the results shown.

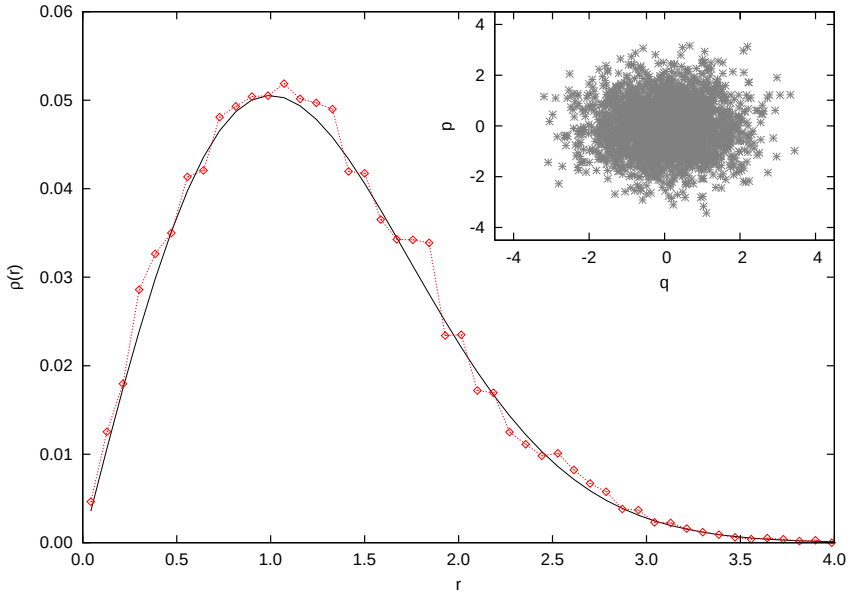

Figure 6.7c: Radial distribution (main figure) of phase space and the occupied phase space (inset figure) for the simulation of an harmonic oscillator attached to a hybrid configurational-kinetic temperature Nosè-Hoover (CKTNH) chain thermostat, showing the dynamics of the physical system sampled the phase space in an ergodic manner. The solid line in the main figure is the analytical radial distribution of phase space. The results were obtained using a time step of $\tau = 2.5 \cdot 10^{-3}$ with thermostat masses of $M_\zeta = 10$ and $M_s = 1$. The equations of motion were integrated using the symmetric Trotter propagator (STP) integration scheme.

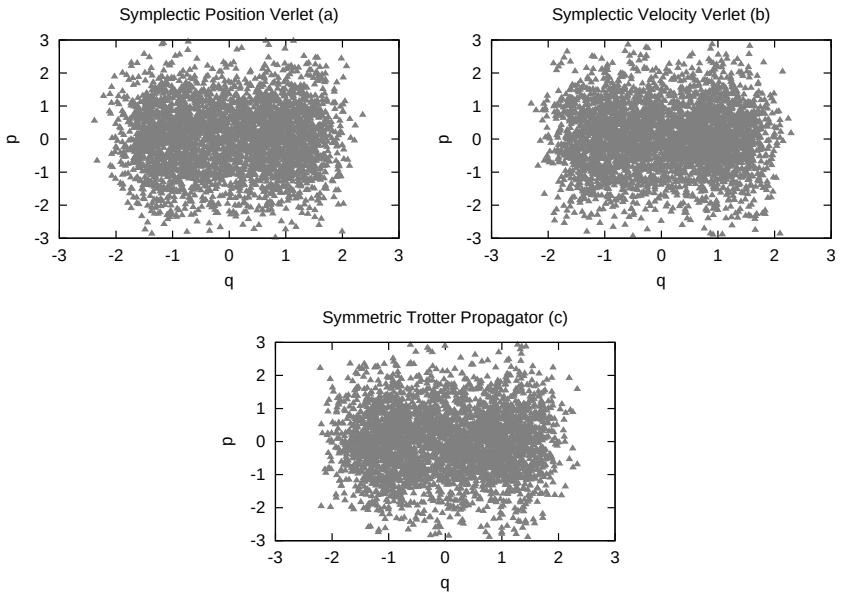

Figure 6.8: Occupied phase space for the simulation of a quartic oscillator attached to a hybrid configurational-kinetic temperature Nosè-Hoover (CKTNH) chain thermostat, for each of the three integration schemes discussed previously. The top left, (a), and right, (b), figures show results obtained using the symplectic position (SPV) and velocity (SVV) Verlet integration algorithms respectively, and the bottom figure was obtained using the symmetric Trotter propagator (STP) integration scheme. For all three simulations, thermostat masses of $M_\zeta = 10^3$ and $M_s = 1$, with a time step of $\tau = 2.5 \cdot 10^{-3}$, were used.

Chapter 7

Conclusions

This dissertation began by introducing the concept of temperature within the field of Thermostatistics. A microcanonical expression for the temperature was provided, through the seminal work of Rugh [11], which was later generalised by Jepps *et al* [12]. From this generalised expression, it was shown how one can obtain either a so-called kinetic temperature, which is dependent upon the velocities of the particles, and the equipartition theorem of the energy, or a so-called configurational temperature, which is dependent upon the particles' coordinates.

Next, we introduced the theory of Hamiltonian dynamics, as well as the theory of non-Hamiltonian dynamics. We discussed the concept of extended systems, first introduced by Andersen [3], and showed how non-Hamiltonian theory is applicable to such systems. This led to the introduction of thermostats, and the Nosè-Hoover (NH) and Nosè-Hoover chain (NHC) thermostats were introduced and discussed. The NH and NHC thermostats are referred to as kinetic thermostats, as they control the kinetic temperature of a system.

A configurational temperature thermostat, proposed by Braga and Travis [20], was introduced and discussed. We proceeded to reformulate the proposed thermostat into a phase space description, using the methodology outlined in [21] and [29]. It was found that this configurational temperature Nosè-Hoover (CTNH) thermostat did not achieve an ergodic sampling of phase space, particularly for stiff systems. This problem was solved by utilising the concept behind the NHC thermostat, and attaching a kinetic NH thermostat to the CTNH thermostat which in turn is attached to the physical system. We refer to such a thermostat as a hybrid configurational-kinetic temperature Nosè-Hoover (CKTNH) chain thermostat.

Three different algorithms were derived to integrate the equations of motion for both the CTNH and the hybrid CKTNH chain thermostats. These algorithms were referred to as the symplectic position (SPV) and velocity (SVV) Verlet schemes and the symmetric Trotter propagator (STP) scheme. The procedure outlined in [34] and [37] was used to derive the STP scheme, where for physical systems possessing a force non-linear in the generalised coordinate q, a position-dependent, harmonically approximated (PDHA) scheme was used. This PDHA scheme uses a second order Taylor expansion of the potential function when advancing the coordinate, of the physical system, in time.

Both the CTNH and hybrid CKTNH chain thermostats were used to simulate an harmonic oscillator (single well potential) and a quartic oscillator (double well potential). Each of the three integration algorithms (SPV, SVV and STP) were used for each case, where it was found that the STP scheme performed the strongest. The simulation results verified the ergodicity sampling problem of the CTNH thermostat as well as the hybrid CKTNH chain thermostat being a solution. The simulations also showed that although for both thermostats the configurational temperature of the physical system quickly converges to that of the thermostat, in the case of the hybrid CKTNH chain thermostat, the fluctuations around this value are larger than those for the CTNH thermostat. It is hypothesised that this is due to the difference in the temperatures (configurational versus kinetic) which the two thermostats, of which the chain consists, control. This hypothesis has not been tested in the present work, and is a topic for future research.

The results obtained from the simulations which were performed, and which verify the ideas presented in this dissertation, have been combined with those from Mr. E. Obaga, who implemented a CTNH thermostat to simulate a Weeks-Chandler-Andersen (WCA) fluid (a variation of the Lennard-Jones potential), and submitted to the Computer Physics Communications journal for publication. At the time of writing this dissertation, the paper was still in the review process.

In the future we plan to investigate the validity of both the CTNH thermostat and the hybrid CKTNH chain thermostat in non-equilibrium simulations. Additionally, we plan to use the Wigner representation of quantum mechanics [38] to reformulate these thermostats for use in quantum-classical molecular dynamics simulations. This reformulation will be done using the methodology outlined in [39].

Appendix A

Action of Propagator U1

Applying the Liouville operator $L_{1,h}^{\mathrm{CTNH}}$ defined by (see Eq. (5.15))

$$L_{1,h}^{\mathrm{CTNH}} = \left(\frac{p}{m} - kq\frac{p_\zeta}{M_\zeta}\right)\frac{\partial}{\partial q}\,, \tag{A.1}$$

leads to the differential equation

$$\begin{aligned} \dot{q} &= L_{1,h}^{\mathrm{CTNH}} q\,, \\ \Rightarrow \frac{\mathrm{d}q}{\mathrm{d}t} &= \frac{p}{m} - kq\frac{p_\zeta}{M_\zeta}\,. \end{aligned} \tag{A.2}$$

By making the following substitutions

$$A = \frac{p}{m}\,, \tag{A.3a}$$

$$B = k\frac{p_\zeta}{M_\zeta}\,, \tag{A.3b}$$

equation (A.2) becomes

$$\frac{\mathrm{d}q}{\mathrm{d}t} = A - Bq \tag{A.4}$$

$$\int_{q(t)}^{q(t+\tau)} \frac{\mathrm{d}q}{A - Bq} = \int_t^{t+\tau} \mathrm{d}t' = t + \tau - t = \tau \tag{A.5}$$

Making a change of variables in the left hand side

$$z = A - Bq \tag{A.6}$$

$$\mathrm{d}z = -B\mathrm{d}q \tag{A.7}$$

leads to

$$-\frac{1}{B}\int_{A-Bq(t)}^{A-Bq(t+\tau)}\frac{\mathrm{d}z}{z}=\tau \tag{A.8}$$

$$-\frac{1}{B}\ln\left(\frac{A-Bq\left(t+\tau\right)}{A-Bq\left(t\right)}\right)=\tau \tag{A.9}$$

$$\ln\left(\frac{A-Bq\left(t+\tau\right)}{A-Bq\left(t\right)}\right)=-B\tau \tag{A.10}$$

$$\frac{A-Bq\left(t+\tau\right)}{A-Bq\left(t\right)}=\exp\left(-B\tau\right)\ . \tag{A.11}$$

Making $q\left(t+\tau\right)$ the subject of the formula

$$A-Bq\left(t+\tau\right)=\left[A-Bq\left(t\right)\right]\exp\left(-B\tau\right) \tag{A.12}$$

$$-Bq\left(t+\tau\right)=-A+\left[A-Bq\left(t\right)\right]\exp\left(-B\tau\right) \tag{A.13}$$

$$q\left(t+\tau\right)=\frac{A}{B}+\left[q\left(t\right)-\frac{A}{B}\right]\exp\left(-B\tau\right) \tag{A.14}$$

$$=q\left(t\right)\exp\left(-B\tau\right)+\frac{A}{B}-\frac{A}{B}\exp\left(-B\tau\right) \tag{A.15}$$

$$=q\left(t\right)\exp\left(-B\tau\right)+\frac{A}{B}\left[1-\exp\left(-B\tau\right)\right] \tag{A.16}$$

$$=q\left(t\right)\exp\left(-B\tau\right)+2\frac{A}{B}\exp\left(-B\frac{\tau}{2}\right)\left[\frac{\exp\left(B\frac{\tau}{2}\right)-\exp\left(-B\frac{\tau}{2}\right)}{2}\right]\ . \tag{A.17}$$

Using the definition for $\sinh(x)$

$$q\left(t+\tau\right)=q\left(t\right)\exp\left(-B\tau\right)+2\tau\frac{A}{B}\exp\left(-B\frac{\tau}{2}\right)\frac{\sinh\left(B\frac{\tau}{2}\right)}{\tau} \tag{A.18}$$

$$=q\left(t\right)\exp\left(-B\tau\right)+\tau A\left[\frac{\sinh\left(B\frac{\tau}{2}\right)}{B\frac{\tau}{2}}\right]\ . \tag{A.19}$$

Substituting back in Eqs. (A.3)

$$q\left(t+\tau\right)=q\left(t\right)\exp\left(-\tau k\frac{p_\zeta}{M_\zeta}\right)+\tau\frac{p}{m}\exp\left(-\tau\frac{k}{2}\frac{p_\zeta}{M_\zeta}\right)\left[\frac{\sinh\left(\tau\frac{k}{2}\frac{p_\zeta}{M_\zeta}\right)}{\tau\frac{k}{2}\frac{p_\zeta}{M_\zeta}}\right]\ . \tag{A.20}$$

Hence the action of the propagator $U_{1,\mathrm{h}}^{\mathrm{CTNH}}(\tau)$ is given by

$$q\rightarrow q\exp\left(-\tau k\frac{p_\zeta}{M_\zeta}\right)+\tau\frac{p}{m}\exp\left(-\tau\frac{k}{2}\frac{p_\zeta}{M_\zeta}\right)\left[\frac{\sinh\left(\tau\frac{k}{2}\frac{p_\zeta}{M_\zeta}\right)}{\tau\frac{k}{2}\frac{p_\zeta}{M_\zeta}}\right]\Bigg\}:U_{1,\mathrm{h}}^{\mathrm{CTNH}}(\tau)\ . \tag{A.21}$$

For purposes of numerical stability, the term $\sinh\left(x\right)/x$ where x is given by $\tau\frac{k}{2}\frac{p_\zeta}{M_\zeta}$ is calculated using a series expansion

$$\frac{\sinh\left(x\right)}{x}=1+\frac{x^2}{3!}+\frac{x^4}{5!}+\frac{x^6}{7!}+\frac{x^8}{9!}+\mathcal{O}(x^{10})\ . \tag{A.22}$$

Appendix B

Position-Dependent Harmonically Approximated (PDHA) Propagator Derivation

Taking a Taylor series expansion of the potential function, about an arbitrary coordinate q' different to q, and arrested to second order

$$U(q) \simeq U(q') + (q - q') \left.\frac{\partial U(q)}{\partial q}\right|_{q'} + \frac{1}{2}(q - q')^2 \left.\frac{\partial^2 U(q)}{\partial q^2}\right|_{q'} + \mathcal{O}(q^3) \ . \tag{B.1}$$

By definition, for the configurational temperature Nosè-Hoover (CTNH) thermostat

$$G(q') = \left.\frac{\partial^2 U(q)}{\partial q^2}\right|_{q'} . \tag{B.2}$$

Thus the Taylor series expansion, Eq. (B.1), reduces to

$$U(q) \simeq U(q') - (q - q') F(q') + \frac{1}{2}(q - q')^2 G(q') + \mathcal{O}(q^3) \ , \tag{B.3}$$

$$\begin{aligned} \Rightarrow -\frac{\partial U(q)}{\partial q} &\simeq F(q') + G(q')(q' - q) \\ &\simeq F(q') + G(q') q' - G(q') q \ . \end{aligned} \tag{B.4}$$

Substituting Eq. (B.4) into the coordinate equation of motion, Eq. (5.9a), yields

$$\dot{q} = \frac{p}{m} - \frac{p_\zeta}{M_\zeta}\frac{\partial U(q)}{\partial q} \tag{B.5}$$

$$\simeq \frac{p}{m} + \frac{p_\zeta}{M_\zeta}\left[F(q') + G(q') q' - G(q') q\right] \tag{B.6}$$

$$= L_{1,h}^{\mathrm{CTNH}} q \ . \tag{B.7}$$

Solving the differential equation, Eq. (B.7), for q

$$\frac{\mathrm{d}q}{\mathrm{d}t} = \frac{p}{m} + \frac{p_\zeta}{M_\zeta} F\left(q'\right) + \frac{p_\zeta}{M_\zeta} G\left(q'\right) q' - \frac{p_\zeta}{M_\zeta} G\left(q'\right) q \; . \tag{B.8}$$

We make the following substitutions

$$A = \frac{p}{m} + \frac{p_\zeta}{M_\zeta} F\left(q'\right) + \frac{p_\zeta}{M_\zeta} G\left(q'\right) q' \; , \tag{B.9a}$$

$$B = \frac{p_\zeta}{M_\zeta} G\left(q'\right) \; , \tag{B.9b}$$

so that Eq. (B.8) reduces to

$$\frac{\mathrm{d}q}{\mathrm{d}t} = A - Bq \tag{B.10}$$

$$\Rightarrow q\left(t+\tau\right) = q\left(t\right) \exp\left(-B\tau\right) + \tau A \left[\frac{\sinh\left(B\frac{\tau}{2}\right)}{B\frac{\tau}{2}}\right] \; , \tag{B.11}$$

where the result was taken from the derivation in App. A, Eq. (A.19). Substituting back in for Eqs. (B.9), one finds

$$\begin{aligned} q\left(t+\tau\right) = {} & q\left(t\right) \exp\left(-\frac{p_\zeta}{M_\zeta} G\left(q'\right) \tau\right) \\ & + \tau \left[\frac{p}{m} + \frac{p_\zeta}{M_\zeta} F\left(q'\right) + \frac{p_\zeta}{M_\zeta} G\left(q'\right) q'\right] \left[\frac{\sinh\left(\frac{p_\zeta}{M_\zeta} G\left(q'\right) \frac{\tau}{2}\right)}{\frac{p_\zeta}{M_\zeta} G\left(q'\right) \frac{\tau}{2}}\right] \; . \end{aligned} \tag{B.12}$$

Hence, the action of the propagator $\tilde{U}_{1,h}^{\mathrm{CTNH}}$ is

$$\begin{aligned} q \rightarrow {} & q\left(t\right) \exp\left(-\frac{p_\zeta}{M_\zeta} G\left(q'\right) \tau\right) \\ & + \tau \left[\frac{p}{m} + \frac{p_\zeta}{M_\zeta} F\left(q'\right) + \frac{p_\zeta}{M_\zeta} G\left(q'\right) q'\right] \left[\frac{\sinh\left(\frac{p_\zeta}{M_\zeta} G\left(q'\right) \frac{\tau}{2}\right)}{\frac{p_\zeta}{M_\zeta} G\left(q'\right) \frac{\tau}{2}}\right] \Bigg\} : \tilde{U}_{1,h}^{\mathrm{CTNH}}(\tau) \; . \end{aligned} \tag{B.13}$$

Appendix C

Simulation Parameters

Tables C.1 show the relevant parameter values used for the simulations which were conducted. The top table is for the harmonic oscillator simulations and the bottom table is for the quartic oscillator simulations. The notation used in tables C.1 is as follows

HO	:	Harmonic Oscillator (single well)
DW	:	Quartic Oscillator (double well)
CTNH	:	configurational temperature Nosè-Hoover thermostat
CKTNH	:	hybrid configurational-kinetic temperature Nosè-Hoover chain thermostat
STP	:	Symmetric Trotter Propagator integration scheme
SPV	:	Symplectic Position Verlet integration algorithm
SVV	:	Symplectic Velocity Verlet integration algorithm
k_{B}	:	Boltzmann's constant
T	:	thermostat temperature
k	:	Harmonic Oscillator spring constant
a	:	Quartic Oscillator well width
b	:	Quartic Oscillator well depth
m	:	particle mass
M_ζ	:	configurational thermostat mass
M_s	:	kinetic thermostat mass
τ	:	integration time step
n_{yosh}	:	number of Yoshida integration steps
m_{step}	:	maximum number of iterations in the multiple time step scheme
n_{iter}	:	maximum number of iterations when implementing the symplectic integrators
tol	:	iteration tolerance used when implementing the symplectic integrators

Table C.1: Tables showing the relevant input parameters for each of the simulations performed. An explanation of the notation used is provided in App. C.

System	Thermostat	Integrator	k	$k_\mathrm{B}T$	m	M_ζ	M_s	τ	n_yosh	m_step	n_iter	tol
HO	CTNH	STP	1.0	1.0	1.0	10.0	—	$2.5 \cdot 10^{-3}$	—	—	—	—
		SPV	1.0	1.0	1.0	10.0	—	$2.5 \cdot 10^{-3}$	—	—	10	10^{-10}
		SVV	1.0	1.0	1.0	10.0	—	$2.5 \cdot 10^{-3}$	—	—	10	10^{-10}
	CKTNH	STP	1.0	1.0	1.0	10.0	1.0	$2.5 \cdot 10^{-3}$	5	—	—	—
		SPV	1.0	1.0	1.0	10.0	1.0	$2.5 \cdot 10^{-3}$	—	—	15	10^{-15}
		SVV	1.0	1.0	1.0	10.0	1.0	$2.5 \cdot 10^{-3}$	—	—	15	10^{-15}

System	Thermostat	Integrator	a	b	$k_\mathrm{B}T$	m	M_ζ	M_s	τ	n_yosh	m_step	n_iter	tol
DW	CTNH	STP	1.0	-1.0	1.0	1.0	$9.6 \cdot 10^5$	—	$2.5 \cdot 10^{-3}$	5	5	—	—
		SPV	1.0	-1.0	1.0	1.0	$9.6 \cdot 10^5$	—	$2.5 \cdot 10^{-3}$	—	—	20	10^{-15}
		SVV	1.0	-1.0	1.0	1.0	$9.6 \cdot 10^5$	—	$2.5 \cdot 10^{-3}$	—	—	20	10^{-15}
	CKTNH	STP	1.0	-1.0	1.0	1.0	10^3	1.0	$2.5 \cdot 10^{-3}$	5	—	—	—
		SPV	1.0	-1.0	1.0	1.0	10^3	1.0	$2.5 \cdot 10^{-3}$	—	—	100	10^{-50}
		SVV	1.0	-1.0	1.0	1.0	10^3	1.0	$2.5 \cdot 10^{-3}$	—	—	100	10^{-50}

Appendix D

Occupied Phase Spaces

In this appendix, enlarged versions of the occupied phase spaces, discussed earlier in Sec. 6, for each simulation performed, are presented.

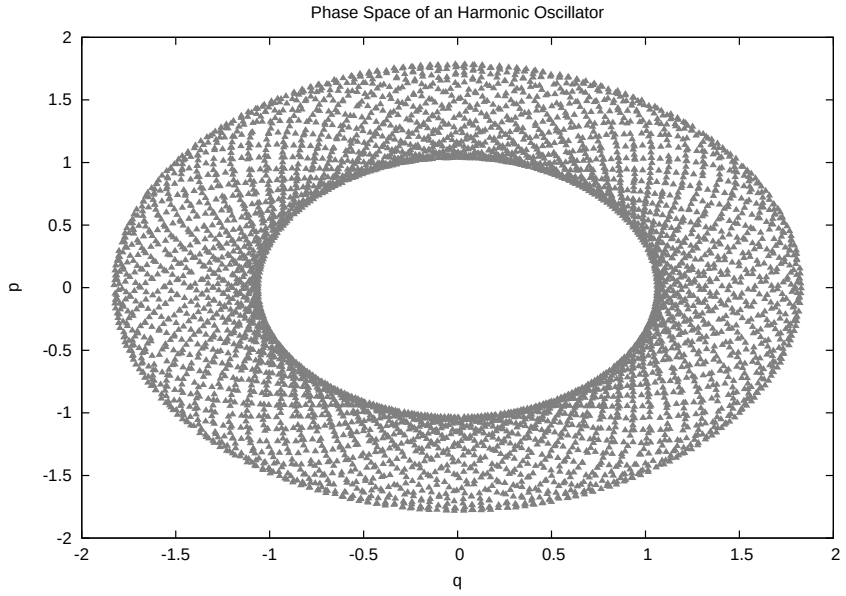

Figure D.1a: Figure showing the occupied phase space for the simulation of an harmonic oscillator system attached to a configurational temperature Nosè-Hoover (CTNH) thermostat, using a symplectic position Verlet (SPV) integration scheme. The figure shows the non-ergodicity property which arises when using the CTNH thermostat to simulate stiff systems. The simulation results were obtained using a thermostat mass of $M_\zeta = 10$ and a time step of $\tau = 2.5 \cdot 10^{-3}$.

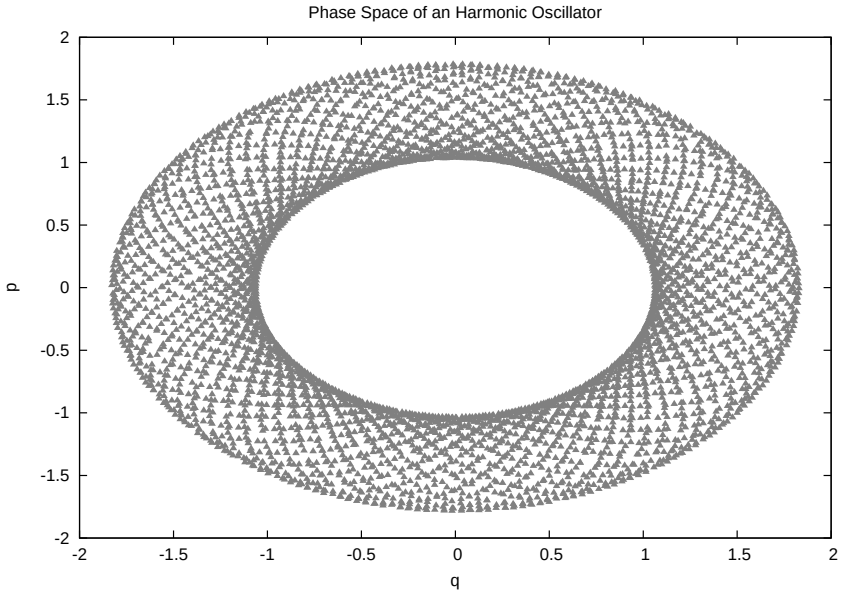

Figure D.1b: Occupied phase space for an harmonic oscillator system attached to a configurational (CTNH) thermostat, showing the lack of an ergodic sampling of phase space by the dynamics of the physical system. The integration of the equations of motion was conducted using a symplectic velocity Verlet (SVV) integration scheme, with a thermostat mass of $M_\zeta = 10$ and a time step of $\tau = 2.5 \cdot 10^{-3}$.

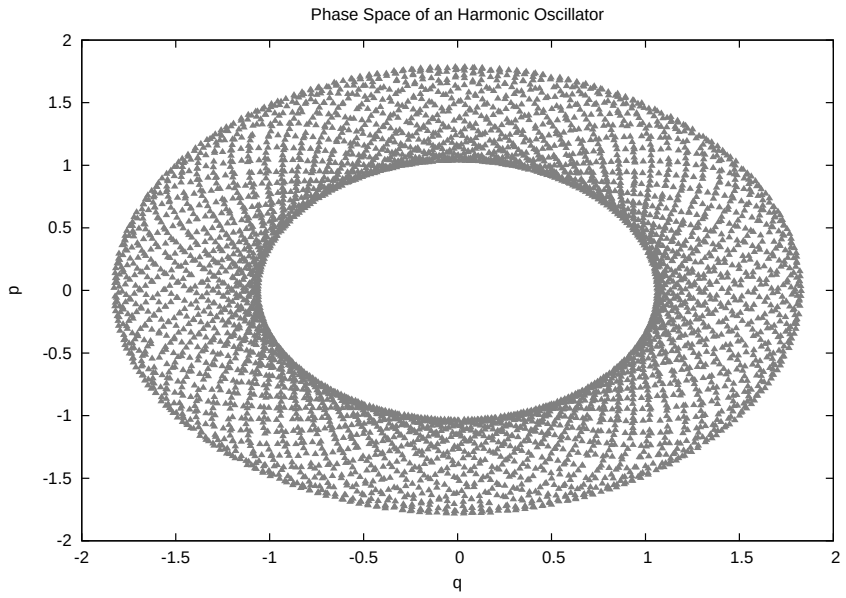

Figure D.1c: Occupied phase space for an harmonic oscillator system attached to a configurational temperature Nosè-Hoover (CTNH) thermostat, showing the lack of ergodicity when using the CTNH thermostat for stiff systems. The equations of motion were integrated using the symmetric Trotter propagator (STP) algorithm. The simulation results were obtained using a thermostat mass of $M_\zeta = 10$ and a time step of $\tau = 2.5 \cdot 10^{-3}$.

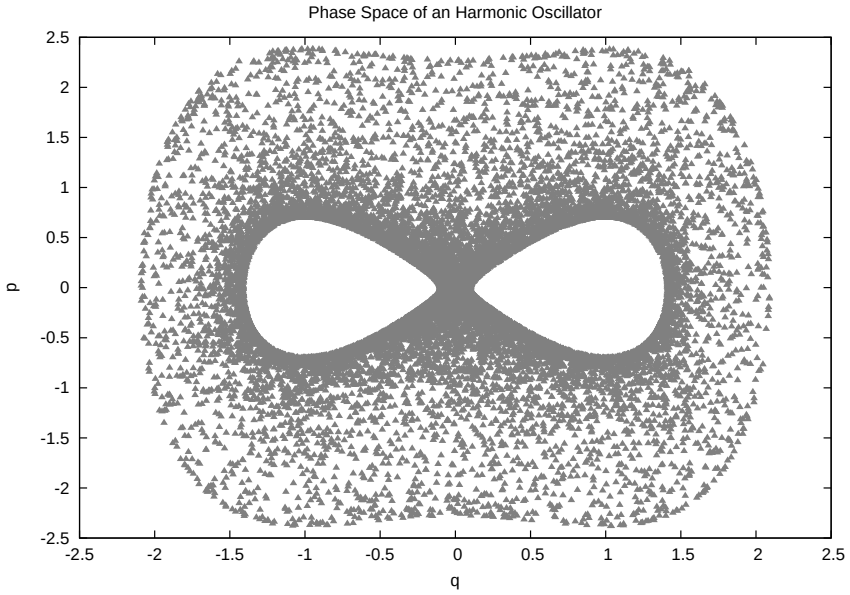

Figure D.2a: Occupied phase space for a double well potential system attached to a configurational temperature Nosè-Hoover (CTNH) thermostat, using a symplectic position Verlet (SPV) integration scheme. The figure shows the non-ergodic manner in which the dynamics of the system sample the phase space. The simulation results were obtained using a thermostat mass of $M_\zeta = 9.6 \cdot 10^5$ and a time step of $\tau = 2.5 \cdot 10^{-3}$.

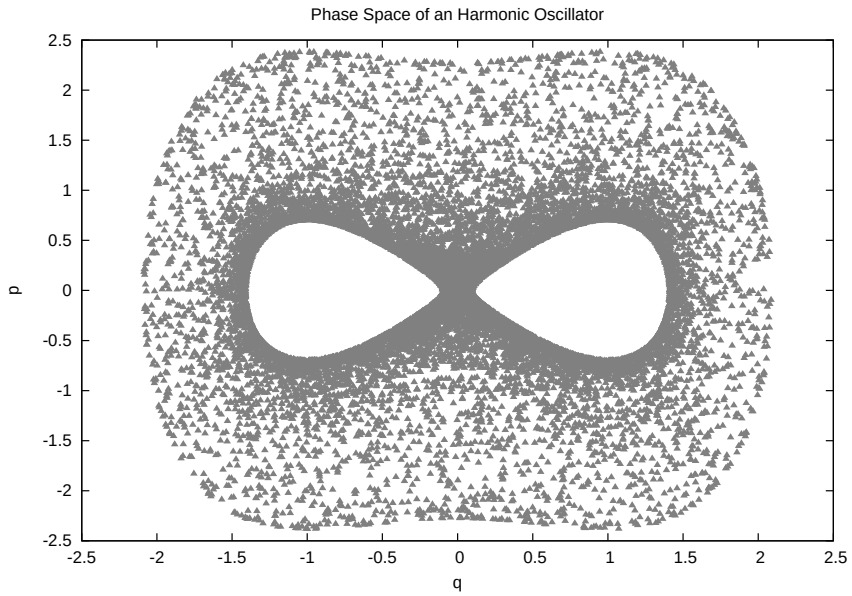

Figure D.2b: Figure showing the occupied phase space for a quartic oscillator attached to a configurational temperature Nosè-Hoover (CTNH) thermostat. The figure shows the property of non-ergodicity which arises when simulating stiff systems using a CTNH thermostat. The equations of motion were integrated using a symplectic velocity Verlet (SVV) integration algorithm, and a thermostat mass of $M_\zeta = 9.6 \cdot 10^5$ with a time step of $\tau = 2.5 \cdot 10^{-3}$ was used.

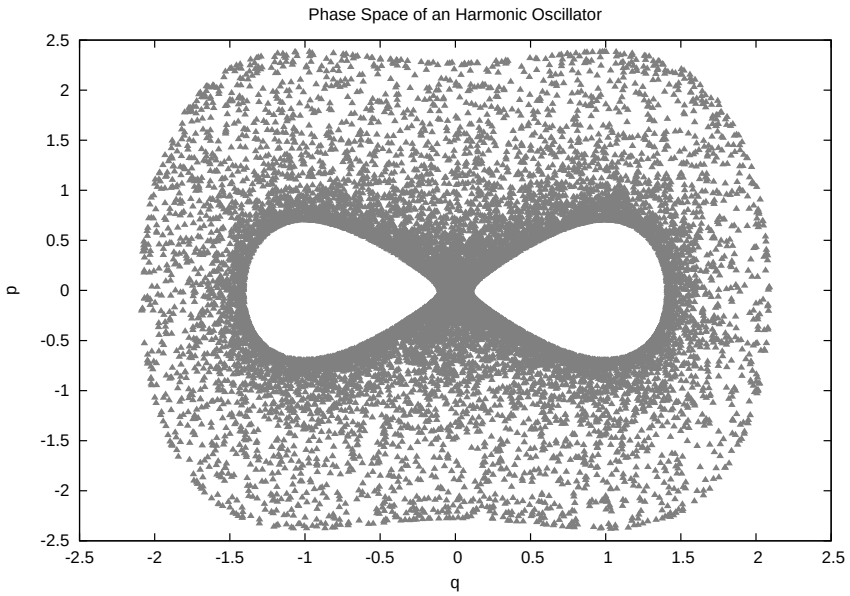

Figure D.2c: Occupied phase space for a quartic oscillator attached to a configurational (CTNH) thermostat, showing the non-ergodic sampling of phase space achieved by the system's dynamics. The equations of motion were integrated using a symmetric Trotter propagator (STP) integration algorithm, as well as the Yoshida and multiple time step procedures. A thermostat mass of $M_\zeta = 9.6 \cdot 10^5$ and a time step of $\tau = 2.5 \cdot 10^{-3}$ was used.

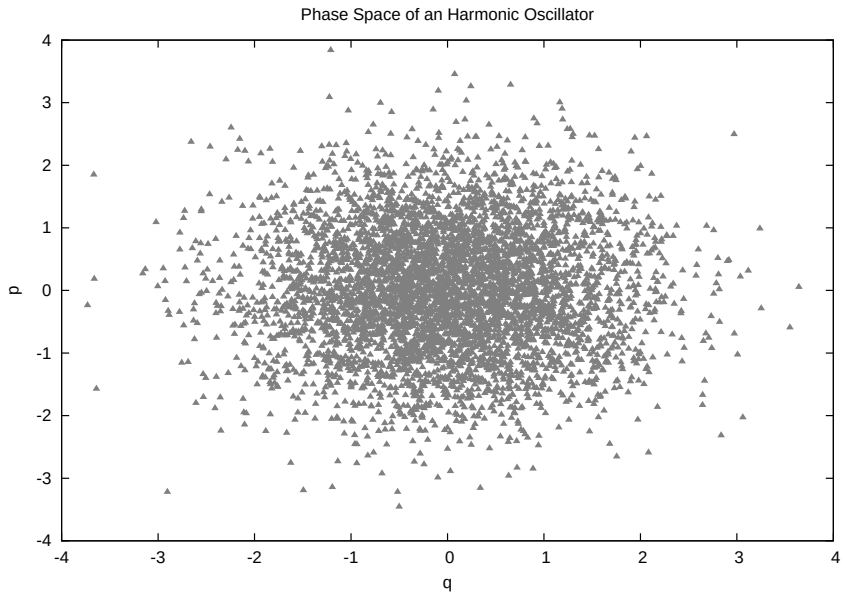

Figure D.3a: Occupied phase space during the simulation of an harmonic oscillator attached to a hybrid configurational-kinetic temperature Nosè-Hoover (CKTNH) chain thermostat, where a symplectic position Verlet (SPV) integration scheme was implemented. The figure shows the ergodic sampling of phase space achieved by the dynamics of the system. Thermostat masses of $M_\zeta = 10$ and $M_s = 1$, and a time step of $\tau = 2.5 \cdot 10^{-3}$ were used.

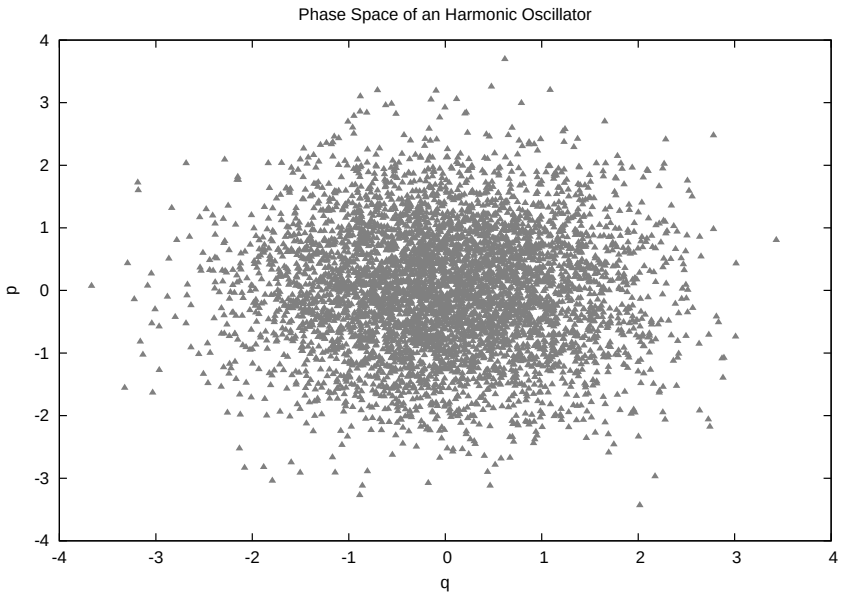

Figure D.3b: Figure showing the phase space occupied during the simulation of an harmonic oscillator attached to a hybrid configurational-kinetic temperature Nosè-Hoover (CKTNH) chain thermostat. Shown in the figure is the ergodic manner in which the dynamics of the system sample phase space. The equations of motion were integrated using a symplectic velocity Verlet (SVV) scheme, with thermostat masses of $M_\zeta = 10$ and $M_s = 1$, and a time step of $\tau = 2.5 \cdot 10^{-3}$.

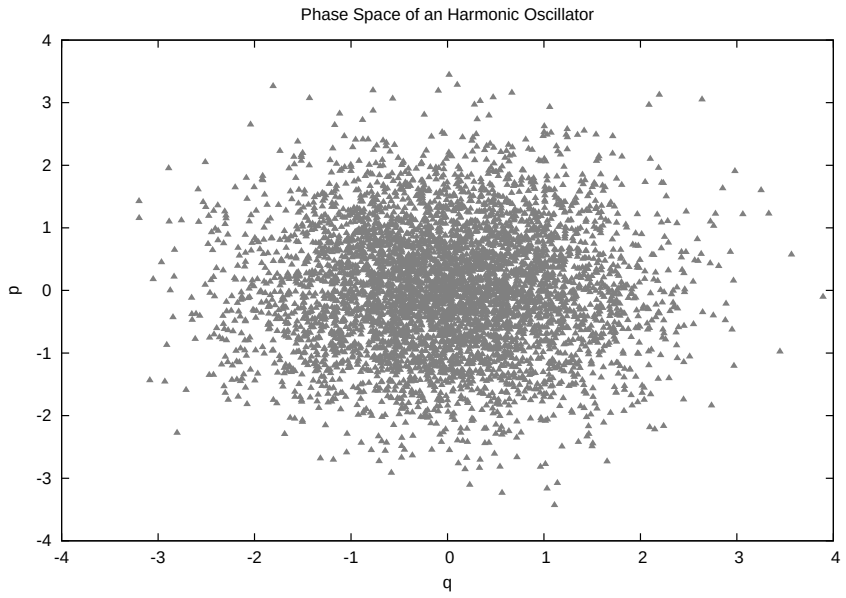

Figure D.3c: Occupied phase space of an harmonic oscillator system attached to a hybrid configurational-kinetic temperature Nosè-Hoover (CKTNH) chain thermostat, showing the property of ergodicity. The equations of motion were integrated using a combination of both the symmetric Trotter propagator (STP) and Yoshida integration schemes. Thermostat masses of $M_\zeta = 10$ and $M_s = 1$, and a time step of $\tau = 2.5 \cdot 10^{-3}$ were used.

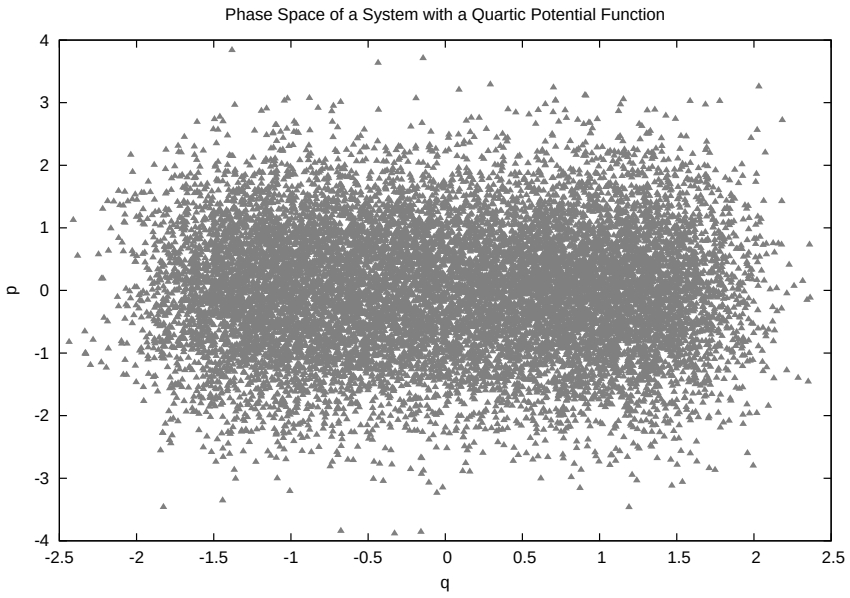

Figure D.4a: Occupied phase space of a quartic oscillator attached to a hybrid configurational-kinetic temperature Nosè-Hoover (CKTNH) chain thermostat, using a symplectic position Verlet (SPV) integration scheme. The figure shows the ergodic manner in which the dynamics of the system sample the phase space. Thermostat masses of $M_\zeta = 10^3$ and $M_s = 1$, and a time step of $\tau = 2.5 \cdot 10^{-3}$, were used to obtain the results shown.

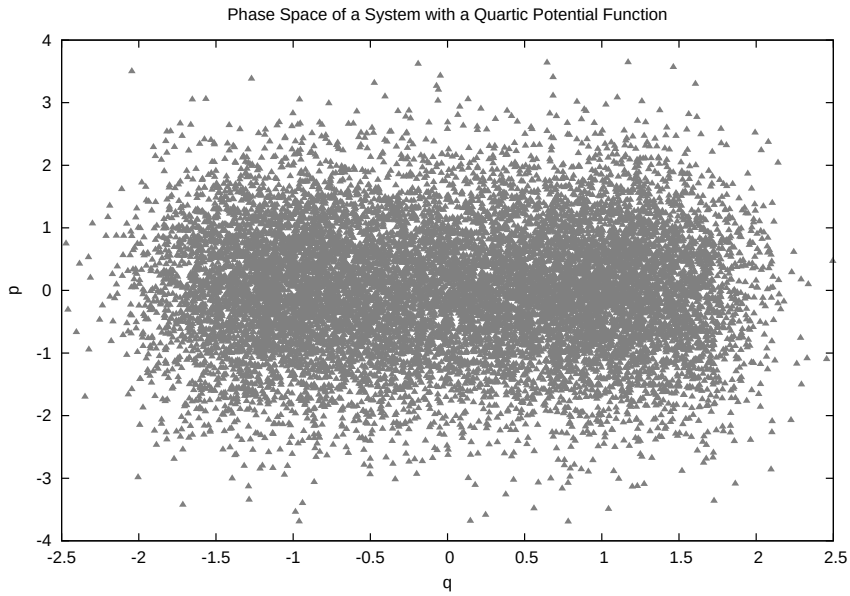

Figure D.4b: Figure showing the phase space occupied during the simulation of a quartic oscillator attached to a hybrid configurational-kinetic temperature Nosè-Hoover (CKTNH) chain thermostat, demonstrating the ergodic nature of the system. The equations of motion were integrated using a symplectic velocity Verlet (SVV) scheme, and the simulation results were obtained using thermostat masses of $M_\zeta = 10^3$ and $M_s = 1$, and a time step of $\tau = 2.5 \cdot 10^{-3}$.

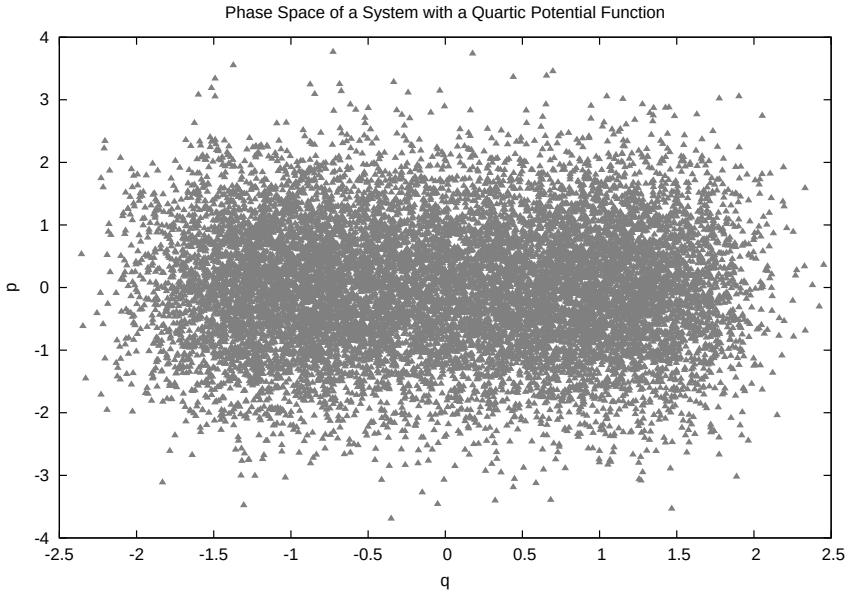

Figure D.4c: Occupied phase space for a double well potential system attached to a hybrid configurational-kinetic temperature Nosè-Hoover (CKTNH) chain thermostat, showing the ergodic sampling of phase space achieved by the dynamics of the system. The equations of motion were integrated using a symmetric Trotter propagator (STP) integration algorithm together with the Yoshida integration scheme. The simulation results were obtained using thermostat masses of $M_\zeta = 10^3$ and $M_s = 1$, and a time step of $\tau = 2.5 \cdot 10^{-3}$.

Appendix E

Publications

The publication on which the researched presented in this thesis is based has been reproduced in the following pages. This publication has been submitted to *Computer Physics Communications*, and, at the time of submission of this thesis, was still in the review process.

Derrick Beckedahl[a], Emmanuel O. Obaga[a], Daniel A. Uken[a], Alessandro Sergi[a,b,*], Mauro Ferrario[c]

[a] *School of Chemistry and Physics, University of KwaZulu-Natal Scottsville 3209 Pietermaritzburg, South Africa*
[b] *Dipartimento di Scienze Matematiche e Informatiche, Scienze Fisiche e Scienze della Terra, Universitá degli Studi di Messina, Contrada Papardo, 98166 Messina, Italy*
[c] *Dipartimento di Scienze Fisiche, Informatiche e Matematiche, Università di Modena e Reggio Emilia Via Campi 213/A, 41125 Modena, Italy*

Abstract

In this paper we reformulate the configurational temperature Nosé-Hoover thermostat of Braga and Travis [J. Chem. Phys. **123**, 134101 (2005)] by means of a quasi-Hamiltonian theory in phase space [Phys. Rev. E **64**, 056125 (2001)]. The quasi-Hamiltonian structure is exploited to introduce a hybrid configurational-kinetic temperature Nosé-Hoover chain thermostat that can achieve a uniform sampling of phase space (also for stiff harmonic systems), as illustrated by simulating the dynamics of one-dimensional harmonic and quartic oscillators. A time-reversible integration algorithm, based on the symmetric Trotter decomposition of the propagator, is presented and tested against the symplectic velocity and position Verlet algorithms. In order to obtain an explicit form for the symmetric Trotter propagator algorithm, in the case of non-harmonic and non-linear interaction potentials, a position-dependent harmonically approximated propagator is introduced. Such a propagator approximates the dynamics of the configurational degrees of freedom as if they were locally moving in a harmonic potential. The resulting approximated locally harmonic dynamics is tested with good results in the case of a one-dimensional quartic oscillator and a three-dimensional N-particle system interacting through a soft Weeks-Chandler-Andersen potential.

Keywords: Non-Hamiltonian thermostat, configurational temperature, time-reversible algorithms
PACS: 05.10.-a, 07.05.Tp, 02.60.Cb
2000 MSC: 82-08, 68U20, 68W01

1. Introduction

It is known that the control of the temperature in molecular dynamics simulations [6, 7, 8, 9, 10] can be implemented through the Gaussian [1], the Nosé-Hoover [2, 3] or the Langevin [4, 5] thermostats. However, a new generation of so-called configurational

*E-mail:asergi@unime.it

thermostats (which control the configurational temperature [11, 12] instead of its kinetic counterpart) has been recently derived. The configurational temperature was initially used to check the validity of Monte Carlo codes [13]. At equilibrium in the microcanonical ensemble, it was found that such a temperature is equivalent to the kinetic one [14]. Successively, configurational thermostats were applied to non-equilibrium simulations, where they were shown to provide certain advantages over traditional kinetic schemes [23]. One such an advantage stems from the need to know the form of the local streaming velocity (starting from which, the correct thermal contribution can be computed) in order to correctly control the temperature by using a kinetic thermostat scheme. However, such a form is not known in general and, when using kinetic schemes, the onset of fictitious string phases [15, 16, 17] or the generation of non-zero off-diagonal stresses [18] in a system under shear flow has been observed. It is worth mentioning, however, that an unbiased kinetic temperature can be defined from particle velocities by taking into account the subtraction of the non-equilibrium velocity field [19]. The interest in the study and use of configurational thermostats lies mostly in the possibility of getting rid of the difficulties discussed above.

In this paper we consider the configurational temperature Nosé-Hoover (CTNH) thermostat of Braga and Travis [22, 23] (which has been also extended to implement an isothermal-isobaric ensemble [20] and to study molecular systems [21]). Our first achievement is to reformulate such a thermostat in a quasi-symplectic phase space form, along the anti-symmetric matrix formalism of Ref. [8]. The phase space form, together with its generalized antisymmetric brackets, is a natural mathematical template for the formulation of both the equilibrium statistical mechanics and the linear response theory of so-called non-Hamiltonian systems [24, 25] (but perhaps, contrary to common use, one should term such systems quasi-Hamiltonian, as it is done in the rest of this paper) such as the CTNH thermostat. One distinctive advantage of the quasi-Hamiltonian phase space formalism [8, 24, 25] is that it allows one to easily find more general equations of motion without losing the property of having a conserved (quasi-)Hamiltonian. Exploiting the quasi-Hamiltonian structure of the CTNH thermostat in phase space, we introduce a hybrid configurational kinetic temperature Nosé-Hoover chain thermostat (called hybrid CKTNH chain thermostat in the rest of the paper) that is able to sample uniformly the equilibrium phase space of stiff systems. This cannot be proven rigorously but, as usual, it can be illustrated numerically by studying the relevant case of a stiff one-dimensional harmonic oscillator. The hybrid CKTNH chain thermostat couples the fictitious momentum of the configurational thermostat to an additional fictitious momentum variable that, in turn, controls the kinetic temperature of the configurational thermostat. A similar idea is notoriously been used in the Nosé-Hoover chain (NHC) thermostat [28].

In order to integrate the phase space equations of motion of both the CTNH and hybrid CKTNH chain thermostats, we use a reversible algorithm based on the symmetric Trotter decomposition of the Liouville propagator (which will be called STP algorithm in the following). For comparison, we also use symplectic position and velocity Verlet algorithm [29]. The STP algorithm can be written in an explicit form only for linear and harmonic potential. For more complicated potential (assuming that they can be expanded in Taylor series), we derive a position-dependent harmonically approximated (PDHA) STP algorithm that is both stable and accurate. We illustrate its validity by simulating a one-dimensional quartic oscillator and a three-dimensional Weeks-Chandler-

Andersen (WCA) fluid [32].

This paper is organized as follows. In Sec. 2 we briefly summarize the definition of configurational temperature and of the CTNH thermostat, as formulated by Braga and Travis. In Sec. 3 we introduce the quasi-Hamiltonian phase space formulation of the CTNH thermostat. Its STP integration scheme is provided in Sec. 3.1, while the symplectic velocity and position Verlet algorithms are given in Appendix A. The PDHA STP algorithm is also explained in Sec. 3.1. The hybrid CKTNH chain thermostat is introduced through the quasi-Hamiltonian phase space formalism in Sec. 4. The STP and PDHA STP algorithms for the hybrid CKTNH chain thermostat are presented in Sec. 4.1, while the symplectic velocity and position Verlet algorithms are given in Appendix B. In Sec. 5 we study a stiff one-dimensional oscillator and compare the performance of the CTNH and hybrid CKTNH chain thermostats finding that the second can reproduce the correct canonical distribution function of the relevant system. In Sec. 6 we study the hybrid CKTNH chain thermostatted dynamics of a quartic one-dimensional oscillator in a symmetric double well potential by means of the PDHA STP algorithm. The PDHA STP integrator of the CTNH thermostat is also studied in Sec. 7 in the case of a three-dimensional N-particle system interacting through a WCA potential [32]. It is found that the PDHA STP integrator performs well for all practical purposes. Finally, our conclusions are given in Sec. 8

2. Configurational Temperature Nosé-Hoover Thermostat

Let us consider a general system of N atoms in three dimensional space described in phase space by the 6N-dimensional vector $X = (q, p)$, where the positions and momenta of the particles are represented (using a multi-dimensional notation) by the two $3N$ dimensional coordinates q and p, respectively. The form of the Hamiltonian is given by

$$\mathcal{H}(X) = \mathcal{K}(p) + \mathcal{U}(q) \ , \tag{1}$$

where $\mathcal{K}$ and $\mathcal{U}$ denote the kinetic and the potential energy of the system, respectively. Various statistical mechanical definitions of temperature can be derived for such a system starting from the basic thermodynamic relation

$$\frac{1}{T} = \left(\frac{\partial S}{\partial E} \right)_V \ , \tag{2}$$

where S is the entropy, E the internal energy, and V the volume. Recently, Rugh [11] introduced a microcanonical definition of temperature given by

$$\frac{1}{k_{\rm B}T} = \left\langle \nabla_X \cdot \frac{\nabla_X \mathcal{H}}{|\nabla_X \mathcal{H}|^2} \right\rangle + \mathcal{O}\left(\frac{1}{N}\right) \ , \tag{3}$$

where ∇_X is the phase-space gradient operator and $k_{\rm B}$ is the Boltzmann constant. Jepps *et al.* [12] have later generalized Eq.(3) to

$$k_{\rm B}T \approx \frac{\langle \nabla_X \mathcal{H} \cdot \Omega(X) \rangle}{\langle \nabla_X \cdot \Omega(X) \rangle} \ , \tag{4}$$

where Ω is a general vector field obeying the properties that $0 < \langle |\nabla_X \mathcal{H} \cdot \Omega(X)| \rangle < \infty$ and $0 < \langle |\nabla_X \cdot \Omega(X)| \rangle < \infty$.

Upon choosing $\Omega(X) = \boldsymbol{\chi}(\nabla_X \mathcal{H})$, where $\boldsymbol{\chi}$ is a matrix satisfying the equation $(\nabla_X \mathcal{H})\boldsymbol{\chi}(\nabla_X \mathcal{H}) \neq 0$, one can obtain two useful expressions for the temperature of the system. The first expression comes from choosing the element of the matrix χ_{ij} as δ_{ij} if i and j refer to the momentum variables and zero otherwise. In this case, Eq.(4) becomes

$$k_{\rm B}T_{\rm kin} = \frac{\langle|\nabla_p \mathcal{K}(p)|^2\rangle}{\langle|\nabla_p^2 \mathcal{K}(p)|\rangle} = \frac{\langle\sum_{i=1}^{3N} p_i^2/m_i^2\rangle}{\langle\sum_{i=1}^{3N}(3N/m_i)\rangle} \,, \tag{5}$$

where $\nabla_{\mathbf{p}}$ is the momentum gradient using the multidimensional notation. In Eq.(5) $\mathcal{K}(p) = \sum_i p_i^2/m_i$ and the index $i = 1, ..., 3N$ has been introduced to indicate unambiguously the operation of summation. Such an index constitutes a momentary departure from the otherwise adopted compact multidimensional notation. It will also be used in the following when clarity demands it. Equation (5) provides a kinetic expression for the temperature, $T_{\rm kin}$, and reduces to the equipartition theorem when all the particle's masses m are equal: $3Nk_{\rm B}T_{\rm kin} = \langle\sum_{i=1}^{3N} p_i^2/m_i\rangle$.

A configurational expression for the temperature, different from that derived in Ref. [11], is obtained by choosing the elements of the matrix $\boldsymbol{\chi}$ as δ_{ij} if i and j refer to coordinate variables and zero otherwise. Such an expression reads

$$k_{\rm B}T_{\rm conf} = \frac{\langle|\nabla_q \mathcal{U}(q)|^2\rangle}{\langle\nabla_q^2 \mathcal{U}(q)\rangle} = \frac{\langle|\sum_{i=1}^{3N} \nabla_{q_i} \mathcal{U}(q)|^2\rangle}{\langle\sum_{i=1}^{3N} \nabla_{q_i}^2 \mathcal{U}(q)\rangle} \,, \tag{6}$$

where ∇_q is the position gradient in phase space.

Using the temperature $T_{\rm conf}$ defined in Eq.(6), Braga and Travis introduced a configurational temperature Nosé-Hoover (CTNH) thermostat [22] defined by equations

$$\dot{q}_i = \frac{p_i}{m_i} - \eta\frac{\partial \mathcal{U}}{\partial q_i} \,, \tag{7}$$

$$\dot{p}_i = -\frac{\partial \mathcal{U}}{\partial q_i} \,, \tag{8}$$

$$\dot{\eta} = \frac{F_\eta}{M_\eta} \,, \tag{9}$$

where $i = 1, \ldots, 3N$, η is the thermostat variable with associated inertial mass M_η and

$$F_\eta = \sum_{i=1}^{3N}\left(\frac{\partial \mathcal{U}}{\partial q_i}\right)^2 - k_{\rm B}T\sum_{i=1}^{3N}\frac{\partial^2 \mathcal{U}}{\partial q_i^2} \,. \tag{10}$$

The above equations of motion admit the conserved quantity

$$H_\eta = H(X) + M_\eta\frac{\eta^2}{2} + k_{\rm B}T\int_0^t\left[\eta(t')\sum_{i=1}^{3N}\frac{\partial^2 \mathcal{U}}{\partial q_i^2}\right]dt' \,. \tag{11}$$

Equations (7-9) have been numerically integrated [26] using the algorithm detailed below, derived in the spirit of the velocity-Verlet algorithm [27]. Taking into account the

distinction between p and $m\dot{q}$ in Eq.s(7-9), the algorithm can be written explicitly as

$$q_i(t+\tau) = q_i(t) + \tau\frac{p_i(t)}{m_i} + \tau\left[\eta(t) + \frac{\tau}{2m_i}\right]F_i(t) \quad (12)$$

$$p_i(t+\tau) = p_i(t) + \frac{\tau}{2}\left[F_i(t) + F_i(t+\tau)\right] \quad (13)$$

$$\eta(t+\tau) = \eta(t) + \frac{\tau}{2M_\eta}\left[F_\eta(t) + F_\eta(t+\tau)\right] \ , \quad (14)$$

where $i = 1, \ldots, 3N$, $F_i = -\partial\mathcal{U}/\partial q_i$ and τ is the time step of integration. The algorithm has been tested in the equilibrium case with respect to the conservation law of Eq.(11) and by comparison with the results in Ref. [22] in the non-equilibrium steady-state conditions. It is important to note that in the case of Eq.s(7-9) the integration algorithm remains explicit.

3. Phase Space Formulation of the CTNH thermostat

The original formulation of the CTNH thermostat has been given by Braga and Travis by means of Eq.s(7-9), the conserved quantity in Eq.(11), and the thermostat force in Eq.(10). However, for further generalizations, it is useful to reformulate it within a phase space approach.

To this end, one can introduce the fictitious variable ζ and its associated momentum $p_\zeta = M_\zeta\eta$. Upon changing the notation so that $M_\zeta = M_\eta$ and $F_\zeta = F_\eta$, one can introduce the conserved quantity

$$H^\zeta = \sum_{i=1}^{3N}\frac{p_i^2}{2m_i} + \mathcal{U}(q) + \frac{p_\zeta^2}{2M_\zeta} + k_{\rm B}T\zeta \quad (15)$$

and the phase space equations of motion (q and p being $3N$-dimensional vectors)

$$\dot{q} = \frac{p}{m} - \frac{p_\zeta}{M_\zeta}\frac{\partial\mathcal{U}}{\partial q} \ , \quad (16)$$

$$\dot{\zeta} = G(q)\frac{p_\zeta}{M_\zeta} \ , \quad (17)$$

$$\dot{p} = -\frac{\partial\mathcal{U}}{\partial q} \ , \quad (18)$$

$$\dot{p}_\zeta = F_\zeta(q) \ , \quad (19)$$

where

$$G(q) = \sum_{i=1}^{3N}\frac{\partial^2\mathcal{U}}{\partial q_i^2} \ . \quad (20)$$

Defining an extended phase space point as $x = (q, \zeta, p, p_\zeta)$, the equations of motion (16-19) can be written in matrix form as

$$\dot{x}_i = \sum_{j=1}^{6N+2}\mathcal{B}_{ij}^{\rm CTNH}\frac{\partial H^\zeta}{\partial x_j} \qquad (i = 1, ..., 6N+2) \ . \quad (21)$$

In Eq.(21), the following $(6N+2)\times(6N+2)$ antisymmetric tensor field has been introduced

$$\boldsymbol{\mathcal{B}}^{\mathrm{CTNH}} = \begin{bmatrix} 0 & 0 & 1 & -\frac{\partial \mathcal{U}}{\partial q} \\ 0 & 0 & 0 & G(q) \\ -1 & 0 & 0 & 0 \\ \frac{\partial \mathcal{U}}{\partial q}^T & -G(q) & 0 & 0 \end{bmatrix} , \tag{22}$$

where we have used a compact notation for the $3N\times 3N$ block diagonal matrices and for the column vector $\partial\mathcal{U}/\partial q$ and its transpose, the row vector $(\partial\mathcal{U}/\partial q)^T$.

The Eq.s(16-19), with the conserved quantity (15), are equivalent to the original Eq.s(7-9),with the conserved quantity in Eq.(11). It is simple to show that, under the assumption of ergodicity, the phase space equation of motions of the Nosé-Hoover configurational thermostat sample the canonical distribution. As a matter of fact, at equilibrium and if the dynamics is ergodic, Eq.s(7-9) generate the distribution function

$$f_{\mathrm{eq}}^{\mathrm{CTNH}} = \delta\left(H^{\zeta}-\mathcal{C}\right)\exp[-w(x)] , \tag{23}$$

where $w(x)$ is a phase space function defined by $dw/dt = \kappa$, and $\kappa = (\partial\mathcal{B}^{\mathrm{CTNH}}_{\alpha\beta}/\partial x_\alpha))\partial H^{\zeta}/\partial x_\beta = -\dot{\zeta}$ is the compressibility of phase space. Upon defining $H^{\zeta,T} = H^{\zeta} - k_{\mathrm{B}}T\zeta$, one easily finds that $\kappa = (1/k_{\mathrm{B}}T)dH^{\zeta,T}/dt$ so that averages of functions of the type $a = a(q,p)$ with the weight in Eq.(23) provide canonical ensemble values. However, the assumption of ergodicity regarding the dynamics defined by Eq.s(16-19) is not correct, at least as far it regards stiff systems. To this end, the phase space formulation and the antisymmetric matrix in Eq.(22) provide a basis for the introduction of a more general, energy-conserving dynamics that is able to sample ergodically the time evolution of stiff systems. This will be dealt with in Sec. 3.1.

3.1. STP Integrators for phase space CTNH thermostat

Upon introducing multidimensional phase space coordinates (q,p) for describing the system of interest, the dynamics of the phase space CTNH thermostat can be defined in terms of the following Liouville operators:

$$L_1^{\mathrm{CTNH}} = \left(\frac{p}{m}+F(q)\frac{p_\zeta}{M_\zeta}\right)\frac{\partial}{\partial q} \tag{24}$$

$$L_2^{\mathrm{CTNH}} = F(q)\frac{\partial}{\partial p} \tag{25}$$

$$L_3^{\mathrm{CTNH}} = G(q)\frac{p_\zeta}{M_\zeta}\frac{\partial}{\partial \zeta} \tag{26}$$

$$L_4^{\mathrm{CTNH}} = F_\zeta(q)\frac{\partial}{\partial p_\zeta} \tag{27}$$

where $F(q)$ is the force acting on the system coordinates q and

$$G(q) = \frac{\partial^2\mathcal{U}}{\partial q^2} \tag{28}$$

$$F_\zeta(q) = \left(\frac{\partial\mathcal{U}}{\partial q}\right)^2 - k_{\mathrm{B}}T\frac{\partial^2\mathcal{U}}{\partial q^2} . \tag{29}$$

The total Liouville operator is obviously defined as $L^{\rm CTNH} = \sum_{i=1}^{4} L_i^{\rm CTNH}$. Denoting the time step with τ, one can introduce the propagators associated to the Liouville operators in Eq.s(24-27): $U_\alpha^{\rm CTNH}(\tau) = \exp(\tau L_\alpha^{\rm CTNH})$, for $\alpha = 1, ..., 4$.

A possible symmetric Trotter factorization of the propagator is given as follows:

$$\begin{aligned} U^{\rm CTNH}(\tau) &= U_4^{\rm CTNH}\left(\frac{\tau}{4}\right) U_3^{\rm CTNH}\left(\frac{\tau}{2}\right) U_4^{\rm CTNH}\left(\frac{\tau}{4}\right) \\ &\times U_2^{\rm CTNH}\left(\frac{\tau}{2}\right) U_1^{\rm CTNH}(\tau)\, U_2^{\rm CTNH}\left(\frac{\tau}{2}\right) \\ &\times U_4^{\rm CTNH}\left(\frac{\tau}{4}\right) U_3^{\rm CTNH}\left(\frac{\tau}{2}\right) U_4^{\rm CTNH}\left(\frac{\tau}{4}\right) . \end{aligned} \tag{30}$$

The action of the propagators $U_\alpha^{\rm CTNH}$ for $\alpha = 2, 3, 4$ can be easily determined:

$$p \to p + \tau F(q)\ \} \quad : \quad U_2^{\rm CTNH}(\tau) , \tag{31}$$

$$\zeta \to \zeta + \tau G(q)\frac{p_\zeta}{M_\zeta}\ \} \quad : \quad U_3^{\rm CTNH}(\tau) , \tag{32}$$

$$p_\zeta \to p_\zeta + \tau F_\zeta(q)\ \} \quad : \quad U_4^{\rm CTNH}(\tau) . \tag{33}$$

However, the action of $U_1^{\rm CTNH}(\tau)$ cannot be determined for a general potential $U(q)$.

If the potential $\mathcal{U}(q) = (1/2)kq^2$ is quadratic (so that the force $F(q)$ is linear in q), the Liouville operator $L_1^{\rm CTNH}$ must be substituted with $L_{1,\rm h}^{\rm CTNH}$:

$$L_{1,\rm h}^{\rm CTNH} = \left(\frac{p}{m} - kq\frac{p_\zeta}{M_\zeta}\right)\frac{\partial}{\partial q} , \tag{34}$$

In the case of quadratic potentials, the action of the propagator $U_{1,\rm h}^{\rm CTNH}(\tau)$, associated to the Liouville operator $L_{1,\rm h}^{\rm CTNH}$ can be determined analytically: one has simply to consider the differential equation $\dot{q} = L_{1,\rm h}^{\rm CTNH} q$ and integrate by parts between 0 and τ. The result is

$$q \to q\exp\left(-\tau k\frac{p_\zeta}{M_\zeta}\right)\left[\frac{\sinh\left(\tau\frac{k}{2}\frac{p_\zeta}{M_\zeta}\right)}{\tau\frac{k}{2}\frac{p_\zeta}{M_\zeta}}\right]\ \} \quad : \quad U_{1,\rm h}^{\rm CTNH}(\tau) . \tag{35}$$

The use of the STP propagator $U^{\rm CTNH}$ defined in Eq.(30) is difficult because of the generally unknown action of the $U_1^{\rm CTNH}(\tau)$ propagator. However, one can expect that for a continuous and sufficiently smooth potential, a linear approximation for the force could be used

$$F(q) \approx F(q_t) - \tilde{k}(q - q_t) , \tag{36}$$

where

$$\tilde{k} = \frac{1}{2}\left.\frac{\partial^2 \mathcal{U}}{\partial q^2}\right|_{q=q_t} . \tag{37}$$

position-dependent numerical spring parameters. Equation (36) clearly stems from a quadratic expansion of the interaction potential $\mathcal{U}$ around the position q_t describing the system at a given time t.

If the approximation of Eq.(36) is performed, the propagator

$$\begin{aligned} q \quad \rightarrow \quad & q \exp\left(-\tau\tilde{k}\frac{p_\zeta}{M_\zeta}\right) + \tau\left(\frac{p}{m} + F(q_t) + \tilde{k}q_t\right)\exp\left(-\tau\frac{\tilde{k}}{2}\frac{p_\zeta}{M_\zeta}\right)\left[\frac{\sinh\left(\tau\frac{\tilde{k}}{2}\frac{p_\zeta}{M_\zeta}\right)}{\tau\frac{\tilde{k}}{2}\frac{p_\zeta}{M_\zeta}}\right] \} \\ : \quad & \tilde{U}_{1,\mathrm{h}}^{\mathrm{CTNH}}(\tau)\ . \end{aligned} \tag{38}$$

can be substituted in place of $U_1^{\mathrm{CTNH}}(\tau)$ in Eq.(30). In such a way, one can obtain a position-dependent harmonically-approximated (PDHA) STP integrator for the CTNH thermostat in general provided the potential is smooth.

The position and velocity Verlet symplectic algorithms for integrating the CTNH thermostat are given in Appendix A.

4. Hybrid Configurational-Kinetic Temperature Nosé-Hoover Chain Thermostat

In order to obtain an ergodic configurational thermostat, one can exploit the idea of creating a chain of thermostats. The prototype of such an idea is given by the Nosè-Hoover chain thermostat [28]. Here, we will consider a hybrid chain where a configurational thermostat, which controls the particles' temperature is chained to a standard Nosé-Hoover (kinetic) thermostat, which, in turn, controls the kinetic energy of the configurational thermostat. We call such a thermostat hybrid Configurational-Kinetic Temperature Nosé-Hoover (CKTNH) chain thermostat. It will be shown, by means of a numerical study of the one-dimensional harmonic oscillator, that the hybrid CKTNH chain thermostat is able to sample correctly the equilibrium canonical distribution, even for stiff systems.

In order to introduce the hybrid CKTNH chain thermostat, one can define the conserved quantity as

$$H^{\zeta s} = \sum_i \frac{p_i^2}{2m_i} + \mathcal{U}(q) + \frac{p_\zeta^2}{2M_\zeta} + \frac{p_s^2}{2M_s} + k_{\mathrm{B}}T(\zeta + s) \tag{39}$$

and the equations of motion as

$$\dot{q} = \frac{p}{m} - \frac{p_\zeta}{M_\zeta}\frac{\partial U}{\partial q} \tag{40}$$

$$\dot{\zeta} = G(q)\frac{p_\zeta}{M_\zeta} \tag{41}$$

$$\dot{s} = \frac{p_s}{M_s} \tag{42}$$

$$\dot{p} = -\frac{\partial U}{\partial q} \tag{43}$$

$$\dot{p}_\zeta = F_\zeta(q) - \frac{p_s}{M_s}p_\zeta \tag{44}$$

$$\dot{p}_s = \frac{p_\zeta^2}{M_\zeta} - k_{\mathrm{B}}T \tag{45}$$

where s, p_s are the additional thermostat variables (with associated mass M_s) chained to ζ, p_{zeta}.

Upon defining the extended phase space point as $\tilde{x} = (q, \zeta, s, p, p_\zeta, p_s)$, the equations of motion (40-45) can be written in matrix form as

$$\dot{\tilde{x}}_\alpha = \sum_\beta \mathcal{B}^{\rm CKTNH}_{\alpha\beta} \frac{\partial H^{\zeta s}}{\partial \tilde{x}_\beta} \tag{46}$$

This can be seen from

$$\boldsymbol{\mathcal{B}}^{\rm CKTNH} = \begin{bmatrix} 0 & 0 & 0 & 1 & -\frac{\partial \mathcal{U}}{\partial q} & 0 \\ 0 & 0 & 0 & 0 & G(q) & 0 \\ 0 & 0 & 0 & 0 & 0 & 1 \\ -1 & 0 & 0 & 0 & 0 & 0 \\ \frac{\partial \mathcal{U}}{\partial q}^T & -G(q) & 0 & 0 & 0 & -p_\zeta \\ 0 & 0 & -1 & 0 & p_\zeta & 0 \end{bmatrix} \tag{47}$$

Under the assumption of ergodicity, Eq.s(40-45) generate the equilibrium distribution function

$$f^{\rm CKTNH}_{\rm eq} = \delta\left(H^{\zeta s} - \mathcal{C}\right) \exp[-\tilde{w}(\tilde{x})] \,, \tag{48}$$

where $\tilde{w}(\tilde{x})$ is the space space function defined by $d\tilde{w}/dt = \tilde{\kappa}$ and $\tilde{\kappa} = (\partial \mathcal{B}^{\rm CKTNH}_{\alpha\beta}/\partial x_\alpha)\partial H^{\zeta s}/\partial x_\beta = -(\dot{\zeta} + \dot{s})$. Upon defining $H^{\zeta s,T} = H^{\zeta s} - k_{\rm B}T(\zeta + s)$, one easily finds that $\tilde{\kappa} = (1/k_{\rm B}T) dH^{\zeta s,T}/dt$ so that averages of functions of the type $a = a(q,p)$ with the weight in Eq.(48) provide canonical ensemble values.

4.1. STP Integrators for the hybrid CKTNH Chain Thermostat

The dynamics of the hybrid CKTNH chain thermostat can be defined in terms of the following Liouville operators:

$$L^{\rm CKTNH}_1 = \left(\frac{p}{m} + F(q)\frac{p_\zeta}{M_\zeta}\right)\frac{\partial}{\partial q} = L^{\rm CTNH}_1 \,, \tag{49}$$

$$L^{\rm CKTNH}_2 = F(q)\frac{\partial}{\partial p} = L^{\rm CTNH}_2 \,, \tag{50}$$

$$L^{\rm CKTNH}_3 = G(q)\frac{p_\zeta}{M_\zeta}\frac{\partial}{\partial \zeta} = L^{\rm CTNH}_3 \,, \tag{51}$$

$$L^{\rm CKTNH}_4 = \frac{p_s}{M_s}\frac{\partial}{\partial s} \,, \tag{52}$$

$$L^{\rm CKTNH}_5 = F_\zeta(q)\frac{\partial}{\partial p_\zeta} = L^{\rm CTNH}_4 \,, \tag{53}$$

$$L^{\rm CKTNH}_6 = -p_\zeta\frac{p_s}{M_s}\frac{\partial}{\partial p_\zeta} \,, \tag{54}$$

$$L^{\rm CKTNH}_7 = \left(\frac{p^2_\zeta}{M_\zeta} - k_{\rm B}T\right)\frac{\partial}{\partial p_s} \,. \tag{55}$$

The total Liouville operator is given by $L^{\rm CKTNH} = \sum_{i=1}^{7} L_i^{\rm CKTNH}$. We can introduce the associated propagators as follows

$$\begin{aligned}
U_1^{\rm CKTNH}(\tau) &= \exp\left[\tau\left(\frac{p}{m} + F(q)\frac{p_\zeta}{M_\zeta}\right)\frac{\partial}{\partial q}\right] \\
&= U_1^{\rm CTNH}(\tau)\,, \qquad (56)\\
U_2^{\rm CKTNH}(\tau) &= \exp\left[\tau F(q)\frac{\partial}{\partial p}\right] = U_2^{\rm CTNH}(\tau)\,, \qquad (57)\\
U_3^{\rm CKTNH}(\tau) &= \exp\left[\tau\left(G(q)\frac{p_\zeta}{M_\zeta}\frac{\partial}{\partial \zeta} + \frac{p_s}{M_s}\frac{\partial}{\partial s}\right)\right], \qquad (58)\\
U_4^{\rm CKTNH}(\tau) &= \exp\left[\tau F_\zeta(q)\frac{\partial}{\partial p_\zeta}\right] = U_4^{\rm CTNH}(\tau)\,, \qquad (59)\\
U_5^{\rm CKTNH}(\tau) &= \exp\left[-\tau p_\zeta \frac{p_s}{M_s}\frac{\partial}{\partial p_\zeta}\right]\,, \qquad (60)\\
U_6^{\rm CKTNH}(\tau) &= \exp\left[\tau\left(\frac{p_\zeta^2}{M_\zeta} - k_{\rm B}T\right)\frac{\partial}{\partial p_s}\right]\,. \qquad (61)
\end{aligned}$$

A possible symmetric Trotter factorization of the exact propagator can be given as follows:

$$\begin{aligned}
U^{\rm CKTNH}(\tau) = &\left[\prod_{n=1}^{n_{\rm yosh}}\prod_{m=1}^{m_s}\left(\prod_{\alpha=1}^{3} U_{7-\alpha}^{\rm CKTNH}\left(\frac{w_n}{m_s}\frac{\tau}{4}\right)\right)\right. \\
\times\quad & \left. U_3^{\rm CKTNH}\left(\frac{w_n}{m_s}\frac{\tau}{2}\right)\left(\prod_{\alpha=1}^{3} U_{3+\alpha}^{\rm CKTNH}\left(\frac{w_n}{m_s}\frac{\tau}{4}\right)\right)\right] \\
\times\quad & U_2^{\rm CKTNH}\left(\frac{\tau}{2}\right) U_1^{\rm CKTNH}(\tau)\, U_2^{\rm CKTNH}\left(\frac{\tau}{2}\right) \\
\times\quad & \left[\prod_{n=1}^{n_{\rm yosh}}\prod_{m=1}^{m_s}\left(\prod_{\alpha=1}^{3} U_{7-\alpha}^{\rm CKTNH}\left(\frac{w_n}{m_s}\frac{\tau}{4}\right)\right)\right. \\
\times\quad & \left. U_3^{\rm CKTNH}\left(\frac{w_n}{m_s}\frac{\tau}{2}\right)\left(\prod_{\alpha=1}^{3} U_{3+\alpha}^{\rm CKTNH}\left(\frac{w_n}{m_s}\frac{\tau}{4}\right)\right)\right]\,,
\end{aligned} \qquad (62)$$

where we have introduced a Yoshida higher order integration scheme [30, 31] and a multiple time step procedure [10, 35] (where m_s is the maximum number of iterations in such a procedure) on the chain of thermostats. If the number of iterations is $n_{\rm yosh} = 3$, the weights w_n (n=1,2,3) take the values $w_1 = w_3 = 1/(2 - 2^{1/3})$ and $w_2 = 1 - 2w_1$; while if $n_{\rm yosh} = 5$, the weights take the values $w_1 = w_2 = w_4 = w_5 = 1/(4 - 4^{1/3})$ and $w_3 = 1 - 4w_1$.

From the propagator in Eq.(62), one can set out to devise a STP integrator by noting that the action of $U_2^{\rm CKTNH}(\tau)$ is identical to that of $U_2^{\rm CTNH}(\tau)$ in Eq.(31) and the action of $U_4^{\rm CKTNH}(\tau)$ is identical to that of $U_4^{\rm CTNH}(\tau)$ in Eq.(33). The action of the other

propagators is easily found to be

$$\left.\begin{array}{rcl} \zeta & \rightarrow & \zeta + \tau G(q) p_\zeta / M_\zeta \\ s & \rightarrow & s + \tau p_s / M_s \end{array}\right\} \; : \; U_3^{\mathrm{CKTNH}}(\tau) \; , \tag{63}$$

$$\left. p_\zeta \rightarrow \exp\left(-\tau p_s / M_s\right) \right\} \; : \; U_5^{\mathrm{CKTNH}}(\tau) \; , \tag{64}$$

$$\left. p_s \rightarrow p_s + \tau \left(p_\zeta^2 / M_\zeta - k_{\mathrm{B}} T \right) \right\} \; : \; U_6^{\mathrm{CKTNH}}(\tau) \; . \tag{65}$$

However, the action of $U_1^{\mathrm{CKTNH}}(\tau)$ is identical to that of $U_1^{\mathrm{CTNH}}(\tau)$ so that one does not know how to apply in the case of a general potential. In the case of a quadratic potential L_1^{CKTNK} goes to $L_{1,\mathrm{h}}^{\mathrm{CKTNH}}$, which is identical to $L_{1,\mathrm{h}}^{\mathrm{CTNH}}$ in Eq.(34). One would then obtain an associated propagator $U_{1,\mathrm{h}}^{\mathrm{CKTNH}}(\tau)$ whose action is identical to that of $U_{1,\mathrm{h}}^{\mathrm{CTNH}}(\tau)$ in Eq.(35). In such a case, the propagator in Eq.(62) would lead to a straightforward STP integrator (after the substitution $U_1^{\mathrm{CKTNH}}(\tau) \rightarrow U_{1,\mathrm{h}}^{\mathrm{CKTNH}}(\tau)$).

For sufficiently smooth potentials, the local quadratic approximation of Eq.(36) would provide the parameters $\tilde{k}$ that once substituted into $U_{1,\mathrm{h}}^{\mathrm{CKTNH}}(\tau)$ would give an approximation, $\tilde{U}_{1,\mathrm{h}}^{\mathrm{CKTNH}}(\tau) = \tilde{U}_{1,\mathrm{h}}^{\mathrm{CTNH}}(\tau)$, where $\tilde{U}_{1,\mathrm{h}}^{\mathrm{CTNH}}(\tau)$ is defined in Eq.(36), to the exact but untreatable $U_1^{\mathrm{CKTNH}}(\tau)$. In such a way, one can obtain a PDHA STP integrator for the hybrid CKTNH chain thermostat.

The position and velocity Verlet algorithm for integrating the dynamics of the hybrid CKTNH chain thermostat (without the PDHA) are given in Appendix B.

5. Harmonic Oscillator

The harmonic oscillator is a paradigmatic model to assess the ergodic property of a thermostat. In the following we consider one-dimensional phase space coordinates (q, p). The potential of the harmonic oscillator is a quadratic function:

$$\mathcal{U}^{\mathrm{h}}(q) = \frac{1}{2} k q^2 \; , \tag{66}$$

where k is the spring constant. For the harmonic potential in Eq.(66), the quantities $G(q)$ and $F_\zeta(q)$ in Eq.s(28) and (29), respectively, become $G(q) \rightarrow G^{\mathrm{h}}(q) = k$ and $F_\zeta(q) \rightarrow F_\zeta^{\mathrm{h}}(q) = k^2 q^2 - k_{\mathrm{B}} T k$

A STP integrator for the harmonic oscillator coupled to a CTNH thermostat can be implemented by considering the action of the propagators in Eq.s(31-33) and (35), together with the total time-reversible approximated propagator $U^{\mathrm{CTNH}}(\tau)$ in Eq.(30) (where one has to perform the substitution $U_1(\tau) \rightarrow U_{1,\mathrm{h}}(\tau)$). The expression for the conserved quantity is given by substituting $\mathcal{U}^{\mathrm{h}}(q)$ in place of $\mathcal{U}(q)$ in Eq.(15).

A STP integrator for the harmonic oscillator coupled to a hybrid CKTNH chain thermostat can be implemented considering the action of the propagator in Eq.(62) and substituting $\mathcal{U}^{\mathrm{h}}$, $F_\zeta^{\mathrm{h}}(q)$ and $G^{\mathrm{h}}(q)$ for their correspondent general quantities where needed. Similarly, the expression for the conserved quantity is given by substituting $\mathcal{U}^{\mathrm{h}}(q)$ in place of $\mathcal{U}^q(q)$ in Eq.(39).

For the sake of comparison, it is also useful to consider the integration of the CTNH and hybrid CKTNH chain thermostatted harmonic oscillator by means of symplectic algorithms. The general framework for determining a symplectic integrator (once the equations of motion are given in terms of multidimensional coordinates) is provided in

Appendix A. The same Appendix shows the algorithm for integrating the dynamics of the CTNH thermostat.

We can set $m = k = k_{\mathrm{B}}T = 1$ and study the conservation property, plot the phase space (q, p), and check whether p and q are distributed according to $\exp[-\beta p^2/2m]$ and $\exp[-\beta k q^2/2]$, respectively.

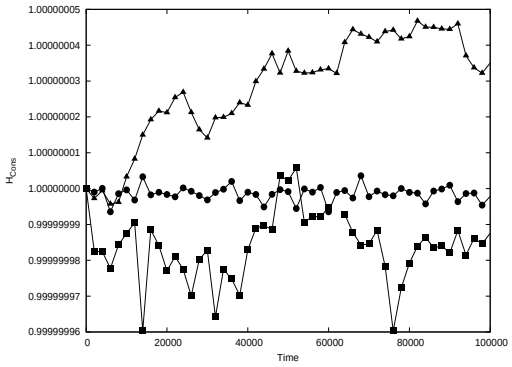

Figure 1: Figure showing the conserved quantity versus time for the position (squares) and velocity (triangles) Verlet symplectic algorithms as well as the STP integration algorithm (circles), for the case of an harmonic oscillator attached to a configurational thermostat. The conserved energies are all normalized. The above results were obtained using a thermostat mass of 2.0, a spring constant of 1.0 and a time step of $1 \cdot 10^{-4}$ for all three calculations.

From Fig. 1. we see that the behavior of the conserved quantity as time evolves is similar for each of the integration algorithms implemented. In addition, the three algorithms appear to be stable over a long time.

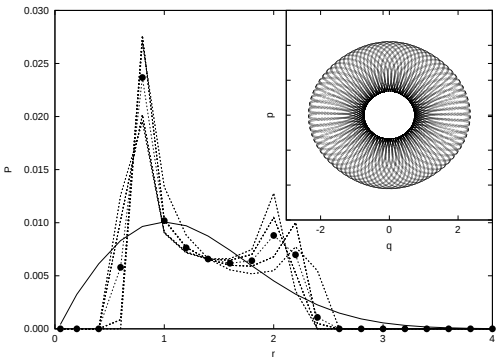

Figure 2: Figure showing the phase space radial distribution (main figure) for an harmonic oscillator attached to a configurational thermostat, using the STP integration algorithm. The solid line is the analytical distribution. The inset figure shows the occupied phase-space for the simulation. The above results were obtained using a thermostat mass of 2.0, a spring constant of 1.0 and a time step of $1 \cdot 10^{-4}$.

From Figure 2 one can see that the configurational thermostat is unable to preserve the ergodicity property of the harmonic oscillator system. In order to overcome this problem

we consider a hybrid configurational-kinetic thermostat. This thermostat consists of a Nosè-Hoover kinetic thermostat attached to a configurational thermostat, which is in turn attached to the system. This hybrid thermostat was implemented for the case of the quadratic harmonic potential, as well as the quartic, double-well potential.

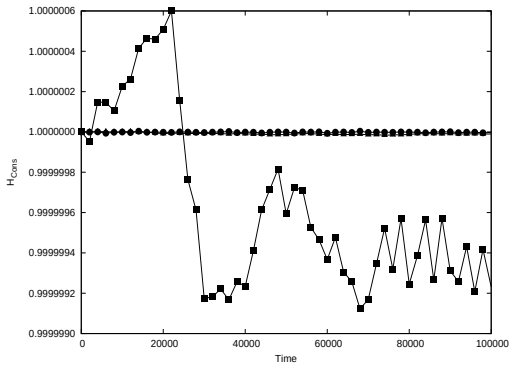

Figure 3: Figure showing the conserved quantity versus time of an harmonic oscillator attached to a hybrid configurational-kinetic chain thermostat, using the STP integration algorithm (circles), compared with results using the configurational thermostat (triangles) and the Nosè-Hoover chain thermostat (squares). The configrational thermostat mass was 2.0, while the hybrid thermostat result was obtained using thermostat masses of $M_\zeta = 10$ and $M_s = 10^{-1}$. The Nosè-Hoover chain thermostat masses were $M_\zeta = M_s = 1.0$. A spring constant of 1.0 and a time step of $1 \cdot 10^{-4}$ were used for all three calculations.

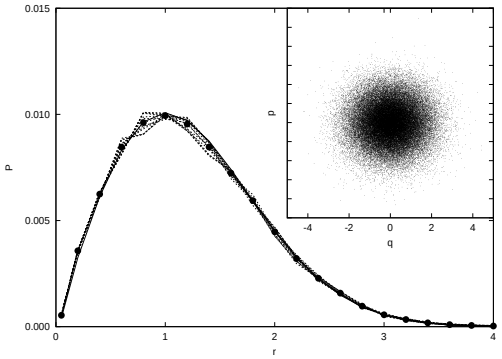

Figure 4: Figure showing the phase space radial distribution (main figure) for an harmonic oscillator attached to a hybrid configurational-kinetic chain thermostat, using the STP integration algorithm. The solid line is the analytical distribution. The inset figure shows the occupied phase space for the simulation. The above results were obtained using thermostat masses of $M_\zeta = 10$ and $M_s = 10^{-1}$, a spring constant of 1.0 and a time step of $1 \cdot 10^{-4}$.

6. Hybrid CKTNH Chain Dynamics in a Quartic Potential

Let us consider a one-dimensional coordinate q in a quartic potential

$$\mathcal{U}^{\rm dw}(q) \;=\; \frac{a}{4}q^4 - \frac{b}{2}q^2 \; . \tag{67}$$

A proper choice of the numerical value of the parameters a and b (which in this work were both taken to be 1) gives to this potential the profile of a symmetric double well.

In order to provide an example in favor of the effectiveness of the PDHA STP integrator, we consider the hybrid CKTNH chain thermostatted dynamics of a particle moving in the potential of Eq.(67). For such a system the thermostat quantities become $G(q) \rightarrow G^{\rm dw}(q) = 3aq^2 - b$ and $F_\zeta \rightarrow F_\zeta^{\rm dw} = \left(aq^3 - bq\right)^2 - k_{\rm B}T\left(3aq^2 - b\right)$. The equations of motion and the conserved quantity are obtained by substituting $G^{\rm dw}(q)$, $F_\zeta^{\rm dw}$ and $\mathcal{U}^{\rm dw}(q)$ into Eq.s(39) and (40-45).

A PDHA STP integrator of the hybrid CKTNH chain thermostatted dynamics is obtained upon approximating $\mathcal{U}^{\rm dw}(q)$ with a quadratic form $\tilde{\mathcal{U}}^{\rm h} = (1/2)\tilde{k}q^2$ and using this latter expression in the STP propagator in Eq.(62). In order to assess the stability of the PDHA STP integrator we have used both position and velocity Verlet symplectic algorithms.

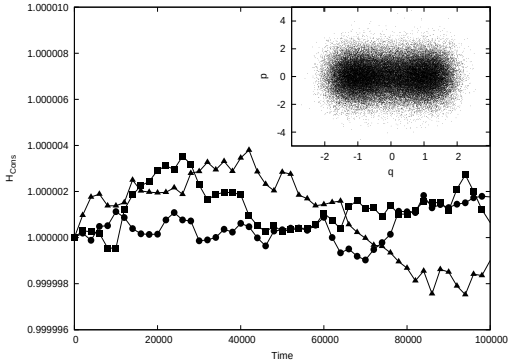

Figure 5: Figure showing the conserved quantity versus time (main figure) for the position (squares) and velocity (triangles) Verlet symplectic algorithms as well as the STP integration algorithm (circles), for the case of a quartic potential function attached to a hybrid configurational-kinetic thermostat. The conserved energies are all normalized. The inset figure shows the occupied phase space for the simulation in the case of the STP algorithm. The above results were obtained using thermostat masses of $M_\zeta = 10$ and $M_s = 10^{-1}$, a spring constant of 1.0 and a time step of $1 \cdot 10^{-4}$ for all three calculations.

The results for the STP scheme, as well as the symplectic algorithms, were obtained using thermostat masses of $M_\zeta = 10$ and $M_s = 10^{-1}$ and a time-step of 0.0001. Yoshida weights and a multiple time-step equal to 5 were also used. The simulations were run for a total of 10^9 integration steps.

From Figures 4 and 5 we can see that when the hybrid configurational-kinetic thermostat is used, we are able to achieve ergodicity for both the harmonic potential and the double-well potential.

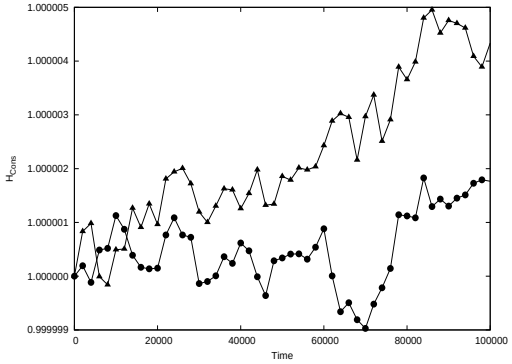

Figure 6: Figure showing the conserved quantity versus time for the STP integration algorithm (circles), in the case of a quartic potential function attached to a hybrid configurational-kinetic thermostat, compared with the result obtained using a Nosè-Hoover chain thermostat. The conserved energies are all normalized. The above results were obtained using thermostat masses of $M_\zeta = 10$ and $M_s = 10^{-1}$ for the hybrid configurational thermostat, while the NHC thermostats mass was set to $M_\zeta = 1.0$ and $M_s = 1.0$. A spring constant of 1.0 and a time step of $1 \cdot 10^{-4}$ were used for both calculations.

7. CTNH Dynamics in a WCA Potential

Let us consider a system of N particles in three-dimensional space. The particles and momenta phase space coordinates will be denoted by q_i and p_i, respectively, where $i = 1, ..., 3N$. Let us also assume that the particles interact through a WCA potential (which is a Lennard-Jones potential cut and shifted at its minimum):

$$\mathcal{U}^{\mathrm{WCA}}(r_{ij}) = \begin{cases} 4\epsilon \left[\left(\frac{\sigma}{r_{ij}} \right)^{12} - \left(\frac{\sigma}{r_{ij}} \right)^{6} \right] + \epsilon & \text{if } r_{ij} \leq r_{\min} \equiv \sigma \sqrt[6]{2} \,, \\ 0 & \text{otherwise} \,, \end{cases} \tag{68}$$

where $r_{ij} = \sqrt{q_{ij} \cdot q_{ij}}$ and $q_{ij} = q_i - q_j$. Such a potential is usually called Weeks-Chandler-Andersen (WCA) potential [32] since it was used by these researchers to develop the perturbative description commonly referred to as the "van der Waals picture of simple fluids" [33, 34]. Since we do not expect stiff modes, it is reasonable to assume the thermostatting of such a system by means of the CTNH thermostat is ergodic. For clarity, we write the CTNH equations of motion for the WCA system. These equations

are:

$$\dot{q}_i = \frac{p_i}{m_i} - \frac{p_\zeta}{M_\zeta}\frac{\partial \mathcal{U}^{\rm WCA}}{\partial q_i} \tag{69}$$

$$\dot{p}_i = -\frac{\partial \mathcal{U}^{\rm WCA}}{\partial q_i} = F_i^{\rm WCA} \tag{70}$$

$$\dot{\zeta} = \sum_{i=1}^{3N}\left(\frac{\partial^2 \mathcal{U}^{\rm WCA}}{\partial q_i^2}\right)\frac{p_\zeta}{M_\zeta} = G^{\rm WCA}(q)\frac{p_\zeta}{M_\zeta} \tag{71}$$

$$\dot{p}_\zeta = = \left[\sum_{i=1}^{3N}(F_i^{\rm WCA})^2 - k_{\rm B}TG^{\rm WCA}(q)\right] = F_\zeta^{\rm WCA} \tag{72}$$

The associated Liouville operators are

$$L_{1,\rm WCA}^{\rm CTNH} = \left(\frac{p}{m} + F^{\rm WCA}(q)\frac{p_\zeta}{M_\zeta}\right)\frac{\partial}{\partial q} \tag{73}$$

$$L_{2,\rm WCA}^{\rm CTNH} = F^{\rm WCA}(q)\frac{\partial}{\partial p} \tag{74}$$

$$L_{3,\rm WCA}^{\rm CTNH} = G^{\rm WCA}(q)\frac{p_\zeta}{M_\zeta}\frac{\partial}{\partial \zeta} \tag{75}$$

$$L_{4,\rm WCA}^{\rm CTNH} = F_\zeta^{\rm WCA}(q)\frac{\partial}{\partial p_\zeta} \tag{76}$$

The propagators associated to the Liouville operators in Eq.s(73-76) are defined as $U_{\alpha,\rm WCA}^{\rm CTNH}(\tau) = \exp[\tau L_{\alpha,\rm WCA}^{\rm CTNH}]$, for $\alpha = 1, ..., 4$. In order to devise an explicit algorithm, the total exact propagator can be factorized as in Sec. 3.1. For the sake of clarity, we rewrite the chosen factorization below:

$$\begin{aligned} U_{\rm WCA}^{\rm CTNH}(\tau) &= U_{4,\rm WCA}^{\rm CTNH}\left(\frac{\tau}{4}\right)U_{3,\rm WCA}^{\rm CTNH}\left(\frac{\tau}{2}\right)U_{4,\rm WCA}^{\rm CTNH}\left(\frac{\tau}{4}\right) \\ &\times U_{2,\rm WCA}^{\rm CTNH}\left(\frac{\tau}{2}\right)U_{1,\rm WCA}^{\rm CTNH}(\tau)\,U_{2,\rm WCA}^{\rm CTNH}\left(\frac{\tau}{2}\right) \\ &\times U_{4,\rm WCA}^{\rm CTNH}\left(\frac{\tau}{4}\right)U_{3,\rm WCA}^{\rm CTNH}\left(\frac{\tau}{2}\right)U_{4,\rm WCA}^{\rm CTNH}\left(\frac{\tau}{4}\right)\ . \end{aligned} \tag{77}$$

The action of $U_{\alpha,\rm WCA}^{\rm CTNH}(\tau)$ for $\alpha = 2, 3, 4$ is given in Eq.s(31-33). The propagator $U_{1,\rm WCA}^{\rm CTNH}(\tau)$ can be approximated locally with a quadratic potential in order to obtain a PDHA-STP scheme of integration. This leads to a modified Liouville operator $L_{1,\rm WCA}^{\rm CTNH} \to \tilde{L}_{1,\rm h}^{\rm CTNH}$ and modified propagator $U_{1,\rm WCA}^{\rm CTNH}(\tau) \to \tilde{U}_{1,\rm h}^{\rm CTNH}(\tau)$. The action of $\tilde{U}_{1,\rm h}^{\rm CTNH}(\tau)$ is known and given by Eq.(38). Upon substituting $\tilde{U}_{1,\rm h}^{\rm CTNH}(\tau)$ in place of $U_{1,\rm WCA}^{\rm CTNH}(\tau)$ in the propagator in Eq.(77), one obtains a PDHA-STP integrator for the WCA potential.

Simulations were run for a system comprising 1000 particles using both the CTNH and NH thermostats. Each calculation was performed using a time step of $2.5 \cdot 10^{-4}$ for 10^6 integration steps. The thermostat temperature $T_{\rm ext}$ was set to 0.722, and the density of the system was 0.8442.

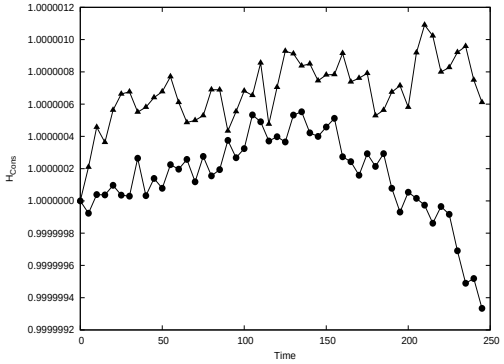

Figure 7: Figure showing the conserved quantity versus time for the Lennard-Jones potential using the configurational thermostat (circles), and the Nosè-Hoover thermostat (triangles). The simulation included 1000 particles. A thermostat mass of $M_\zeta = 10^{20}$ was used for the CTNH thermostat, while the NH thermostat masses was unity. The time-step size was $2.5 \cdot 10^{-4}$, the external temperature $T_{\text{ext}} = 0.722$ and system density 0.8442 for both calculations. The average variance in the conserved quantity, calculated using the configurational thermostat, was determined to be $1.060 \cdot 10^{-7}$, while the variation in the case of the Nosè-Hoover thermostat was found to be $1.523 \cdot 10^{-7}$.

Figure 7 displays the comparison of the conserved quantity for each of the two calculations. We see that both the NH and CTNH methods conserve the quantity with excellent precision, with the CTNH performing slightly better than the NH, thus demonstrating that the quadratic approximation used when propagating the particle positions is sufficient for producing good dynamics.

The run times for each calculation were also compared, and it was found that they were close together, with the NH calculation approximately 10% faster than that of the CTNH.

8. Conclusion

We have recasted the configurational temperature Nosé-Hoover thermostat using the phase space quasi-Hamiltonian formalism. Within this latter mathematical language, we have introduced a hybrid configurational-kinetic temperature Nosé-Hoover chain thermostat that can achieve a uniform sampling of phase space for stiff harmonic systems. This has been illustrated by simulating the dynamics of one-dimensional harmonic and quartic oscillators. A time-reversible integration algorithm, based on the symmetric Trotter decomposition of the propagator, has also been presented and tested against the symplectic velocity and position Verlet algorithms. In order to obtain an explicit form for the symmetric Trotter propagator algorithm, in the case of non-harmonic and non-linear interaction potentials, a position-dependent harmonically approximated propagator has bee devised. Such a propagator approximates the dynamics of the configurational degrees of freedom as if they were locally moving in a harmonic potential. The resulting approximated locally harmonic dynamics was tested with good results in the case of a one-dimensional quartic oscillator and a three-dimensional N-particle system interacting through a soft Weeks-Chandler-Andersen potential.

Appendix A. Symplectic Algorithms

Consider equations of motion written in the form

$$\dot{q} = H_p(q,p)\,, \tag{A.1}$$
$$\dot{p} = -H_q(q,p)\,, \tag{A.2}$$

where (q,p) can be interpreted as multidimensional coordinates and $H_q = \partial H/\partial q$, $H_p = \partial H/\partial p$, with H denoting the Hamiltonian function of the system under study. The symplectic formulation of the velocity Verlet algorithm is given by

$$p(t+\tau/2) = p(t) - \frac{\tau}{2} H_q(q(t), p(t+\tau/2)) \tag{A.3}$$
$$\begin{aligned} q(t+\tau) &= q(t) + \frac{\tau}{2}\left[H_p(q(t), p(t+\tau/2))\right. \\ &+ \left. H_p(q(t+\tau), p(t+\tau/2))\right] \end{aligned} \tag{A.4}$$
$$p(t+\tau) = p(t+\tau/2) - \frac{\tau}{2} H_q(q(t+\tau), p(t+\tau/2)) \tag{A.5}$$

while the symplectic formulation of the position Verlet algorithm is given by

$$q(t+\tau/2) = q(t) + \frac{\tau}{2} H_p(q(t+\tau/2), p(t)) \tag{A.6}$$
$$\begin{aligned} p(t+\tau) &= p(t) - \frac{\tau}{2}\left[H_q(q(t+\tau/2), p(t))\right. \\ &+ \left. H_q(q(t+\tau/2), p(t+\tau))\right] \end{aligned} \tag{A.7}$$
$$q(t+\tau) = q(t+\tau/2) + \frac{\tau}{2} H_p(q(t+\tau/2), p(t+\tau)) \tag{A.8}$$

For the phase space CTNH thermostat, the symplectic velocity Verlet algorithm reads

$$p(t+\tau/2) = p(t) + \frac{\tau}{2} F(q(t)) \tag{A.9}$$
$$p_\zeta(t+\tau/2) = p_\zeta(t) + \frac{\tau}{2} F_\zeta(q(t)) \tag{A.10}$$
$$\begin{aligned} q(t+\tau) &= q(t) + \tau\frac{p(t+\tau/2)}{m} + \frac{\tau}{2}\frac{p_\zeta(t+\tau/2)}{M_\zeta} \\ &\times \left[F(q(t)) + F(q(t+\tau))\right] \end{aligned} \tag{A.11}$$
$$\begin{aligned} \zeta(t+\tau) &= \zeta(t) + \frac{\tau}{2}\frac{p_\zeta(t+\tau/2)}{M_\zeta} \\ &\times \left[G(q(t)) + G(q(t+\tau))\right] \end{aligned} \tag{A.12}$$
$$p(t+\tau) = p(t+\tau/2) + \frac{\tau}{2} F(q(t+\tau)) \tag{A.13}$$
$$p_\zeta(t+\tau) = p_\zeta(t+\tau/2) + \frac{\tau}{2} F_\zeta(q(t+\tau)) \tag{A.14}$$

Because of the dependencies in Eqs (A.11-A.12) the algorithm is implicit and can be solved by iterating over (A.11-A.12).

The symplectic position Verlet algorithm for the CTNH thermostat is given by

$$
\begin{aligned}
q(t+\tau/2) &= q(t) + \frac{\tau}{2}\frac{p(t)}{m} + \frac{\tau}{2}\frac{p_\zeta(t)}{M_\zeta}F(q(t+\tau/2)) && \text{(A.15)}\\
\zeta(t+\tau/2) &= \zeta(t) + \frac{\tau}{2}\frac{p_\zeta(t)}{M_\zeta}G(q(t+\tau/2)) && \text{(A.16)}\\
p(t+\tau) &= p(t) + \tau F(q(t+\tau/2)) && \text{(A.17)}\\
p_\zeta(t+\tau) &= p_\zeta(t) + \tau F_\zeta(q(t+\tau/2)) && \text{(A.18)}\\
q(t+\tau) &= q(t+\tau/2) + \frac{\tau}{2}\frac{p(t+\tau)}{m}\\
&+ \frac{\tau}{2}\frac{p_\zeta(t+\tau)}{M_\zeta}F(q(t+\tau/2)) && \text{(A.19)}\\
\zeta(t+\tau) &= \zeta(t+\tau/2)\\
&+ \frac{\tau}{2}\frac{p_\zeta(t+\tau)}{M_\zeta}\left(\sum_i \frac{\partial^2 U}{\partial q_i^2}\right)_{q=q(t+\tau/2)} && \text{(A.20)}
\end{aligned}
$$

Equations (A.15-A.18) must be iterated.

Appendix B. Symplectic integration algorithm of the hybrid CKTNH chain thermostat

Writing explicitly the symplectic velocity Verlet algorithm for the hybrid CKTNH chain thermostat, one obtains

$$
\begin{aligned}
p(t+\tau/2) &= p(t) + \frac{\tau}{2} F(q(t)) && \text{(B.1)}\\
p_\zeta(t+\tau/2) &= p_\zeta(t) - \frac{\tau}{2}\frac{p_s(t+\tau/2)}{M_s} p_\zeta(t+\tau/2) \\
&+ \frac{\tau}{2} F_\zeta(q(t)) && \text{(B.2)}\\
p_s(t+\tau/2) &= p_s(t) + \frac{\tau}{2}\frac{p_\zeta^2(t+\tau/2)}{M_\zeta} - \frac{\tau}{2} k_{\mathrm{B}} T && \text{(B.3)}\\
q(t+\tau) &= q(t) + \tau\frac{p(t+\tau/2)}{m} + \frac{\tau}{2}\frac{p_\zeta(t+\tau/2)}{M_\zeta} \\
&\times [F(q(t)) + F(q(t+\tau))] && \text{(B.4)}\\
\zeta(t+\tau) &= \zeta(t) + \frac{\tau}{2}\frac{p_\zeta(t+\tau/2)}{M_\zeta} \\
&\times [G(q(t)) + G(q(t+\tau))] && \text{(B.5)}\\
s(t+\tau) &= s(t) + \tau\frac{p_s(t+\tau/2)}{M_s} && \text{(B.6)}\\
p(t+\tau) &= p(t+\tau/2) + \frac{\tau}{2} F(q(t+\tau)) && \text{(B.7)}\\
p_\zeta(t+\tau) &= p_\zeta(t+\tau/2) - \frac{\tau}{2}\frac{p_s(t+\tau/2)}{M_s} p_\zeta(t+\tau/2) \\
&+ \frac{\tau}{2} F_\zeta(q(t+\tau)) && \text{(B.8)}\\
p_s(t+\tau) &= p_s(t+\tau/2) + \frac{\tau}{2}\frac{p_\zeta^2(t+\tau/2)}{M_\zeta} - \frac{\tau}{2} k_{\mathrm{B}} T \\
& && \text{(B.9)}
\end{aligned}
$$

Equations (B.2-B.4) must be iterated.

The symplectic position Verlet algorithm for the hybrid CKTNH chain thermostat

reads

$$q(t+\tau/2) = q(t) + \frac{\tau}{2}\frac{p(t)}{m} + \frac{\tau}{2}\frac{p_\zeta(t)}{M_\zeta}F(q(t+\tau/2)) \tag{B.10}$$

$$\zeta(t+\tau/2) = \zeta(t) + \frac{\tau}{2}\frac{p_\zeta(t)}{M_\zeta}G(q(t+\tau/2)) \tag{B.11}$$

$$s(t+\tau/2) = s(t) + \frac{\tau}{2}\frac{p_s(t)}{M_s} \tag{B.12}$$

$$p(t+\tau) = p(t) + \tau F(q(t+\tau/2)) \tag{B.13}$$

$$\begin{aligned} p_\zeta(t+\tau) &= p_\zeta(t) + \tau F_\zeta(q(t+\tau/2)) \\ &- \frac{\tau}{2M_s}\left[p_s(t)p_\zeta(t) + p_s(t+\tau)p_\zeta(t+\tau)\right] \end{aligned} \tag{B.14}$$

$$p_s(t+\tau) = p_s(t) + \frac{\tau}{2M_\zeta}\left[p_\zeta^2(t) + p_\zeta^2(t+\tau)\right] - \tau k_{\mathrm{B}}T \tag{B.15}$$

$$\begin{aligned} q(t+\tau) &= q(t+\tau/2) + \frac{\tau}{2}\frac{p(t+\tau)}{m} \\ &+ \frac{\tau}{2}\frac{p_\zeta(t+\tau)}{M_\zeta}F(q(t+\tau/2)) \end{aligned} \tag{B.16}$$

$$\zeta(t+\tau) = \zeta(t+\tau/2) + \frac{\tau}{2}\frac{p_\zeta(t+\tau)}{M_\zeta}G(q(t+\tau/2)) \tag{B.17}$$

$$s(t+\tau) = s(t+\tau/2) + \frac{\tau}{2}\frac{p_s(t+\tau)}{M_s} \tag{B.18}$$

Equations (B.10) and (B.14-B.15) must be iterated.

References

[1] D. J. Evans, W. G. Hoover, B. H. Failor, B. Moran, and A. J. C. Ladd, Phys. Rev. A **28** 1016 (1983).
[2] S. Nosè, J. Chem. Phys. **81** 511 (1984).
[3] W. G. Hoover, Phys. Rev. A **31** 1695 (1985).
[4] T. Schneider and E. Stoll, Phys. Rev. B **17** 1302 (1978).
[5] G. S. Grest and K. Kremer. Phys. Rev. A **33** 3628 (1986).
[6] R. Hartkamp, S. Bernardi, and B. D. Todd, J. Chem. Phys. **136** 064105 (2012).
[7] A. Sergi, M. Ferrario and D. Costa, Molec. Phys. **97** 825 (1999).
[8] A. Sergi and M. Ferrario, Phys. Rev. E **64** 056125 (2001).
[9] M. Reguzzoni, M. Ferrario, S. Zapperi, and M. C. Righi, Proc. Natl. Acad. Sci. USA **107** 1311 (2010).
[10] G. J. Martyna, M. E. Tuckerman, D. J. Tobias, and M. L. Klein, Molec. Phys. **87** 1117 (1996).
[11] H. H. Rugh, Phys. Rev. Lett. **78**, 772 (1997).
[12] O. G. Jepps, G. Ayton, and D. J. Evans, Phys. Rev. E **62**, 4757 (2000).
[13] B. D. Butler, G. Ayton, O. G. Jepps and D. J. Evans, J. Chem. Phys. 109, 6519 (1998).
[14] G. Rickayzen and J. G. Powles, J. Chem. Phys. 114, 4333 (2001)
[15] J. J. Erpenbeck, Phys. Rev. Lett. **52**, 1333 (1984).

[16] D. J. Evans and G. P. Morriss, Phys. Rev. Lett. **56**, 2172 (1986).
[17] D. J. Evans, S. T. Cui, H. J. M. Hamley, and G. C. Straty, Phys. Rev. A **46**, 6731 (1992).
[18] K. P. Travis, P. J. Daivis, and D. J. Evans, J. Chem. Phys. **103**, 10638 (1995).
[19] W. Loose and G. Ciccotti, Phys. Rev. A **45**, 3859 (1992).
[20] C. Braga and K. P. Travis, J. Chem. Phys. **124**, 104102 (2006).
[21] K. P. Travis and C. Braga, J. Chem. Phys. **128**, 014111 (2008).
[22] C. Braga and K. P. Travis, J. Chem. Phys. **123**, 134101 (2005).
[23] K. P. Travis and C. Braga, Molec. Phys. **104**, 3735 (2006).
[24] A. Sergi, Phys. Rev. E **67** 021101 (2003).
[25] A. Sergi and P. V. Giaquinta, J. Stat. Mech.: Th. and Exper. **02** P02013 (2007).
[26] D. Costa, A. Sergi, and M. Ferrario, J. Chem. Phys. **138** 184501 (2013).
[27] M. P. Allen and D. J. Tildesley, *Computer Simulation of Liquids* (Clarendon Press, Oxford, 1987).
[28] G. J. Martyna, M. L. Klein, and M. Tuckerman, J. Chem. Phys. **97** 2635 (1992).
[29] E. Hairer, C. Lubich, and G. Wanner, Geometric Numerical Integration. Structure-Preserving Algorithms for Ordinary Differential Equations Springer Series in Comput. Mathematics, Vol. 31 (Springer-Verlag, Berlin, 2002).
[30] H. Yoshida, Phys. Lett. A **150** 262 (1990).
[31] M. Suzuki, J. Math. Phys. **32** 400 (1991).
[32] J. D. Weeks, D. Chandler, and H. C. Andersen, J. Chem. Phys. **54** 5237 (1971).
[33] H. C. Andersen, J. D. Weeks, and D. Chandler, Phys. Rev. A **4** 1597 (1971).
[34] J.-P. Hansen and I. R. McDonald, Theory of Simple Liquids, 3rd ed. (Academic Press, Amsterdam, 2006).
[35] M. Tuckerman, B. J. Berne, and G. J. Martyna, J. Chem. Phys. **97**, 1990 (1992).

Bibliography

1. M.P. Allen and D.J. Tildesley. *Computer Simulation of Liquids*. Clarendon Press, 1989.

2. D. Frenkel and B. Smit. *Understanding Molecular Simulation: From Algorithms to Applications*. Elsevier Science, 2001.

3. H. C. Andersen. Molecular dynamics simulations at constant pressure and/or temperature. *J. Chem. Phys.*, 72, 1980.

4. A. Sergi and P. V. Giaquinta. On Computational Strategies within Molecular Dynamics Simulation. *Phys. Essays*, 20, 2007.

5. D. J. Evans, W. G. Hoover, B. H. Failor, B. Moran, and A. J. C. Ladd. Nonequilibrium molecular dynamics via Gauss's principle of least constraint. *Phys. Rev. A*, 28, 1983.

6. T. Schneider and E. Stoll. Molecular-dynamics study of a three-dimensional one-component model for distortive phase transitions. *Phys. Rev. B*, 17, 1978.

7. G. S. Grest and K. Kremer. Molecular dynamics simulation for polymers in the presence of a heat bath. *Phys. Rev. A*, 33, 1986.

8. S. Nosè. A unified formulation of the constant temperature molecular dynamics methods. *J. Chem. Phys.*, 81, 1984.

9. W. G. Hoover. Canonical dynamics: Equilibrium phase-space distributions. *Phys. Rev. A*, 31, 1985.

10. G. J. Martyna, M. L. Klein, and M. Tuckerman. Nosè-Hoover chains: The canonical ensemble via continuous dynamics. *J. Chem. Phys.*, 97, 1992.

11. H. H. Rugh. Dynamical Approach to Temperature. *Phys. Rev. Lett.*, 78, 1997.

12. O. G. Jepps, G. Ayton, and D. J. Evans. Microscopic expressions for the thermodynamic temperature. *Phys. Rev. E*, 62, 2000.

13. B. D. Butler, G. Ayton, O. G. Jepps, and D. J. Evans. Configurational temperature: Verification of Monte Carlo simulations. *J. Chem. Phys.*, 109, 1998.

14. G. Rickayzen and J. G. Powles. Temperature in the classical microcanonical ensemble. *J. Chem. Phys.*, 114, 2001.

15. K. P. Travis and C. Braga. Configurational temperature and pressure molecular dynamics: review of current methodology and applications to the shear flow of a simple fluid. *Molec. Phys.*, 104, 2006.

16. J. J. Erpenbeck. Shear Viscosity of the Hard-Sphere Fluid via Nonequilibrium Molecular Dynamics. *Phys. Rev. Lett.*, 52, 1984.

17. D. J. Evans and G. P. Morriss. Shear Thickening and Turbulence in Simple Fluids. *Phys. Rev. Lett.*, 56, 1986.

18. D. J. Evans, S. T. Cui, H. J. M. Hanley, and G. C. Straty. Conditions for the existence of a reentrant solid phase in a sheared atomic fluid. *Phys. Rev. A*, 46, 1992.

19. K. P. Travis, P. J. Daivis, and D. J. Evans. Thermostats for molecular fluids undergoing shear flow: Application to liquid chlorine. *J. Chem. Phys.*, 103, 1995.

20. C. Braga and K. P. Travis. A configurational temperature Nosè-Hoover thermostat. *J. Chem. Phys.*, 123, 2005.

21. A. Sergi and M. Ferrario. Non-Hamiltonian equations of motion with a conserved energy. *Phys. Rev. E*, 64, 2001.

22. M. Tuckerman. *Statistical Mechanics: Theory and Molecular Simulation.* OUP Oxford, 2010.

23. H.B. Callen. *Thermodynamics and an Introduction to Thermostatistics.* Wiley, 1985.

24. R.H. Swendsen. *An Introduction to Statistical Mechanics and Thermodynamics*. OUP Oxford, 2012.

25. H. H. Rugh. A geometric, dynamical approach to thermodynamics. *J. Phys. A*, 31, 1998.

26. H. Goldstein, C.P. Poole, and J.L. Safko. *Classical Mechanics*. Addison Wesley, 2002.

27. Joseph L McCauley. *Classical mechanics : transformations, flows, integrable, and chaotic dynamics*. Cambridge University Press, 1997.

28. S. Nosè. A molecular dynamics method for simulations in the canonical ensemble. *Molec. Phys.*, 52, 1984.

29. A. Sergi. Non-Hamiltonian equilibrium statistical mechanics. *Phys. Rev. E*, 67, 2003.

30. M. Tuckerman, Y. Liu, G. Ciccotti, and G. J. Martyna. Non-Hamiltonian molecular dynamics: Generalizing Hamiltonian phase space principles to non-Hamiltonian systems. *J. Chem. Phys.*, 115, 2001.

31. M. E. Tuckerman, C. J. Mundy, and G. J. Martyna. On the classical statistical mechanics of non-Hamiltonian systems. *Europhys. Lett.*, 45, 1999.

32. J. Delhommelle and D. J. Evans. Configurational temperature thermostat for fluids undergoing shear flow: application to liquid chlorine. *Molec. Phys.*, 99, 2001.

33. L. Lue, O. G. Jepps, J. Delhommelle, and D. J. Evans. Configurational thermostats for molecular systems. *Molec. Phys.*, 100, 2002.

34. M. Tuckerman, B. J. Berne, and G. J. Martyna. Reversible multiple time scale molecular dynamics. *J. Chem. Phys.*, 97, 1992.

35. H. Yoshida. Construction of higher order symplectic integrators. *Phys. Lett. A*, 150, 1990.

36. M. Suzuki. General theory of fractal path integrals with applications to many-body theories and statistical physics. *J. Math. Phys.*, 32, 1991.

37. G. J. Martyna, M. E. Tuckerman, D. J. Tobias, and M. L. Klein. Explicit reversible integrators for extended systems dynamics. *Molec. Phys.*, 87, 1996.

38. E. Wigner. On the Quantum Correction For Thermodynamic Equilibrium. *Phys. Rev.*, 40, 1932.

39. A. Sergi and F. Petruccione. Nosè-Hoover dynamics in quantum phase space. *J. Phys. A*, 41, 2008.